2-14-2014

Broadband PIFA Rectenna Design for a Multi-Source Energy Harvesting Device

Jillian Erickson

Jillian Erickson

Candidate

Electrical and Computer Engineering

Department

This thesis is approved, and it is acceptable in quality and form for publication:

Approved by the Thesis Committee:

Dr. Christos Christodoulou , Chairperson

Dr. Edl Schamiloglu

Dr. Youssef Tawk

Dr. Silvio Barbin

BROADBAND PIFA RECTENNA DESIGN FOR A MULTI-SOURCE ENERGY HARVESTING DEVICE

by

Jillian Erickson

B.A., Applied Mathematics, University of New Mexico, 2008

THESIS

Submitted in Partial Fulfillment of the
Requirements for the Degree of

Master of Science
Electrical Engineering

The University of New Mexico
Albuquerque, New Mexico

December 2013

Acknowledgements

I would like to start out by expressing my deepest gratitude to my advisor, Dr. Christos Christodoulou, for providing me the opportunity to work on this project and for his guidance throughout my research. He is an amazing professor and advisor and it was an honor to work with him. I would also like to thank Dr. Edl Schamiloglu and Dr. Silvio Barbin for being a part of my thesis committee and taking the time to review my thesis.

I would like to thank Dr. Youssef Tawk for also being a part of my thesis committee and for his continuous help in the design and fabrication of my project. He spent hours aiding me with my research and for that I am truly grateful.

I would like to also thank Dr. Olga Lavrova and the SEPTET team. I have been blessed with a hard working group of people to work with which has made performing this research more enjoyable.

I am also extremely lucky to have had help from Georgios Atmatzakis and Firas Ayoub who took time away from their own research to aide me in taking measurements and fabricating my antenna. Thank you so much for all of your help.

Lastly, I would like to thank Jason Sparks and my parents for their continuous support and for believing in me every step of the way. I am extremely lucky to have people in my life who have so much faith in me.

BROADBAND PIFA RECTENNA DESIGN FOR A MULTI-SOURCE ENERGY HARVESTING DEVICE

by

Jillian Erickson

B.A., Applied Mathematics, University of New Mexico, 2008

M.S., Electrical Engineering, University of New Mexico, 2013

ABSTRACT

Combining different energy harvesting devices to optimize output power is crucial to the achievement of sustainable energy. This thesis focuses on the design, simulation and fabrication of a broadband Planar Inverted-F Antenna (PIFA) constructed for energy harvesting and its integration with a solar cell. An assessment of available ambient RF energy was performed by surveying power density levels from 700MHz to 18GHz. The measured spectrum was then used to determine the bandwidth for our rectifying antenna. The PIFA design was chosen for its small size and low profile, in order to limit the area covering the solar panel. The purpose of this antenna is to harvest power during the times that solar energy is unavailable. The thorough analysis, design and fabrication specifics of the antenna and its integration with the solar panel are discussed in detail. Future work involving the implementation of a PIFA array to optimize the amount of energy harvested is also presented.

TABLE OF CONTENTS

LIST OF FIGURES

LIST OF TABLES

Chapter 1

Introduction

The growth of multifunction, high efficiency energy harvesters has greatly increased in the past few years. Using several energy sources available in the environment such as, solar, thermal, and RF, researchers have been able to come up with new ways to optimize harvesting efficiency and output power. The process of energy harvesting involves capturing ambient energy in the environment and converting it into power that can be stored and reused at any time. The available power being retrieved from a harvesting device is very limited, which is why studies are being done to integrate different energy harvesting techniques to optimize the output. An example layout of this kind of device is shown below.

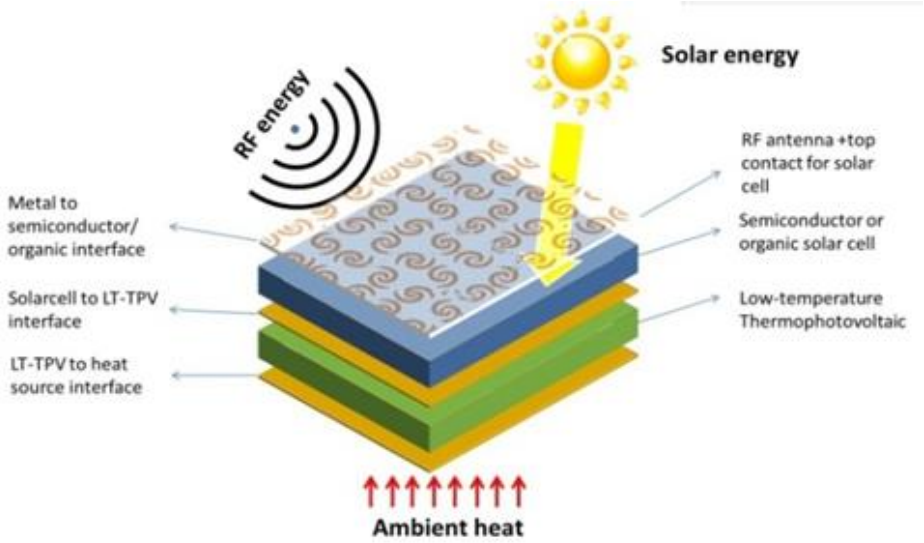

Figure 1.1: An example of a multi-source energy harvesting device [1].

To maximize efficiency, these energy harvesters will be able to read the environment and harvest the energy that is the most prominent at the time. A general objective function for this kind of device is

$$E[x(t), y(t)\tau(t); \alpha] = \sum_i \int_{t \in \pi_i} P_i(x_i(s), y_i(s); \alpha_i) ds \quad (1)$$

[1]

where E is the total energy output of a specified amount of time, $x(t)$ is the environment factors, $y(t) = (y_1(t) \ldots y_N(t))$ are time-varying performance controls for each component, $\alpha = (\alpha_1 \ldots \alpha_N)$ are a collection of fixed design control parameters, $\tau_i(t)$ is the characteristic function for the time interval of operation of the i-th component, and P_i is the instantaneous power output of the i-th component [1]. With these parameters, the goal is to find power functions for each harvesting technique and optimize the total energy output.

For this thesis, the ambient energy focused on is RF. Radio frequency energy surrounds us from applications that have high electromagnetic fields. These fields come from sources such as Wi-Fi, cell phone towers, radio signals, broadcast television signals, among others. Each source radiates at a different frequency. When harvesting RF energy it is important to understand where in the frequency spectrum you will be receiving the most amount of RF power from the surrounding environment. Table 1.1 shows different frequency levels and examples of the applications using them.

Table 1.1: Different frequency ranges and their applications.

Frequency Band	**Frequency Range**	**Applications**
Low Frequency	30 to 300kHz	Navigation, time standards
Medium Frequency	300kHz to 3 MHz	Marine/aircraft navigation, AM broadcast
High Frequency	3 to 30MHz	Broadcasting, mobile radio, amateur radio
Very High Frequency	30 to 300MHz	Land mobile, FM/TV

		broadcast
Ultra-High Frequency	300MHz to 3GHz	Cell phones, mobile radio, WLAN, personal-area networks
Super-High Frequency	3 to 30GHz	Satellite, radar, backhaul, TV
Extremely High Frequency	30 to 300GHz	Satellite, radar, backhaul, experimental

The more broadband the RF energy harvester, the more energy you will be able to harvest from different sources and, in turn, the more efficient your device will be.

The device used to harvest RF energy is called a rectenna. A rectenna is a rectifying antenna that is used to convert microwave energy to DC electricity. Most rectenna designs consist of an antenna that radiates for the desired frequency range, an RF diode that rectifies the AC current to produce a DC signal, and a resistive load. Although the idea of the rectenna came from Nicola Tesla over a hundred years ago, the dream was not brought to life until May 1963 at the Spencer Laboratory of Raytheon Company. The first rectenna ever constructed consisted of a half-wave dipole antenna with a single semiconductor diode placed above a reflecting plane followed by a resistive load [2]. The directivity of this antenna can be seen in Figure 1.2. Since this point, it has been a goal to increase the conversion efficiency of the rectenna element. The conversion efficiency measures how accurately the RF power received by the antenna is converted to DC power. The greatest conversion efficiency ever recorded from a fabricated design was achieved in 1977 by B. C. Brown using a GaAsPt Schottky diode. The conversion efficiency was 90.6% with an input microwave power level of 8W [2].

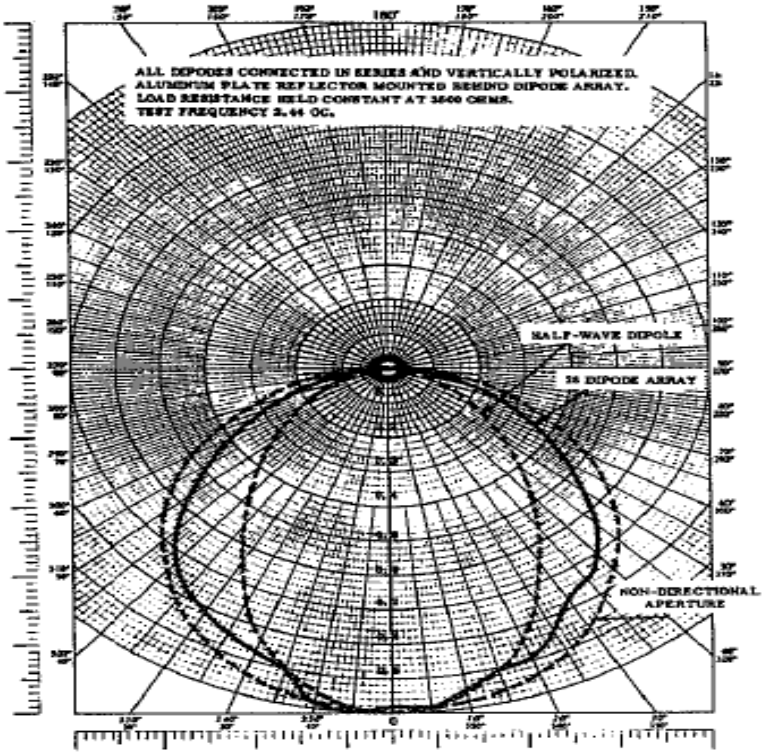

Figure 1.2: Directivity of first rectenna fabricated in May 1963 [2].

Since the fabrication of the first rectenna in 1963, researchers have been finding new ways to develop and expand the rectenna design. A recent development has been a thin-film printed-circuit rectenna for high altitude atmospheric platform and space use [3]. Expansion in the efficiency, bandwidth and size have all been researched and improved in the last several years.

The focus of the research described in this thesis is to measure the power levels produced by ambient RF frequency in different environments and fabricate a working rectenna that will harvest this energy. Once this is accomplished we will integrate the working rectenna design with a solar cell and compare the power harvested from the solar cell with the rectenna and without the rectenna. The motivation of this work is to create a multi-source energy harvesting device that will output the optimal amount of power in different environments.

The remainder of this thesis is organized as follows. Chapter 2 discusses the measurements recorded with the PXA spectrum analyzer and how these results are used to determine the bandwidth of the rectenna. Chapter 3 discusses the design, simulation and fabrication of a narrowband patch antenna. After the fabrication of the patch antenna, the rectifying circuit is measured and tested for efficiency. Chapter 4 talks about the design, simulation and fabrication of the broadband PIFA antenna followed by the construction of the rectifying circuit. The results for the efficiency of this design are also included. Chapter 5 discussed the integration of the PIFA and a solar cell. Lastly, chapter 6 will conclude this thesis with a discussion of the results and a brief introduction of possible future work.

Chapter 2

Review of the Literature

2.1 Introduction

Rectifying antennas, or rectennas, have become very popular over the past few years due to the increasing need for new ways to recycle energy. New advancements in antenna design, circuit design, and efficiency optimization have fueled the study of RF energy harvesting. In this chapter we will introduce some studies on rectenna design and the advancements that have already taken place.

2.2 Rectenna Designs

The paper entitled "Power efficiency and optimum load formulas on RF rectifiers featuring flow-angle equations" [4] is a good introduction to different rectifying circuit layouts and how they work. This paper introduces three pairs of circuits that work for RF rectification. For each circuit they assign a finite RF power and resistive load and calculate the efficiency. To start, the simple one diode scheme is discussed in both the series and shunt topology. For the series layout (figure 2.1) the inductor L makes a DC ground path from the diode to the resistive load. It also chokes the i_2 current against the RF current. The capacitor, C, after the diode makes an RF ground path from the source to the diode, as well as smoothes the output ripple [4].

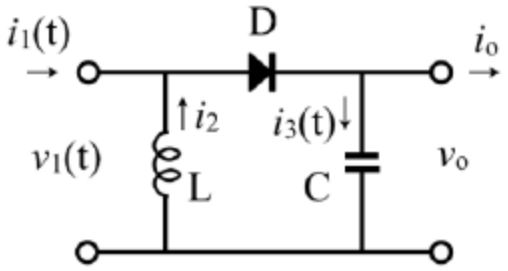

Figure 2.1: A single diode with series topology schematic [4].

The diode in this model is assumed to be a perfect one-way switching model. Therefore the waveform can be described in two states; when the diode is on and when it is off. The equations for these two states are

$$\mathrm{D} = \mathrm{ON}, v_1(t) = v_0, i_1(t) = \frac{1}{r}(v_s cos\omega t - v_0), -t_1 < t < t_1 \tag{2}$$

$$\mathrm{D} = \mathrm{OFF}, i_1(t) = -i_2, v_1(t) = v_s cos\omega t + r i_2, t_1 < t < T - t_1 \tag{3}$$

[4]

These two waveforms are plotted in figure 2.2. It can be seen that while an RF source is received as a pure sinusoidal wave ($v_s(t)$), it is distorted due to the smoothing capacitor for the rectifying input when the diode is ON.

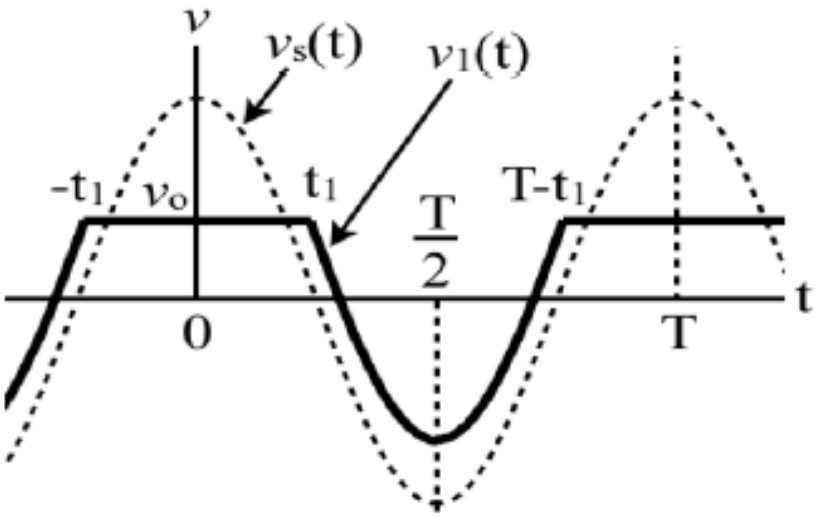

Figure 2.2: Waveforms produced from the two diode switching states [4]

The DC output current and voltage obtain from this system can be written as

$$i_0 = \frac{v_s cos\phi}{R-r} = \frac{v_s}{\pi r}(sin\phi - \phi cos\phi) \quad [4] \tag{4}$$

$$v_0 = Ri_0 = \frac{Rv_s}{\pi r}(sin\phi - \phi cos\phi) = \frac{v_s}{\pi}(sin\phi + (\pi - \phi)cos\phi) \quad [4] \tag{5}$$

and $P_o = i_o v_o$. The efficiency can then be found by

$$\eta = \frac{P_o}{P_s} \quad [4] \tag{6}$$

For this system the maximum efficiency was found to be 81.1% at $R/r = 1$, where R is the output load and r is the internal resistance.

The next single diode layout discussed the single-shunt topology (figure 2.3). The characterization of this circuit is done by interchanging voltage/current, ON/OFF, *L/C*, and *R/r* from the formulas in the single-series layout.

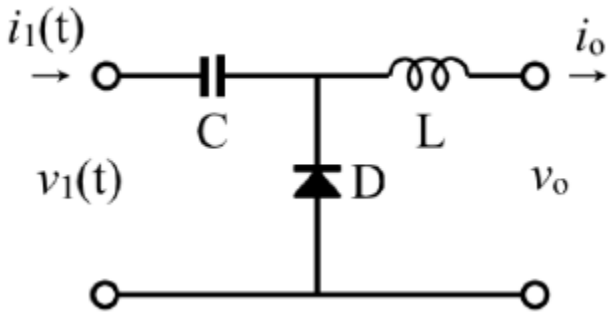

Figure 2.3: A single-shunt diode topology schematic [4].

The equations for the switching diode for this layout are

$$\mathrm{D} = \mathrm{ON}, v_1(t) = -v_0, i_1(t) = \frac{1}{r}(v_s cos\omega t + v_0), -t_1 < t < t_1 \tag{7}$$

$$\mathrm{D} = \mathrm{OFF}, i_1(t) = i_0, v_1(t) = v_s cos\omega t + r i_0, t_1 < t < T - t_1 \quad [4] \tag{8}$$

The power performance in this case is exactly the same as the single-series diode in agreement with the duality theorem which states that the impedance terms can be reversed while the power terms will be unchanged.

Next, the bridge topology will be explained. The layout for this circuit is shown in figure 2.4 and is a widely used topology for full-wave rectification.

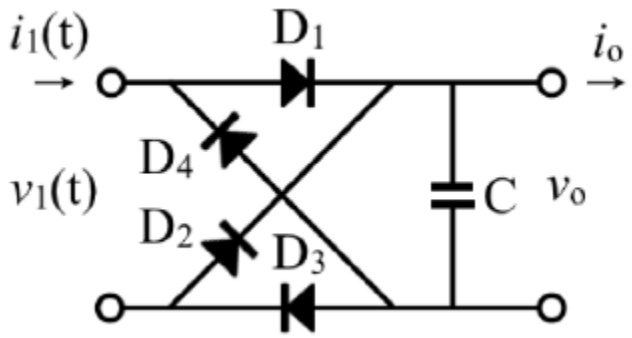

Figure 2.4: Schematic of the bridge topology [4].

For this design a reactance is only needed at the output port due to the DC currents being generated from the two branches cancel each other at the input. The capacitor at the output is used for output smoothing and works as a power efficiency enhancement. Since there are two pairs of diodes, there are four waveform states.

$$\mathrm{D}_{1,3} = \mathrm{ON}, \mathrm{D}_{2,4} = \mathrm{OFF}, v_0 < v_s(t), -t_1 < t < t_1 \tag{9}$$

$$\mathrm{D}_{1,2,3,4} = \mathrm{OFF}, -v_0 < v_s(t) < v_0, t_1 < t < T/2 - t_1 \tag{10}$$

$$\mathrm{D}_{1,3} = \mathrm{OFF}, \mathrm{D}_{2,4} = \mathrm{ON}, v_s(t) < -v_0, T/2 - t_1 < t < T/2 + t_1 \tag{11}$$

$$\mathrm{D}_{1,2,3,4} = \mathrm{OFF}, -v_0 < v_s(t) < v_0, T/2 + t_1 < t < T - t_1 \tag{12}$$

[4]

It is noted that the two diode pairs cannot be on at the same time. However, if the output shunt capacitor was replaced with a series inductor the two diode pairs could be on at the same time but not off at the same time. These waveform states would become

$$\mathrm{D}_{1,3} = \mathrm{ON}, \mathrm{D}_{2,4} = \mathrm{OFF}, ri_0 < v_s(t), -t_1 < t < t_1 \tag{13}$$

$$\mathrm{D}_{1,2,3,4} = \mathrm{ON}, -ri_0 < v_s(t) < ri_0, t_1 < t < T/2 - t_1 \tag{14}$$

$$\mathrm{D}_{1,3} = \mathrm{OFF}, \mathrm{D}_{2,4} = \mathrm{ON}, v_s(t) < -ri_0, T/2 - t_1 < t < T/2 + t_1 \tag{15}$$

$$\mathrm{D}_{1,2,3,4} = \mathrm{ON}, -ri_0 < v_s(t) < ri_0, T/2 + t_1 < t < T - t_1 \tag{16}$$

[4]

The maximum efficiency for these two layouts was found to be 92.3%. It was concluded that the output capacitor in the first bridge is important to successfully receive the optimal amount of DC power from the circuit. Also, the choke inductor in the second bridge enhances the current and saves the voltage in its smoothing process.

The final layout pair discussed is the doubler topology. The double-voltage circuit shows two diodes and two capacitors in figure 2.5.

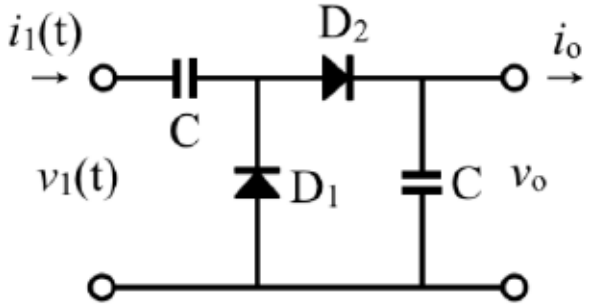

Figure 2.5: Schematic of a double-voltage topology [4].

In this circuit, a half cycle of input voltage travels through one diode and the opposite half cycle goes through another in turn. The voltage sums up double and charges the output capacitor. This scenario has four waveform states

$$\mathrm{D}_1 = \mathrm{OFF}, \mathrm{D}_2 = \mathrm{ON}, v_0 < 2v_s(t), -t_1 < t < t_1 \tag{17}$$

$$\mathrm{D}_{1,2} = \mathrm{OFF}, -v_0 < 2v_s(t) < v_0, t_1 < t < T/2 - t_1 \tag{18}$$

$$\mathrm{D}_1 = \mathrm{ON}, \mathrm{D}_2 = \mathrm{OFF}, 2v_s < -v_0, T/2 - t_1 < t < T/2 + t_1 \tag{19}$$

$$\mathrm{D}_{1,2} = \mathrm{OFF}, -v_0 < 2v_s(t) < v_0, T/2 + t_1 < t < T - t_1 \tag{20}$$

[4]

For this layout the maximum efficiency was 92.3%. The optimal load resistance for this circuit is four times higher than the first bridge topology. It is concluded that the double-voltage and the half-current output from the same input power. From the duality theorem, the formulas for the double current topology were then derived (figure 2.6). The ON/OFF states, voltage/current, and source/load were interchanged and the four waveform states became [4]

$$\mathrm{D}_1 = \mathrm{ON}, \mathrm{D}_2 = \mathrm{OFF}, ri_0 < 2v_s(t), -t_1 < t < t_1 \tag{21}$$

$$\mathrm{D}_{1,2} = \mathrm{ON}, -ri_0 < 2v_s(t) < ri_0, t_1 < t < T/2 - t_1 \tag{22}$$

$$\mathrm{D}_1 = \mathrm{OFF}, \mathrm{D}_2 = \mathrm{ON}, 2v_s(t) < -ri_0, T/2 - t_1 < t < T/2 + t_1 \tag{23}$$

$$\mathrm{D}_{1,2} = \mathrm{ON}, -ri_0 < 2v_s(t) < ri_0, T/2 + t_1 < t < T - t_1 \text{ [4]} \tag{24}$$

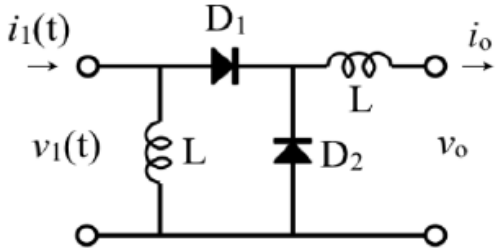

Figure 2.6: Schematic of a double-current topology [4].

For this circuit the maximum efficiency is the same as the double-voltage topology, 92.3%. The three circuit pairs and corresponding maximum efficiencies in this paper are very helpful when designing the optimal rectenna. To maximize the amount of DC power harvested from the circuit it is important to understand how the components are working with respect to each other.

The next few papers discussed different rectenna designs. Authors in [5] designed a circularly polarized rectenna with low profile for wireless power transmission. The layout for this rectenna circuit included a matching network to the diode and a DC-pass filter that consisted of a chip capacitor and a λ/4 microstrip line. Figure 2.7 depicts the layout of this rectifying circuit.

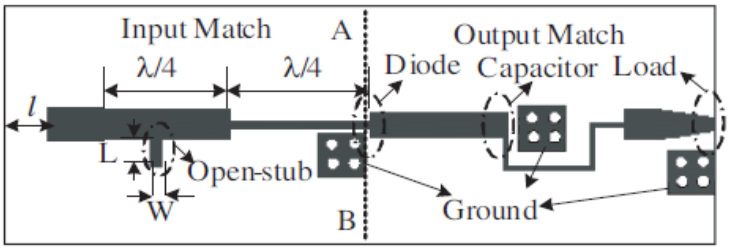

Figure 2.7: Rectifying circuit layout [5].

The rectifying circuit was first tested without the antenna using Agilent 83623L as the microwave source. As discussed above, the conversion efficiency can be calculated and used show how well the rectifying circuit is converting RF to DC power. This equation is

$$\eta = \frac{P_{out}}{P_{in}} = \frac{V_D^2}{R_L P_{in}} \quad [5] \qquad (25)$$

where P_{in} and P_{out} are the incident RF power and output DC power respectively. In this study the highest RF to DC conversion efficiency calculated was 81.4% at an input power of 110mW. The load of this circuit is 320 Ω and the frequency is at 5.8 GHz. Conversion efficiency drops drastically when the input power is greater than 110mW. This drop occurs because the diode voltage exceeds the breakdown voltage. Figure 2.8 shows the conversion efficiency with respect to the input power.

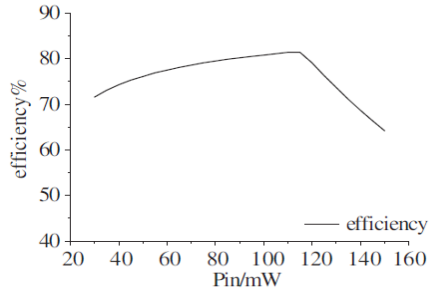

Figure 2.8: Relation between conversion efficiency and input power (mW) [5].

The antenna used in this study is a circularly polarized, truncated-corner patch antenna and the substrate used is FR4. Circularly polarized rectennas are used because they are able to output constant DC power at different polarization angles [5]. This antenna was simulated using a transmitting horn antenna with linear polarization. The gain of the antenna was 16.6 dB and the distance from the rectenna to the transmitting horn was 72cm, which places the rectenna in the far field for the horn.

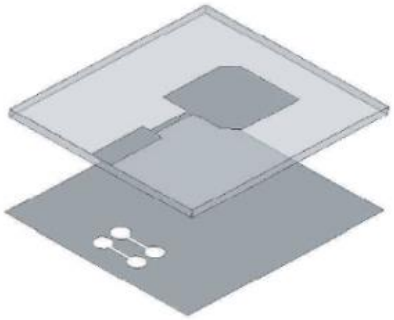

Figure 2.9: Truncated-corner patch antenna etched on an FR4 substrate [5].

Using the Friis transmission formula the power expected from the rectenna can be calculated with:

$$P_{RM} = (\frac{\lambda}{4\pi r})^2 P_t G_t G_r \quad [5] \tag{26}$$

where P_t is the power from the transmitting antenna, G_t is the gain from the transmitting antenna, G_r is the gain from the receiving antenna and λ is the wavelength for 5.8 GHz.

The receiving antenna and rectifying circuit are connected SMA connectors and tested. When this device was simulated at 5.68 GHz a voltage of 4.34 V was obtained and the highest conversion efficiency was 68.4% on a load of 298 Ω. Below is a plot of the RF-DC conversion efficiency with voltage versus the frequency

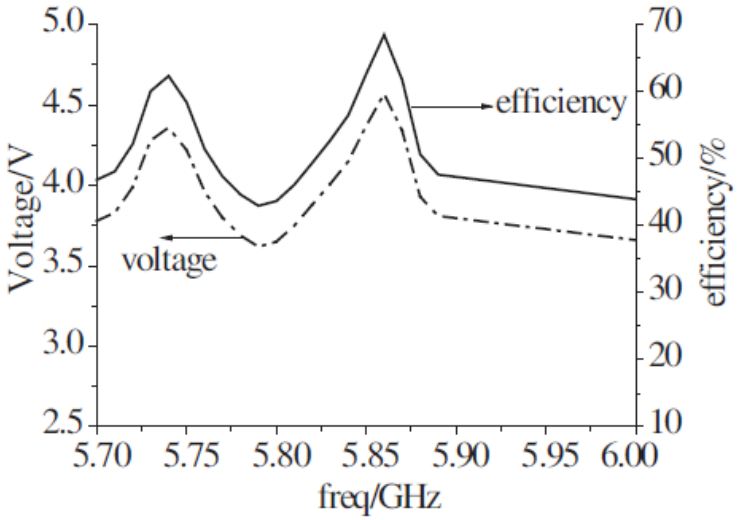

Figure 2.10: Conversion efficiency and voltage versus frequency for a rectenna [5].

The conclusion of this study resulted in a working rectenna design. This compact rectenna with low profile can be applied to RFID and wireless sensor [5]. The frequency where this rectenna was able to harvest the most power is between 5 GHz and 6 GHz.

A tricky aspect of designing a broadband rectenna is modeling the matching network between the antenna and the rectifying diode. Authors in [6] were able to design a 64-element dual-circularly polarized spiral rectenna array meant to radiate for a frequency band from 2-18 GHz. In this study the matching network was eliminated and the diode was attached directly to the antenna feed. The spiral antenna was simulated in CAD tools and resulted in a one-port frequency-dependent impedance that became the diode load [6]. The layout for this rectenna design is seen in figure 2.11.

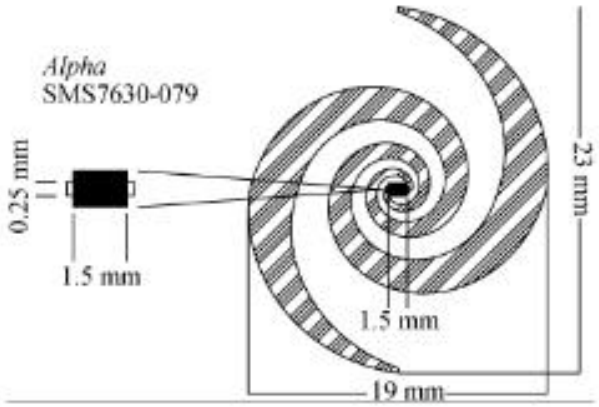

Figure 2.11: Spiral rectenna layout with attached Schottky diode [6].

The rectified DC power and conversion efficiency in this design is characterized by the DC load, RF frequency, polarization and incident angle for power density between 10^{-5}-10^{-1} mW/cm^2. The simulated and measured performance of this rectenna element is below in figure 2.12.

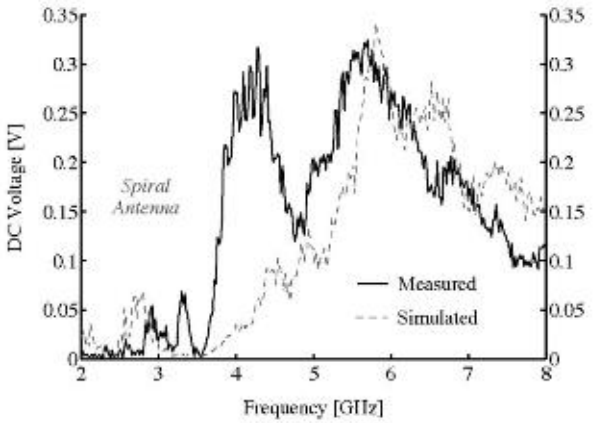

Figure 2.12: Simulated and measure DC voltage with respect to frequency [6].

With these results a broadband rectenna array is constructed. The spiral array consists of 64 elements all left and right-handed circularly polarized. In this layout the RF power is received independently from each element and then summed after rectification as DC currents. The amount of power received by this array is dependent upon the angle of incidence of the RF plane wave. Polarization performance is optimized by alternating left and right circular polarization between the elements. An additional rotation of 90˚ for each element is also put into place.

Although this ensures a flat polarization response, the array suffers a 3 dB input polarization loss for every incident energy polarization [6].

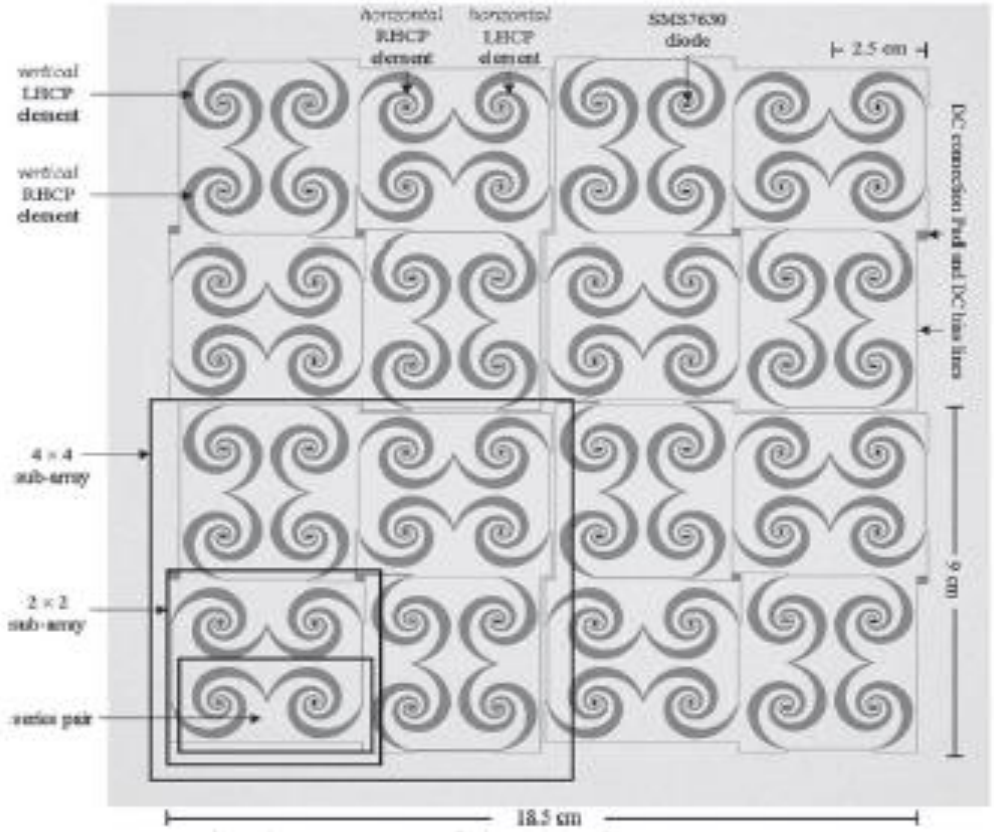

Figure 2.13: Spiral rectenna array layout [6].

To test the efficiency of this design, the array is placed in an environment varying the generated frequency and generated power level. First, a frequency from 2-8 GHz is produced and then an incident power level between 0.1 $\mu W/cm^2$ and 0.1 mW/cm^2 is generated. The rectified power from each source is measured independently and then turned on simultaneously to view the difference. The process was repeated for 10,000 random input pairs. The results can be seen in figure 2.14.

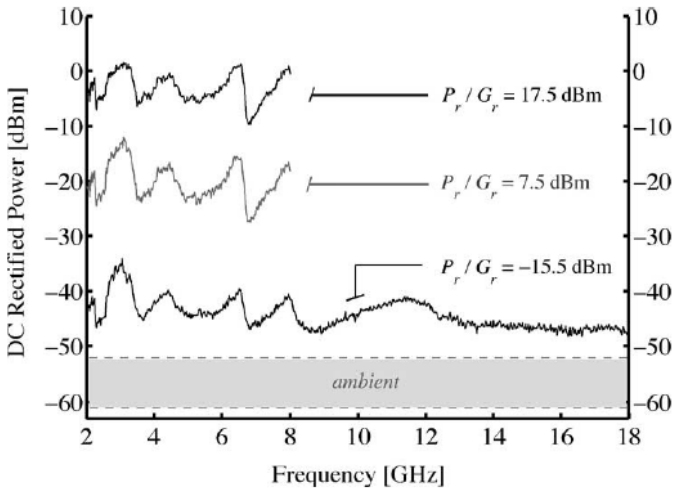

Figure 2.14: Measured broad-band frequency response for three distinct power levels. The grey area towards the bottom represents the rectified power levels that occurred due to ambient background signals. [6]

The results of this paper show that is possible to collect energy by receiving and rectifying two orthogonal polarizations independently and adding the power after rectification.

Authors in [7] present a rectenna design that is tunable for 900 MHz to 2.45 GHz. This rectenna design, as seen is figure 2.15, consists of a receiving antenna, an HF filter, a diode and a DC output filter. The input filter is the matching network between the impedance of the antenna and the diode. In this study they tested their single diode as both series mounted and shunt mounted.

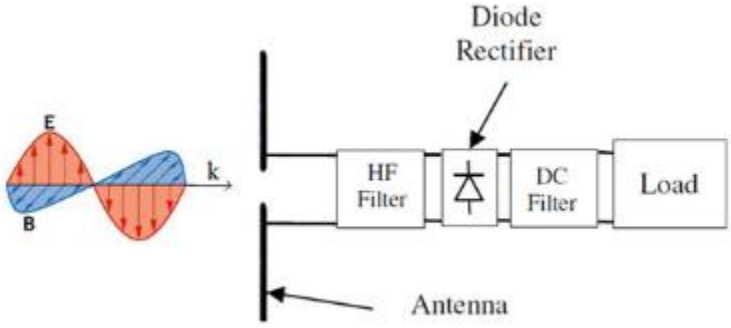

Figure 2.15: Basic rectenna design [7].

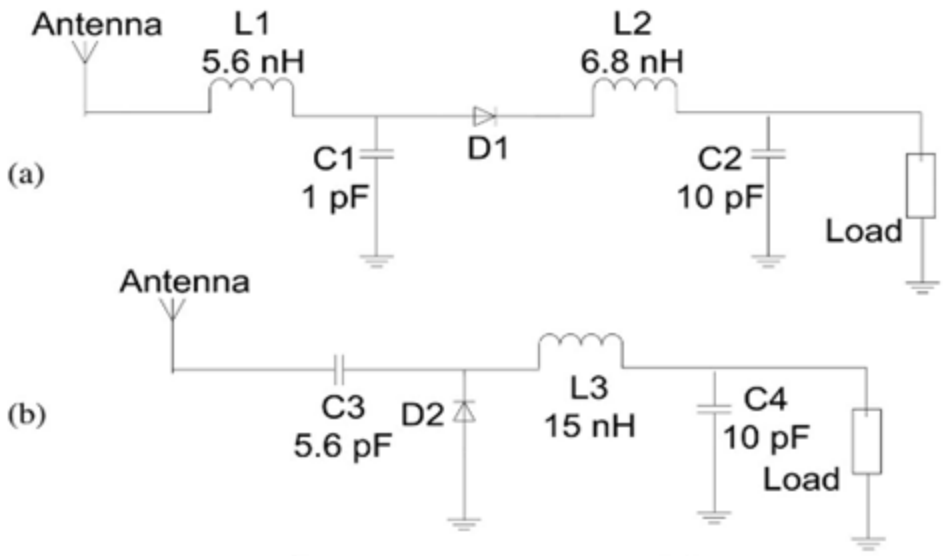

Figure 2.16: Layout for (a) series-mounted and (b) shunt-mounted diode [7].

The series-mounted diode, seen in figure 2.16 (a), is structured for low power levels. The diode used for this circuit is the HSMS2850 by Agilent with a load of 2.4 kΩ. The results for the series-mounted diode are seen in figure 2.17 (a). The maximum efficiency obtained is between -5 and 0 dBm and is approximately 50% with a voltage of 2.1V. It is also seen that the output DC voltage reaches as high as 4.5V at 20 dBm. However, at the higher power levels the diode losses become significant due to the diode series resistance.

a.

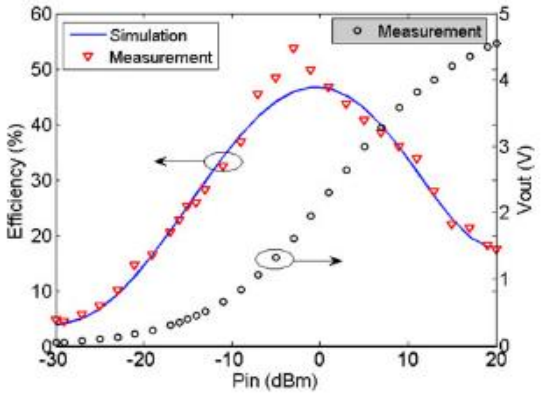

b.

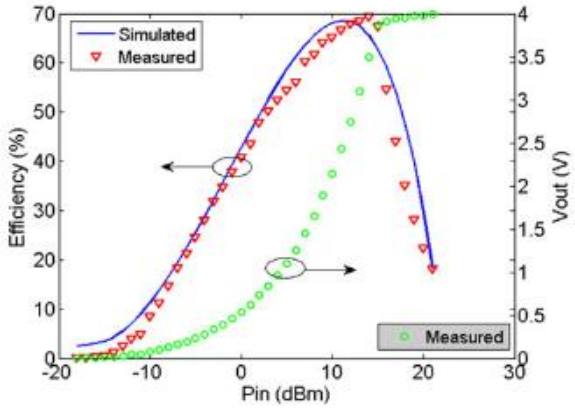

Figure 2.17: (a) Simulated and measured efficiency and output voltage for series-mounted diode; (b) simulated and measured efficiency and output voltage for shunt-mounted diode [7].

The shunt-mounted diode, seen in figure 2.16 (b), is designed for a 0-20 dBm input power level range. The model number for this diode is HSMS2860 manufactured by Agilent Technologies. Results for this layout show a conversion efficiency of 70% at input power 15 dBm. These results are seen in figure 2.17 (b). The optimal load for this input power lever is 750 Ω. In this circuit, for power levels around 15 dBm, the efficiency decreases due to the internal diode ohmic loss. With both the series and the shunt-mounted diodes both high and low input power levels can be accounted for. However, this paper also incorporates a bride rectifier (figure 2.18). The bridge rectifying circuit is mainly used for low frequency AC-DC conversion. The HSMS2820 diode is used in this circuit for the reason that this set up has high power-handling capabilities if a high breakdown voltage diode is used.

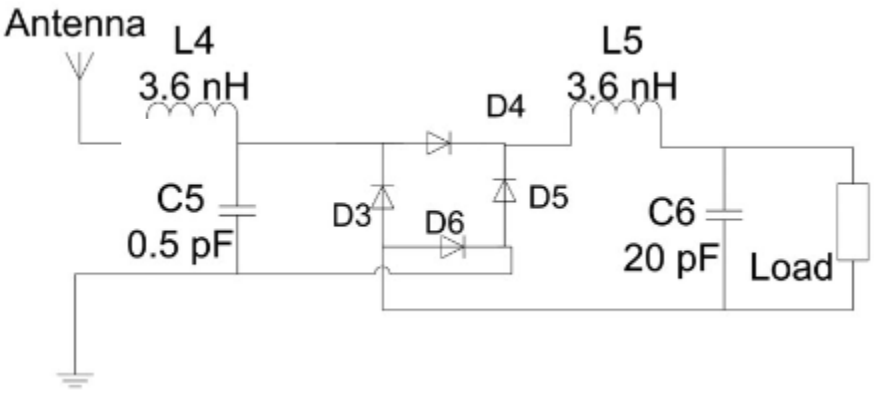

Figure 2.18: Schematic of bridge rectifying circuit [7].

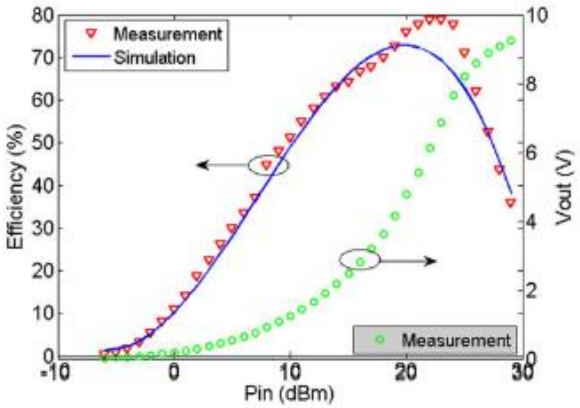

Figure 2.19: Bride rectifier simulation results [7].

The simulation for this circuit shows a peak conversion efficiency at 78% for 23 dBm of input power. However, after 23 dBm the efficiency drops drastically. The optimal load for this input power is 200 Ω.

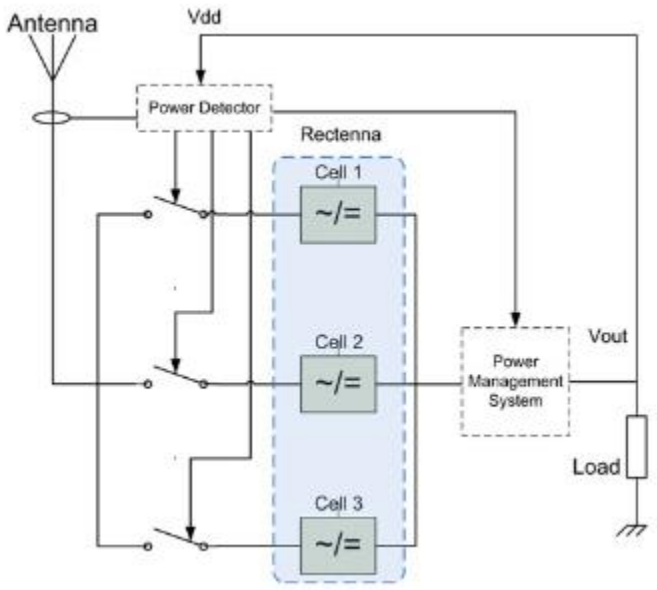

Figure 2.20: Schematic for a reconfigurable rectenna design [7].

The goal of this paper was to create a configurable rectenna design that is optimized to the input power level. To do this the available incident power is measured using a passive RF detector at any given moment, which gives a DC voltage level proportional to the incident power level. The schematics for this proposed rectenna circuit is seen in figure 2.20. The power detector will determine the amount of input power received from the antenna by using a 10 dB directional coupler and a high-impedance diode detector. The series-mounted diode circuit is used for detected power levels less than 1 dBm, the shunt-mounted diode circuit is used for input powers from 1 dBm to 15 dBm, and the bridge rectified circuit is used for detected power levels greater than 15 dBm. The maximum conversion efficiency is 50% at -3 dBm, 68% at 14 dBm, and 78% at 23 dBm for the series-mounted, shunt-mounted and bridge diode circuit respectively.

Authors in [8] developed a dual-frequency circularly polarized antenna made to work at 2.45 and 5.8 GHz. The layout for this antenna, as seen in figure 2.21, consists of two nested microstrip-fed shorted annular ring-slot antennas and two rectifier circuits. The two annular ring-slot antenna structures were formed to operate at two frequencies; a low-band (2.45 GHz) and a high-band (5.8 GHz). Both the low and high band antennas are then fed with a transmission line and quarter-wave transformer for impedance matching.

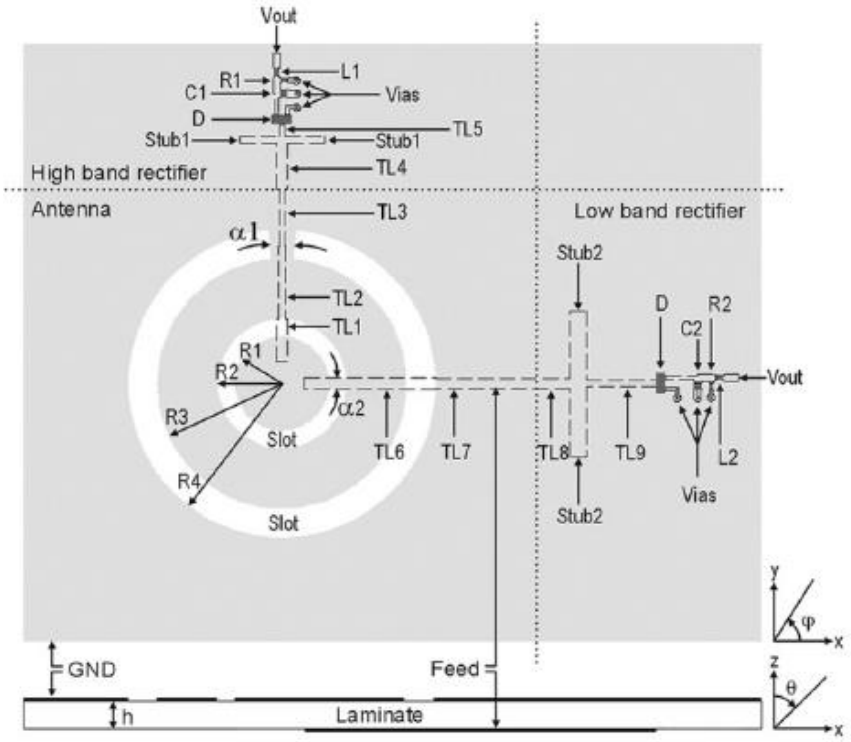

Figure 2.21: Layout for a dual frequency circularly polarized rectenna [8].

The rectifying circuits for this antenna consist of a rectifying diode (HSMS-2862), storage capacitor, load resistor and choke inductor. In this paper the diodes were connected as a voltage-doubler circuit, meaning that the diode is series-mounted for DC and parallel for input microwave frequency.

The measured and simulated reflection coefficients for the antenna are seen in figure 2.22. There are some simulated inefficiencies seen around 5 GHz and higher for the antenna

return loss. According to the authors of [8] these inefficiencies are due to inaccuracies in antenna manufacturing. The performance of this rectenna was measured at one and two meter distances. An output of over 2V was received when 20 dBm was transmitted at one meter and 24 dBm was transmitted at 2 meters. The maximum efficiency of the low-band rectifying antenna (2.45 GHz) was 62% for 24 dBm of transmitted power, 20 dB of transmitted gain and at a distance of 2 meters. For the high-band rectenna (5.8 GHz) the maximum efficiency was 19% at a transmitted power of 32 dBm, transmitted gain of 20 dB, and a distance of 2 meters. Calculated and measured maximum efficiencies agreed well for the rectifier circuits at an input power of -5 dBm to 0 dBm.

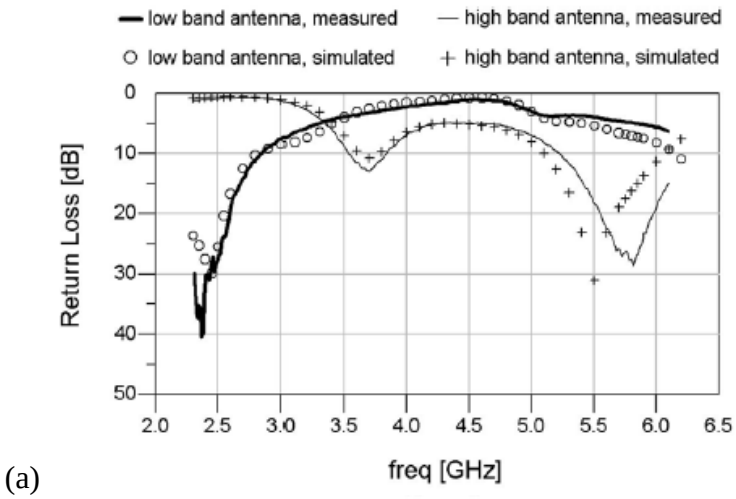

(a)

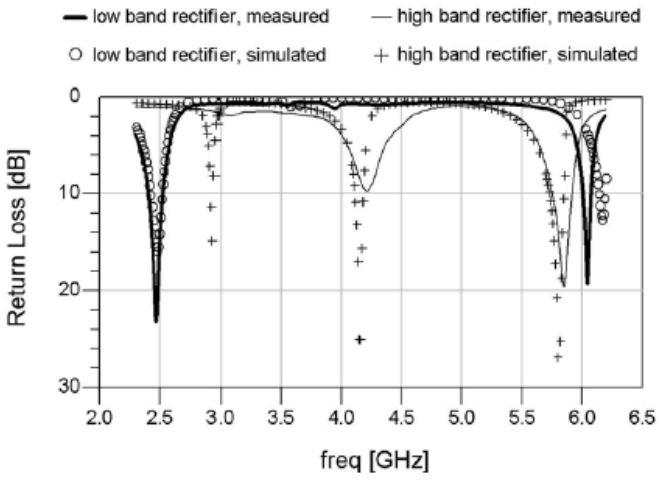

(b)

Figure 2.22: Return loss for (a) antenna and (b) rectifier [8].

Authors in [9] used a device called PowerCast™ and studied various parameters related to the feasibility of harvesting energy from ambient RF power to energize wireless sensor nodes. In this papers three different parameters are studied. The first is the study of the ambient RF power along several frequency bands. The survey of the RF power spectrum was done at six different locations inside the King Fahd University campus using a GW INSTEK spectrum analyzer. Table 2.1 shows several results from this survey.

Table 2.1: Ambient RF power survey for several different frequencies [9].

Peak No	Peak Freq. (MHz)	Peak Power (dBm)
1	952	-37
2	939.5998	-39
3	922.24	-43.9
4	177	-42.7
5	178	-42.7
6	179	-42.7
7	181	-42.9
8	183	-43.2
9	184	-43.4

The PowerCast™ can only harvest power greater than -10 dBm therefore it is determined from the data in Table 2.1 that none of the frequencies surveyed in this paper were in the power range of the PowerCast™. It is concluded that the PowerCast™ is not capable of harvesting ambient RF energy.

For the rest of the study a 915 MHz 3W transmitter with 60˚ directional antenna, a 915 MHz directional Patch antenna and a 915 MHz omnidirectional dipole antenna were used to harvest the required RF energy. Testing was performed in two different areas: outdoor free-field

and indoor reverberant environment. The outdoor experiment was performed on the football field of King Fahd University and the indoor experiment was done in a room with dimensions 40ftx25ftx8.5ft. Both indoor and outdoor experiments were conducted along the same radial lines to be able to compare the two. The results of this study showed that charging time, $T_{C,}$ of the harvester and the RSSI (signal strength) followed a regular trend in the outdoor experiments as compared to irregular trends inside the room with reflective walls. In figure 2.23 the signal strength versus the radial distance from the antenna is shown for both the outdoor (a) and indoor (b) experiments.

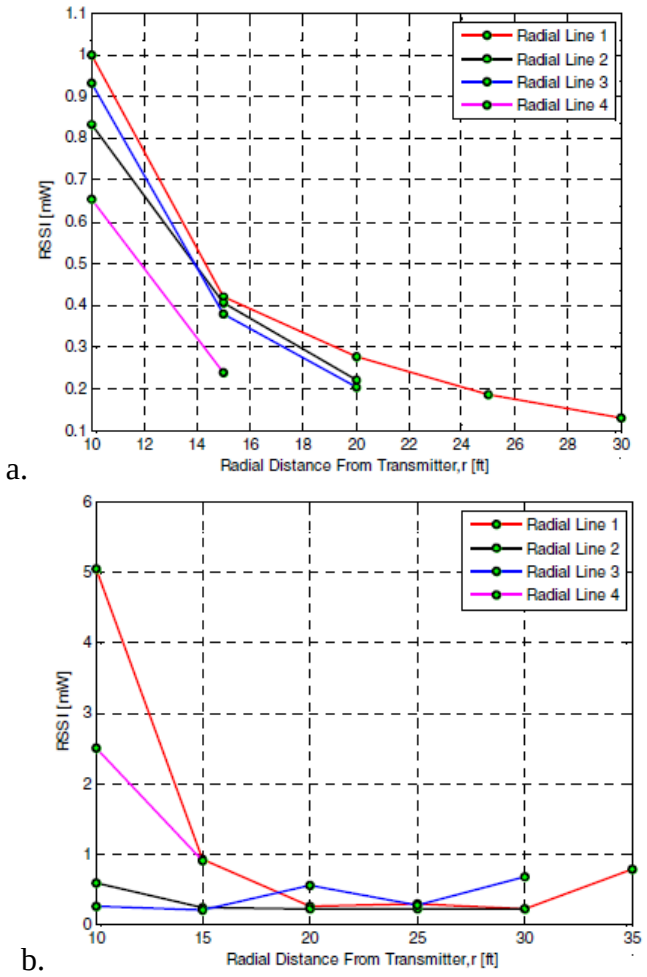

Figure 2.23: RSSI versus radial distance for both outdoor (a) and indoor (b) experiments [9].

2.3 Integration of the rectenna with a solar cell

In this work, our goal is to place the rectenna on a solar cell to make a multi-source energy harvesting device. Authors in [10] were able to integrate a meshed patch antenna onto a solar cell. In this study the glass of the solar cell was used as the substrate for the antenna. The layout for this antenna is seen in figure 2.24. A patch antenna of this design is used because of the large percentage of see-through area.

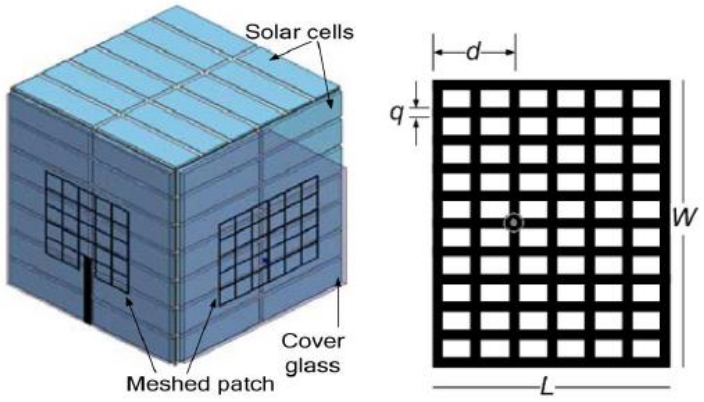

Figure 2.24: Patch antenna design integrated on solar cell cube [10].

The configuration of the antenna on the solar cell starts with the antenna being printed on top of the solar cell cover glass. Underneath this glass is a layer of photovoltaic cells. The effect of conductivity on the antenna was studied by modeling the solar cell layer as silicon. The conductivity was then continuously increased (from 0 to 100 S/m) to evaluate the performance of the antenna integrated on a substrate on top of the silicon layer (ε_r = 11.9). The silicon layer was backed with a perfect electric conductor and the thickness of the solar cell is 0.16 mm. It was found that when the conductivity was from 0 to 1 S/m the results were equivalent to reducing the total thickness of the substrate. Any value above 1 S/m did not show significant change.

Two antennas were fabricated in this study. One was printed with conductive ink on a polyethylene terephthalate glycol thermoplastic sheet and the second was fabricated from

electroformed meshed conductor. Both antennas were then integrated onto a plastic substrate with a relative permittivity of 2.4 at 1 MHz and a thickness of 0.762 mm. They were then attached to the top of the solar cell. To verify the efficiency of the meshed antenna to the solar cell, a solid patch antenna was made from the same conductive ink.

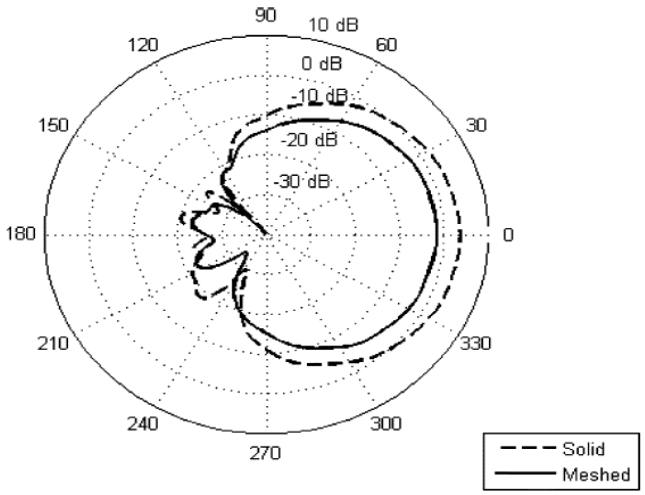

Figure 2.25: Radiation pattern for the meshed and solid antenna design [10].

The radiation pattern for both the antenna integrated on the solar cell and the solid patch antenna can be seen in figure 2.25. It is shown that both antennas possess the same radiation pattern shape and only a small change in directivity (8.6 dB for the solid antenna and 8.4 dB for the meshed antenna. As a result of this study it was found that it is feasible to design an antenna integrated to a solar cell and maintain proper functioning of the solar cell if the transparency of the antenna is greater than 90%. The radiation patter is not greatly affected when the antenna is meshed with the solar cell cover.

Another study of implementing an antenna to a solar cell by the authors in [11] was done with a transparent antenna. The patch antenna (see figure 2.26) in this paper was constructed with a thin sheet of clear polyester with a conductive coating. The covering for this antenna has a minimum visible light transmission of 7% and a sheet resistivity of 4.5 Ω/sq.

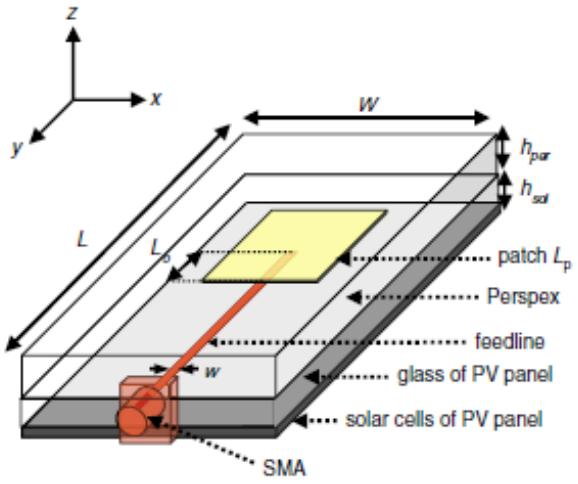

Figure 2.26: Proposed transparent antenna design [11].

The antenna is coupled to a copper microstrip line, which is sandwiched between Perspex glass and a solar cell glass layer. The Perspex glass has an ε_r of 2.6, tan δ of 0.015 and has an overall visible light transmission of 92%.

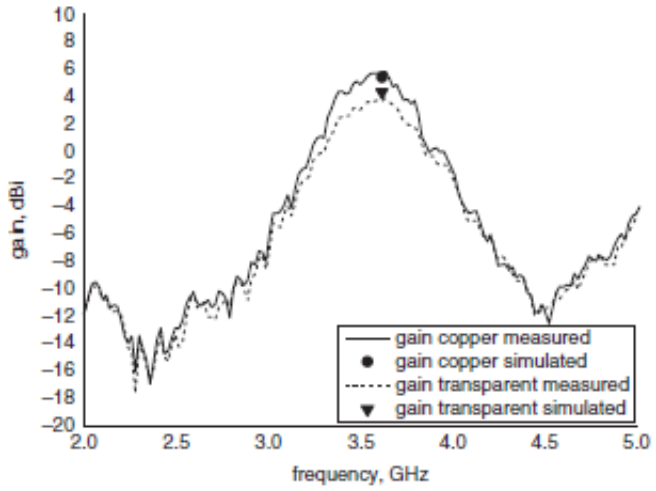

Figure 2.27: Gain measured and simulated results for transparent and copper antennas [11].

The gain results for this antenna are seen in figure 2.27. For the transparent antenna the measured gain was greater than 2.5 dBi for the frequencies 3.4 – 3.8 GHz with a peak of 3.96 dBi. For the copper antenna the measured gain was greater than 3.4 dBi across frequency range with a peak

of 5.81 dBi. The difference in gain values between the two antennas was 1.85 dB. In this paper it was shown that transparent antenna for solar panel integration is feasible and the measured gain is appropriate for wireless communications and sensor networks.

It is observed in this chapter that the study of harvesting energy from ambient RF signals has been an important study over the last several years. Using the literature discussed above, this thesis will design and fabricate an original broadband antenna and discuss how it affects and is affected by the integration of a solar cell.

Chapter Three

Frequency Analysis and Antenna Design

In this chapter we discuss the results of the measurements taken with our PXA spectrum analyzer and how they were used to determine the rectenna bandwidth and ultimately the antenna design. We start with a brief introduction to the hardware used to measure the RF spectrum and where the data was gathered. A discussion of the results will be an introduction to why the specific antenna design was chosen for this thesis.

3.1 PXA Spectrum Analyzer

The first thing to look at when building a rectenna was what kind of RF power will be received from the frequency spectrum. In order to do this Agilent's PXA Spectrum Analyzer (figure 3.1) was used. When working in real-time, this spectrum analyzer can detect intermittent signals with duration as short as 3.57 µs.

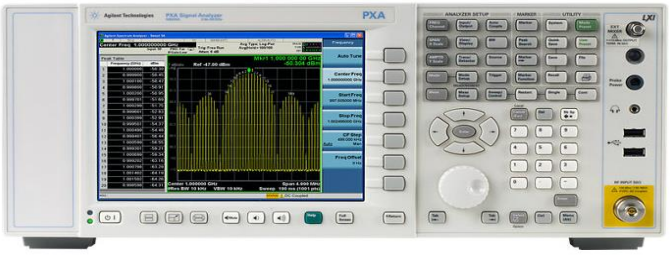

Figure 3.1: Photograph of Agilent's PXA spectrum analyzer

The spectrum analyzer used in this thesis is known as a swept analyzer. The way this type of analyzer works is it sweeps across the input frequency range and displays all the amplitudes found in that range.

3.2 Spectrum Analyzer Measurements: University of New Mexico

For this particular study, the PXA spectrum analyzer was placed in different areas around the Electrical Engineering department at the University of New Mexico and a building, Cosmiac, located near the airport. The purpose of these measurements was to be able to locate the different frequencies where the greatest power density levels are observed. The antenna used for these measurements was a horn antenna with a radiating bandwidth of 700 MHz to 18 GHz and a linear polarization. The setup of for these measurements is seen in figure 3.2.

Figure 3.2: Setup for spectrum analyzer measurements.

The first set of measurements was taken on the second floor of the ECE building located on the UNM campus, as seen in figure 3.3. The horn was facing west and the polarization was tested for both horizontal and vertical. The highest power levels observed for horizontal polarization are listed in table 3.1 and the vertical polarization power levels are in table 3.2.

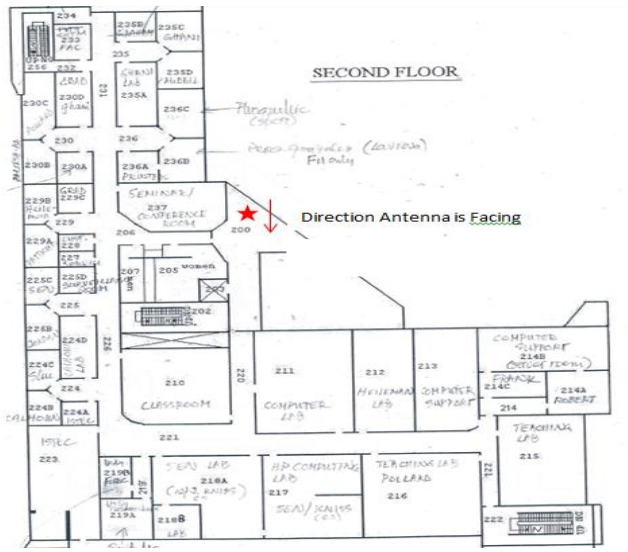

Figure 3.3: Location of antenna and spectrum analyzer for first set of measurements.

Table 3.1: Highest power levels for horizontal polarization (inside).

Frequency	Power
2.154 GHz	-36.88dBm
1.932 GHz	-42.8167dBm
2.1480 GHz	-43.8092dBm
1.9380 GHz	-50.0708dBm
2.1420 GHz	-50.8633dBm

Table 3.2: Highest power levels for vertical polarization (inside).

Frequency	Power
1.932GHz	-33.2139dBm
2.154GHz	-33.6547dBm
2.148GHz	-39.1949dBm
1.938GHz	-42.7059dBm
2.142GHz	-44.7395dBm

The measured spectrum for this location is seen in figure 3.4. The frequency that provides the most power for horizontal polarization occurs at 2.154 GHz and the power received is -36.88 dB. The greatest power received for vertical polarization is at 1.932 GHz and is - 33.2139 dBm. For both horizontal and vertical polarization it was found that the highest power levels lie between 1.5 GHz and 2.5 GHz.

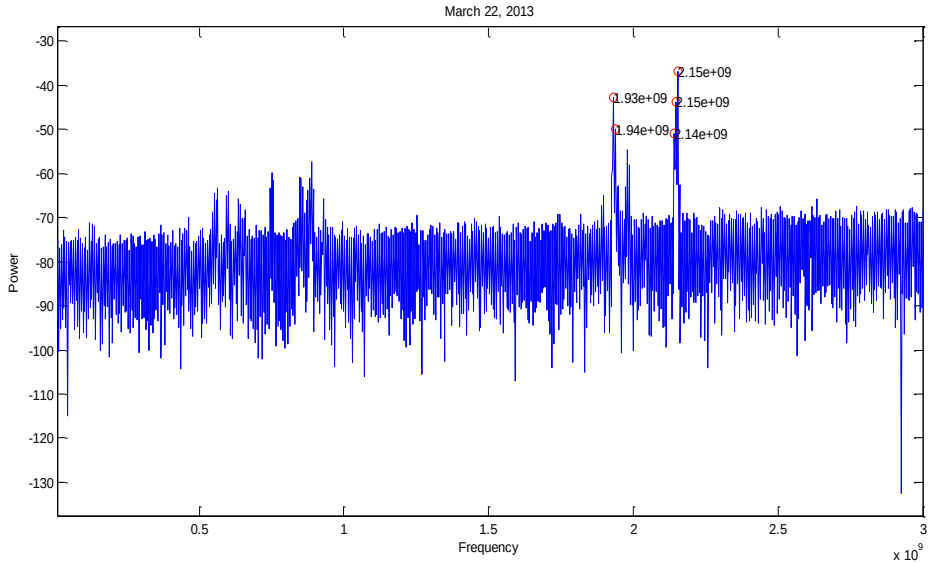

a.

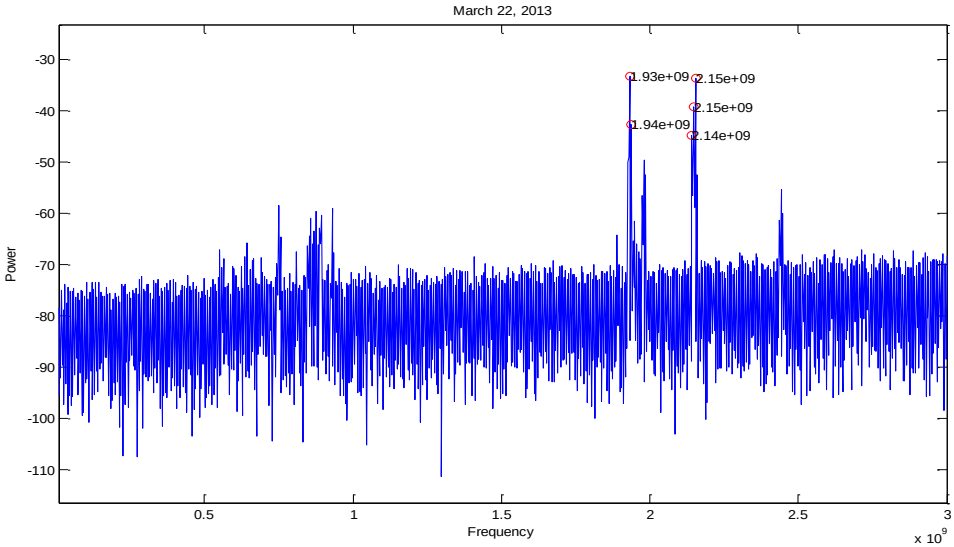

b.

Figure 3.4: Spectrum for first testing site. (a) Horizontal polarization (b) Vertical polarization

The next set of measurements was taken outside of the ECE building at UNM. The spectrum analyzer was set up on the southeast side of the building with the antenna pointing east. The location of the setup can be viewed in figure 3.5. The highest power levels observed for horizontal polarization are listed in table 3.3 and the vertical polarization power levels are in table 3.4.

Figure 3.5: Outdoor set up of the spectrum analyzer

Table 3.3: Highest Power Levels for Horizontal Polarization (outside)

Frequency	Power
2.154GHz	-23.8913dBm
2.148GHz	-27.8514dBm
1.932GHz	-28.9841dBm
2.142GHz	-31.0897dBm
2.151GHz	-36.3211dBm

Table 3.4: Highest Power Levels for Horizontal Polarization (outside)

Frequency	Power
2.148GHz	-28.368dBm
2.154GHz	-29.6341dBm
1.932GHz	-36.0961dBm
2.142GHz	-39.4297dBm
2.145GHz	-43.7875dBm

The results for both the horizontal and vertical polarizations are shown in figure 3.6. These plots show that the peak for horizontal polarization occurs around 2.154 GHz and is -23.8913 dBm. The peak for vertical polarization also occurs around 2.148 GHz and is -28.2680 dBm.

a.

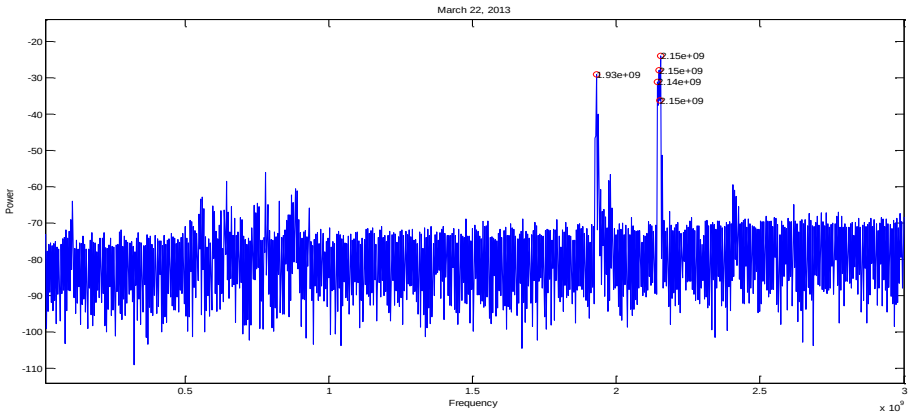

b.

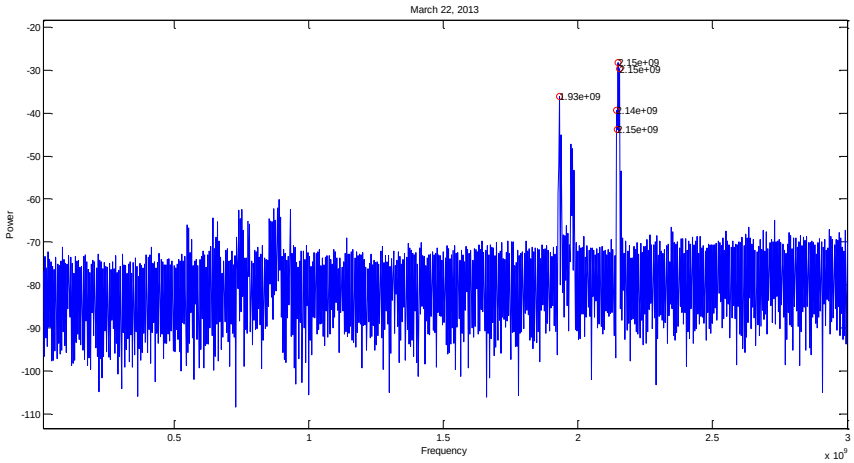

Figure 3.6: Outdoor measurements using the PXA spectrum analyzer

As in the previous test, the greatest power received in both cases occurs between 1.5 GHz and 2.5 GHz. In reviewing the measurements between the indoor and outdoor setups, it is clear that more power is received when the measurements are recorded outdoors. For horizontal polarization a difference of 12.9887 dB is seen and with vertical polarization there is a difference of 4.9459 dBm.

To get a more accurate representation of the ambient RF power available it was necessary to keep the spectrum analyzer in one place and take measurements throughout the day. For the next measurement set, the spectrum analyzer was set up in an office in the ECE building and the RF power was tracked at different time points. The location of this set up is seen in figure 3.7.

Figure 3.7: Location for the third set of measurements.

These measurements were taken using the same horn antenna as in the previous measurement set and the polarization was horizontal. The measurements were taken throughout the day on March 23, 2013. The highest power and corresponding frequency can be seen in table 3.5 and the spectrum throughout the day in shown in figure 3.8.

Table 3.5: Highest power received at different times throughout the day and the corresponding frequencies.

Date and time	Frequency	Power
March 23, 2013 8:52am	2.14 GHz	-17.6363 dBm
March 23, 2013 9:52am	2.14 GHz	-24.4493 dBm
March 23, 2013 10:52am	2.14 GHz	-25.0163 dBm
March 23, 2013 12:17pm	2.14 GHz	-18.1019 dBm
March 23, 2013 1:32pm	2.14 GHz	-24.1978 dBm
March 23, 2013 3:47pm	2.15 GHz	-22.4271 dBm
March 23, 2013 7:02pm	2.15 GHz	-22.7975 dBm
March 23, 2013 9:32pm	2.14 GHz	-16.644 dBm

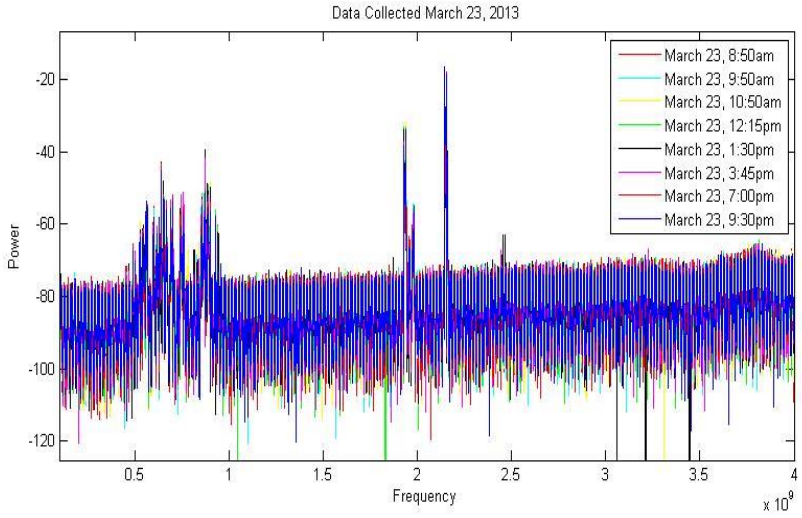

Figure 3.8: Power spectrum from data collected on March 23, 2013.

Throughout the day the frequencies with the most power remain fairly consistent. The average of the frequencies producing the highest power level is 2.1425 GHz and the average high power level over the eight time points is -21.4088 dBm. At 9:32 pm the highest power level was -16.644 dBm received at 2.14 GHz

3.3 Spectrum Analyzer Measurements - Cosmiac: Center for Configurable Space Microsystems Innovations and Applications Center

After reviewing this data it was decided to take the spectrum analyzer to another location to see if the results vary. The location of this building is seen in figure 3.9. The Cosmiac location is close to the airport and was chosen to see what kind of power could be observed from the corresponding airport frequencies.

Figure 3.9: Overhead photograph of the Cosmiac facility.

The setup for the spectrum analyzer was tested and the optimal location for the antenna was found. Since the rectenna being designed for this thesis is meant to be integrated with a solar cell, it is important to focus on the power density at times when the solar energy will not be available. For this reason the emphasis of the measurements at this location are in the evening. Table 3.6 shows the highest power level and corresponding frequency for different times collected from June 20-21, 2013. The spectrum for these measurements is seen in figure 3.10.

Table 3.6: Highest power and corresponding frequency collected the evening of June 20, 2013

Date and Time	Frequency	Power
June 20, 2013 5:00pm	752.8 MHz	-42.2238 dBm
June 20, 2013 9:00pm	2.1454 GHz	-37.7045 dBm
June 20, 2013 10:00pm	1.980 GHz	-40.1043 dBm
June 20, 2013 11:00pm	2.1454 GHz	-39.1844 dBm
June 21, 2013 12:00am	2.1520 GHz	-42.0462 dBm
June 21, 2013 8:00am	1.9804 GHz	-40.3858 dBm

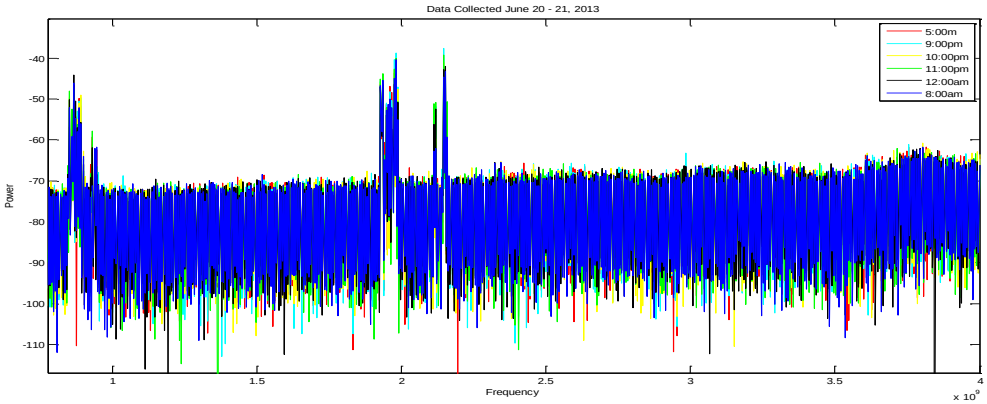

Figure 3.10: Spectrum for power vs. frequency collected on the evening of June 20, 2013.

A majority of power is concentrated between the frequencies of 1.5 GHz and 2.5 GHz. A higher power spike is noticed around 700-800 MHz as well. The average frequency for the high power levels is 1.8593 GHz and average power is -40.27 dBm. The highest power level recorded occurred on June 20, 2013 at 9:00 pm with a frequency of 2.1454 GHz. The highest power level

at this location is -37.7045 dBm, which about a 21 dBm difference between locations; with UNM having a higher power level.

Another set of measurements were taken from June 24, 2013 at 4:00 pm until June 25, 2013 at 11:45 am to compare to those taken on the 20th of June. The highest power and corresponding frequencies for these measurements are seen in Table 3.7.

Table 3.7: Highest power level and corresponding frequency recorded on June 24-25.

Date and Time	Frequency	Power Level
June 24, 2013 4:00pm	1.9804 GHz	-43.1605 dBm
June 24, 2013 6:00pm	1.9804 GHz	-44.8221 dBm
June 24, 2013 8:30pm	2.1454 GHz	-39.8317 dBm
June 24, 2013 9:30pm	1.9540 GHz	-43.6726 dBm
June 24, 2013 10:30pm	1.9738 GHz	-42.6522 dBm
June 24, 2013 11:30pm	2.1124 GHz	-40.9595 dBm
June 25, 2013 9:15 am	2.1454 GHz	-42.9010 dBm
June 25, 2013 11:45 am	2.1520 GHz	-40.0116 dBm

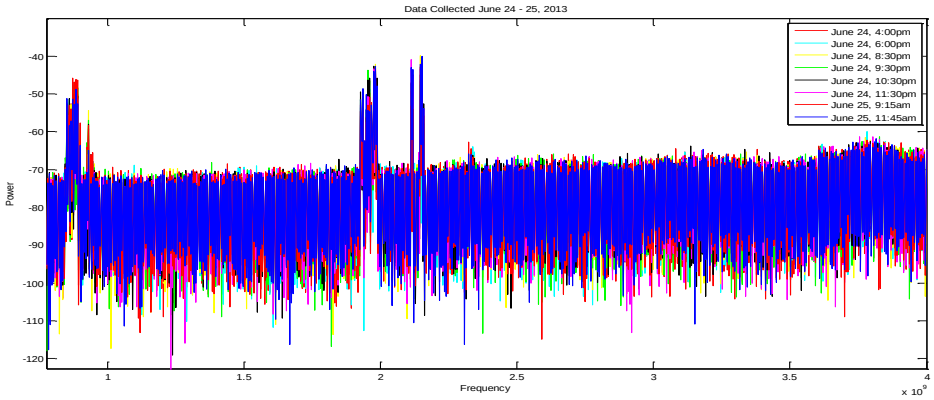

Figure 3.11: Spectrum for measurements collected on June 24-25.

The above plot shows the spectrum of power versus frequency for the collected data. As in the other data sets, the frequencies with the most power remain fairly constant throughout the different time points. The highest power level is seen on June 24, 2013 at 8:30 pm with a frequency of 2.1454 GHz and power level of -39.8317 dBm. Some measurements were taken the morning and afternoon of the 25th to ensure that the power level was not drastically changing

during the evening hours as compared to the daytime. The average frequency for the peak power level is 2.055 GHz and the average power level is -42.25 dB.

The data from both locations was reviewed and plotted to view the range where the highest power density level was received. In the following figure one can see that a bulk of the power was within the 1.5 – 2.5 GHz range.

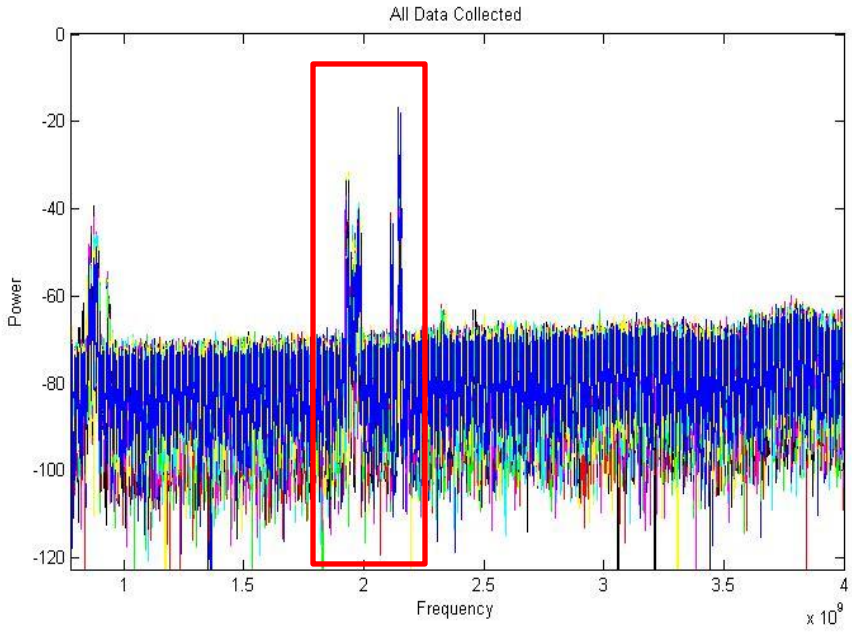

Figure 3.12: Plotted spectrum for all frequency data to highlight desired bandwidth

It was decided that this frequency range would be the ideal bandwidth design for the rectenna.

3.4 Patch Antenna – 2.2 GHz

The goal for the rectenna design in this project is to fabricate a model that will collect ambient RF energy in the frequency ranges where the highest power is observed. In order to do this, the antenna must be broadband. A broadband rectifying circuit, however, can be fairly tricky to design. As a starting point, the modeling of a simpler narrowband rectenna was done to

better understand the rectifying characteristics before building a more complex broadband model. For the simple design, a patch antenna radiating at 2.2 GHz was chosen.

The patch antenna design has become very popular due to its low profile, low cost, and easy fabrication. The antenna constructed for this project is a patch antenna fed by a microstrip transmission line. The patch antenna, microstrip line and ground plane are made up of copper which is a high conductivity material. A model of this antenna is seen in figure 3.13.

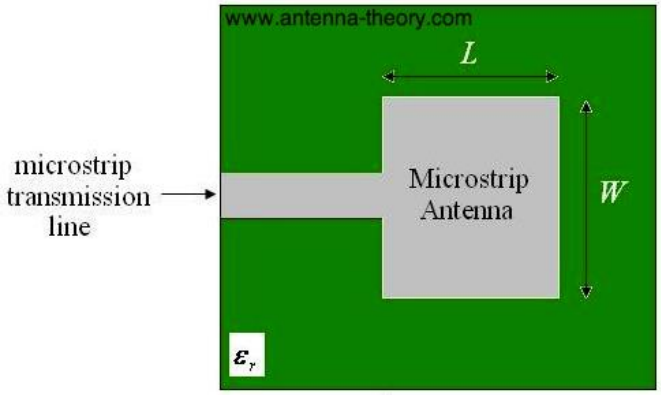

Figure 3.13: Layout for a microstrip antenna [12].

The patch is represented by the length (L) and the width (W) and is set on a specified substrate that has a certain thickness (h) and permittivity (ε_r). The frequency in which the patch antenna is able to operate is determined by the length of the patch and the permittivity of the substrate. The equation for resonating frequency, f_r, is seen below

$$f_r = \frac{1}{2L\sqrt{\epsilon_o}\sqrt{\mu_o\epsilon_o}} \quad [13] \tag{27}$$

The substrate used for this patch antenna is Rogers 5880. This substrate has a relative permittivity is 2.2 and the thickness is 1.6 mm. The desired frequency for this design is 2.2 GHz. By using the equations below the length and width for the patch antenna were calculated.

$$W = \frac{1}{2f_r\sqrt{\mu_o\epsilon_o}}\sqrt{\frac{2}{\epsilon_r + 1}} \tag{28}$$

$$L = \frac{1}{2f_r\sqrt{\epsilon_{reff}}\sqrt{\mu_o\epsilon_o}} - 2\Delta L \quad [13] \tag{29}$$

In the second equation, ΔL is the length required for effective dielectric constant. This length can be found using the following equation [13]:

$$\frac{\Delta L}{h} = 0.412\frac{(\epsilon_{eff}+0.3)(\frac{W}{h}+0.264)}{(\epsilon_{eff}-0.258)(\frac{W}{h}+0.8)} \quad [13] \tag{30}$$

The design and simulation for the patch antenna used in this project was done in Ansoft's HFSS program. The resonating frequency was set for 2.2 GHz with an inset transmission line designed to have an output impedance of 50 Ω. The length of the designed patch is 4.52 cm and the width is 5.39 cm. The transmission line has a length of 4.154 cm, a width of 0.485 cm, and is inset by 1.381 cm. Figure 3.14 shows the model for this antenna.

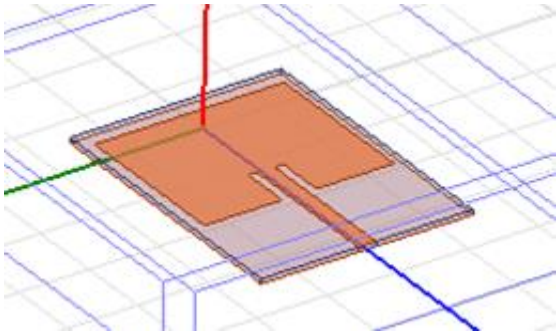

Figure 3.14: 2.2GHz patch antenna model.

Using HFSS this design was simulated to view different performance characteristics. The simulation results for this antenna are seen in figure 3.15 (a-f). Figure 3.15 (a) shows the return loss for the antenna. The return loss has a power level of -26.0967 dBm at 2.2 GHz. It is seen in this plot that the bandwidth is very narrow. Figure 3.15 (b-c) shows the gain for the patch. The image for (b) is a 3-D model for the gain. The maximum gain is in red and the peak occurs at 7.3655 dB. For (c) the 2-D gain image is seen where theta and the gain are the X and Y axis respectively, and two lines represent the gain for phi equal to zero degree (red) and 90 degrees

(black). The radiation patter for the gain is observed in figure 3.15(d) and (e) for both phi and theta respectively. The radiation pattern shows angular dependence of the strength of the electromagnetic field produced by the antenna.

a.

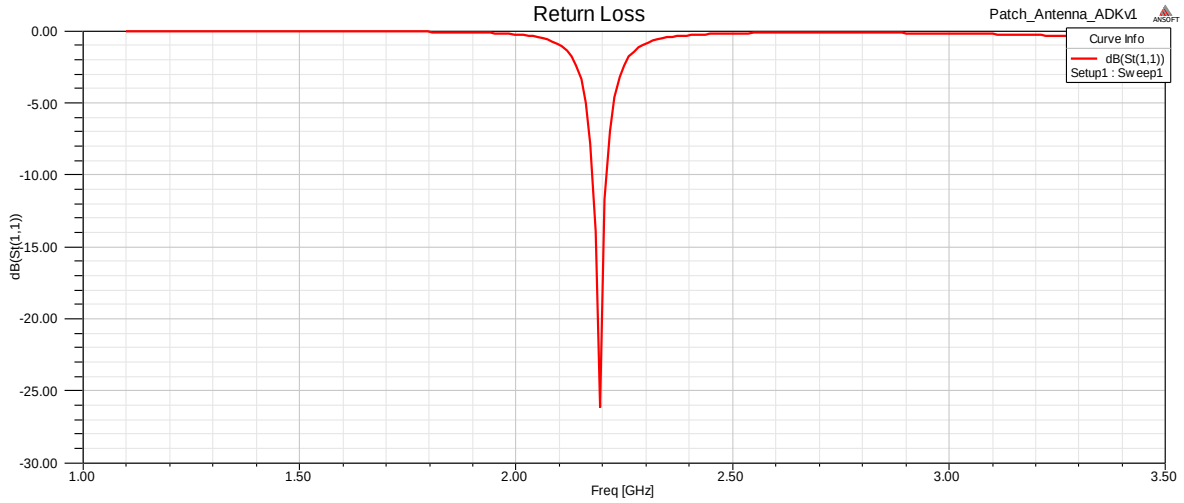

b.

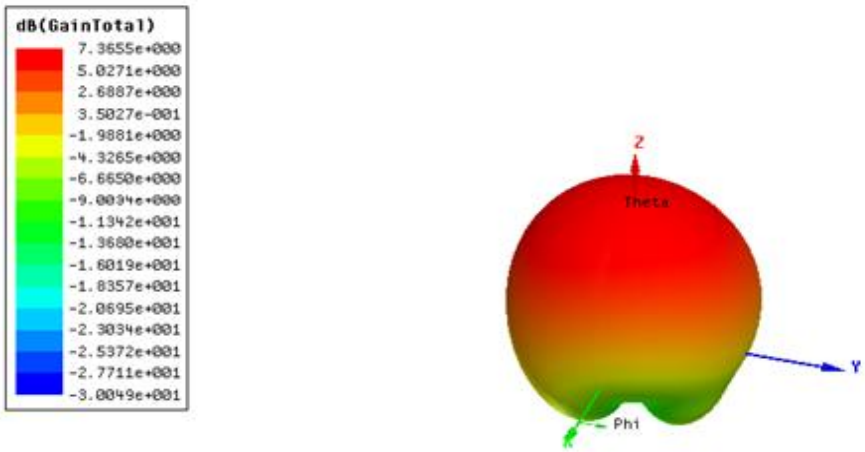

c.

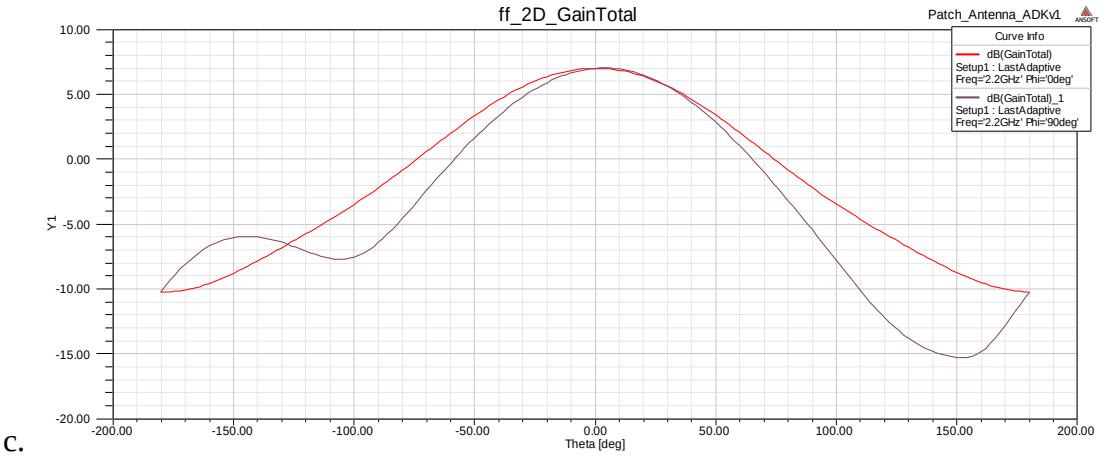

d.

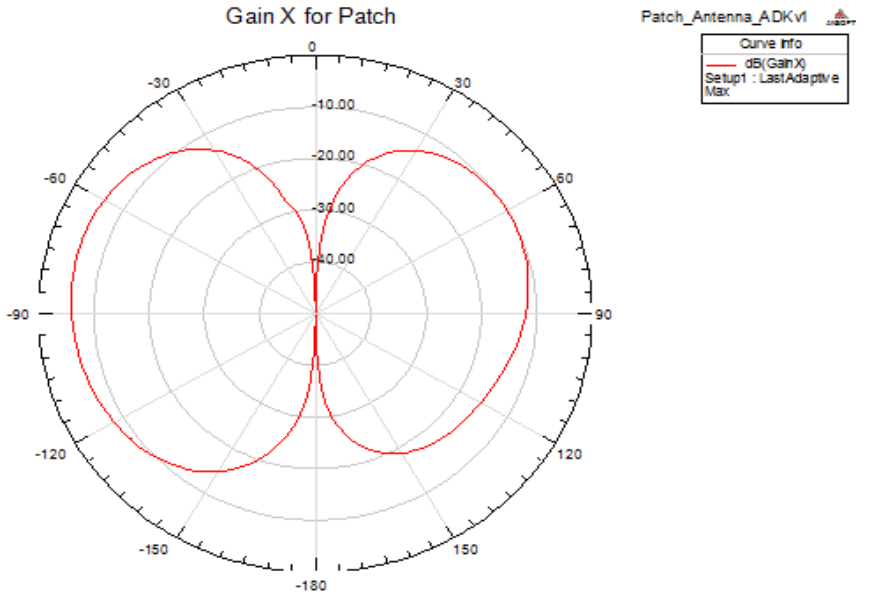

e.

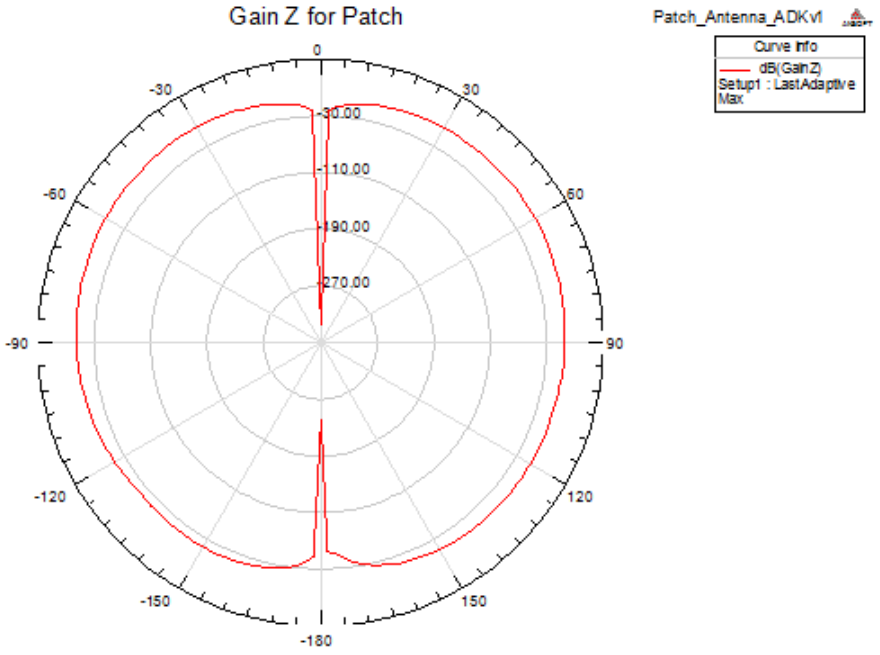

Figure 3.15: Simulation results for 2.2 GHz Patch antenna (a) return loss (b)3-D gain (c)2-D gain (d) gain radiation pattern as a function of phi (e) gain radiation pattern as a function of theta

The fabricated image of this antenna is shown in figure 3.16.

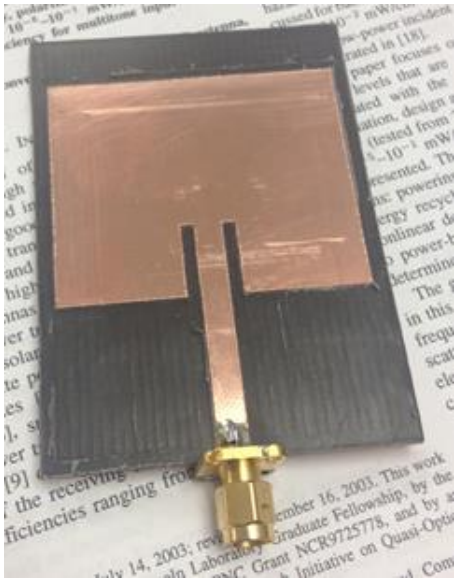

Figure 3.16: Fabricated 2.2GHz patch antenna.

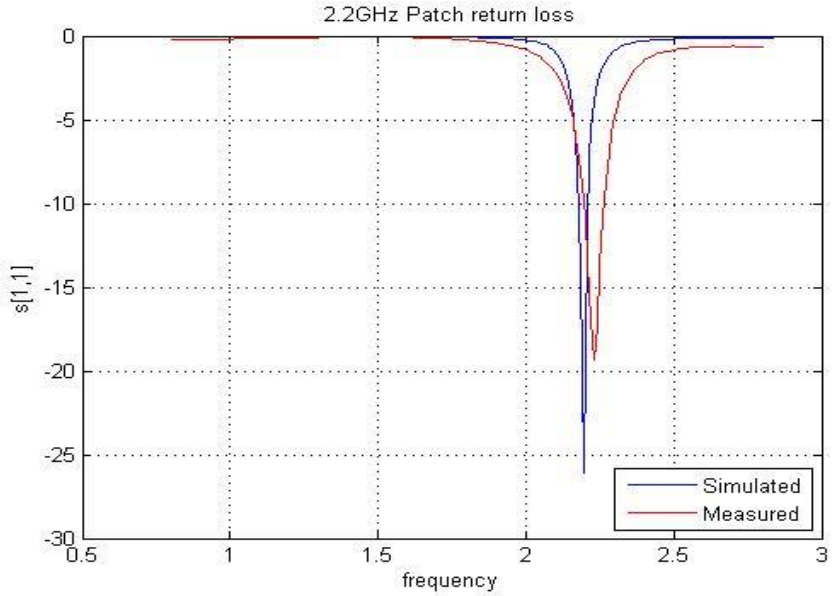

Figure 3.17: Measured S_{11} parameters for the fabricated patch antenna.

In the above figure, the return loss of both the simulated antenna and fabricated antnna is shown. The simulated plot has a resonant frequency viewed at -26.0967 dBm that occurs at 2.1945 GHz and the measured plot has an f_r of -19.3710 dBm occurring at 2.22 GHz. With the patch antenna working and radiating around 2.2 GHz, it was time to design and fabricate the rectifying circuit.

3.5 Narrowband Rectifying Circuit

A rectifier is a device that converts an alternating current (AC) to a direct current (DC). The rectifying circuit for this device was designed using Agilent's ADS software. Since the return loss for the fabricated patch antenna was measured at 2.22 GHz, this frequency was used to model the rectifying circuit as well. The design consists of a matching network, a Schottky diode, a DC filter and a resistive load. The substrate used for this circuit is Rogers 5880.

To construct the matching network the input impedance of 1.042+j62.055 Ohms to the diode was found. Then, using the Smith Chart utility in ADS, the matching network was designed to connect the 50 Ω impedance from the antenna to the input impedance of the diode. The matching is shown in figure 3.18.

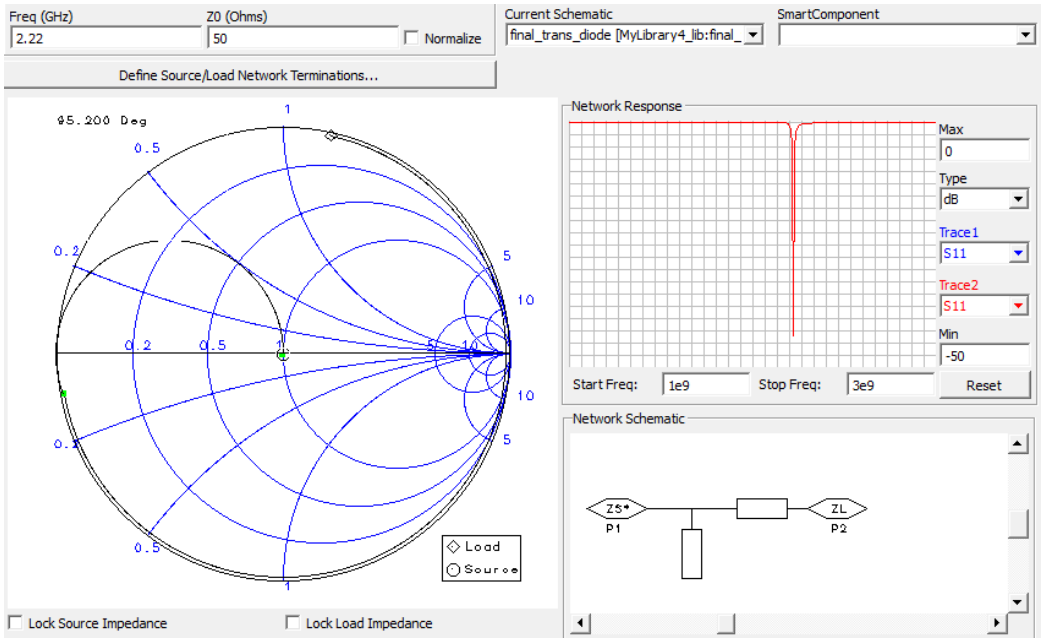

Figure 3.18: Matching for 2.22 GHz from 50 Ω to the input impedance of the diode.

Matching between the 50 Ω impedance from the antenna to the diode uses a shunt transmission line followed by a series transmission line. The shunt transmission line has a length of 26.0102 mm and the series transmission line has a length of 33.7956 mm. The transmission line width for the network is 4.879560 mm. After the matching network, an RF choke is put in place. For this,

an inductor with the value 1 nH is used. Following the inductor is the Schottky diode. A Schottky diode is used in rectifying circuits because it has a low forward voltage drop and fast switching action. The diode used for this model is SKYWORKS® SMS7630-079 (figure 3.20). This diode was used for its zero bias characteristics and its ability to perform for frequencies up to 24 GHz.

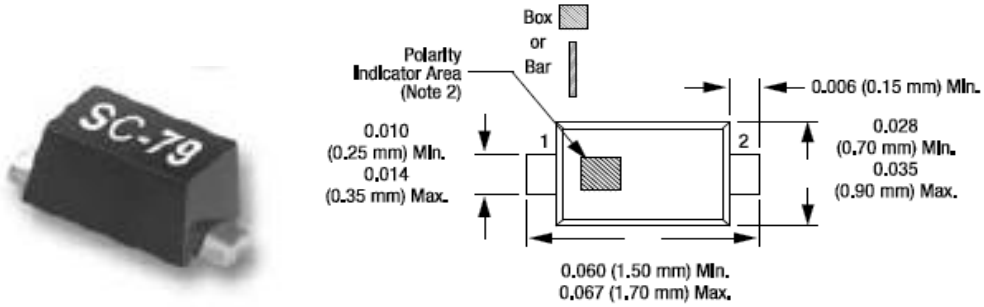

Figure 3.19: A picture of a SKYWORKS SMS7630-079 and its layout.

Following the diode there is a filter capacitor and a resistor load. The capacitor value is 1 µF and the resistor is 100 kΩ. The layout of this circuit is seen in figure 3.20. The inductor, capacitor and resistor are grounded using a via ground.

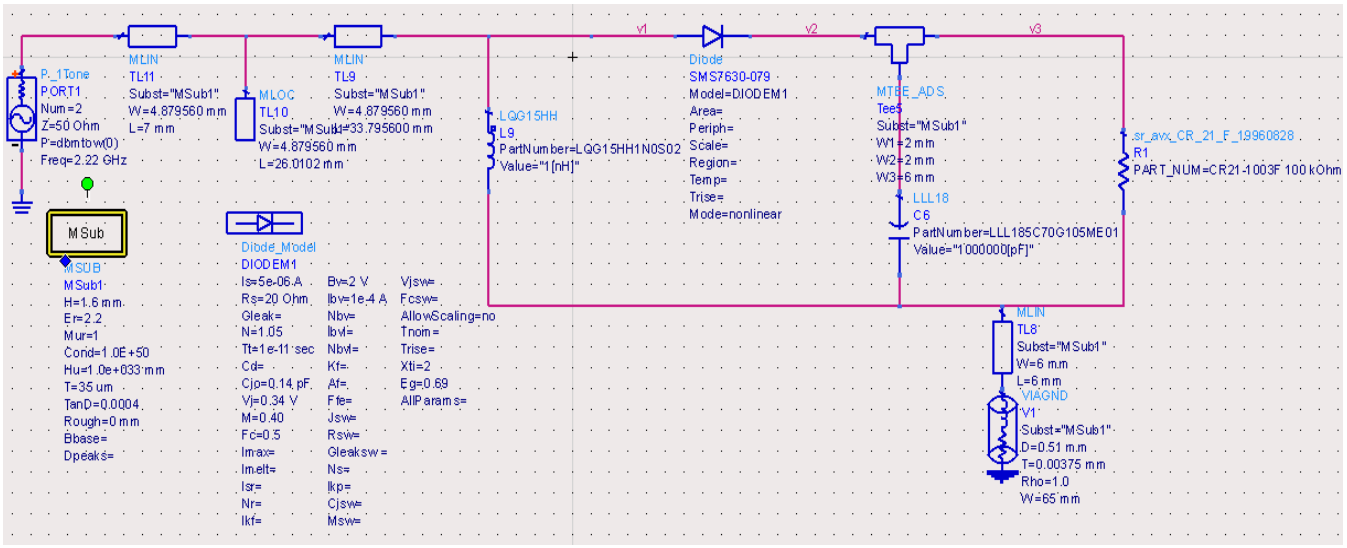

Figure 3.20: ADS circuit layout.

The S_{11} parameters were simulated and a harmonic balance was performed for this design. These results are seen in figures 3.21 and 3.22. The reflection occurs at 2.22 GHz and has a power level of -26.646 dBm. Also, using a harmonic balance simulation with this circuit design, the presence of a DC voltage is verified. A DC current means that there are no oscillations which is why the DC power can be measured at 0 GHz. At 0 GHz the power is 5.694 dBm.

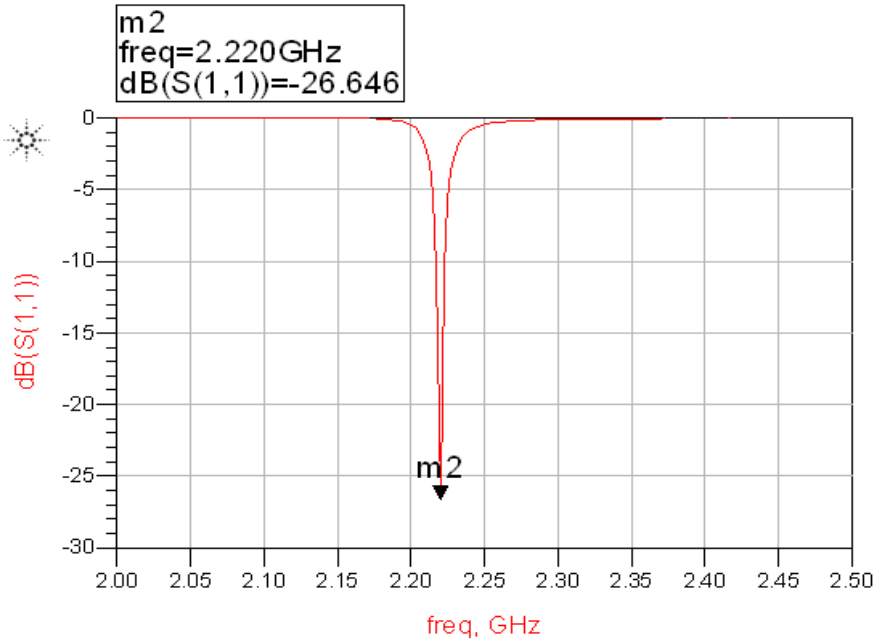

Figure 3.21: Simulated S_{11} parameters for the rectifying circuit.

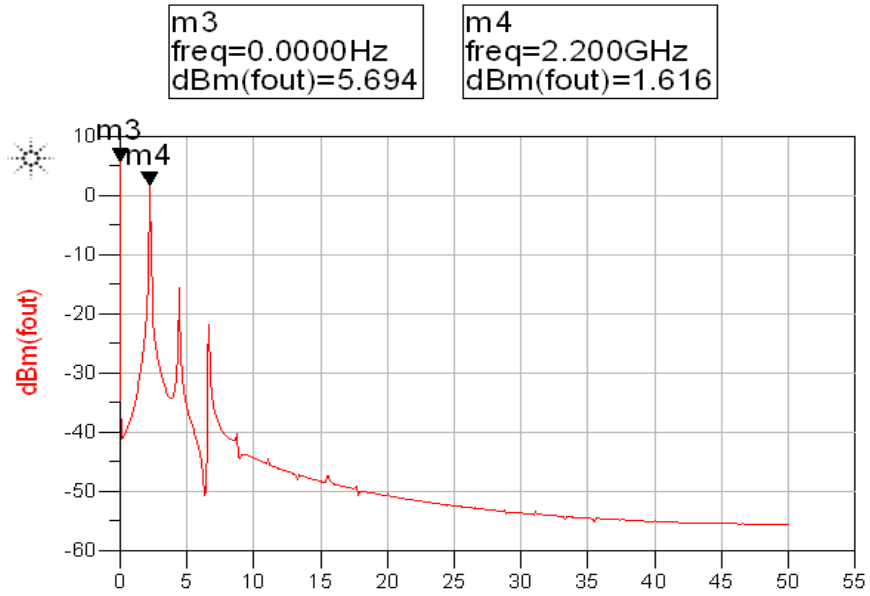

Figure 3.22: Simulated harmonic balance for the rectifying circuit.

The layout for this circuit was constructed in the ADS (figure 3.23) and exported for fabrication. The fabricated image of this circuit is seen in figure 3.24.

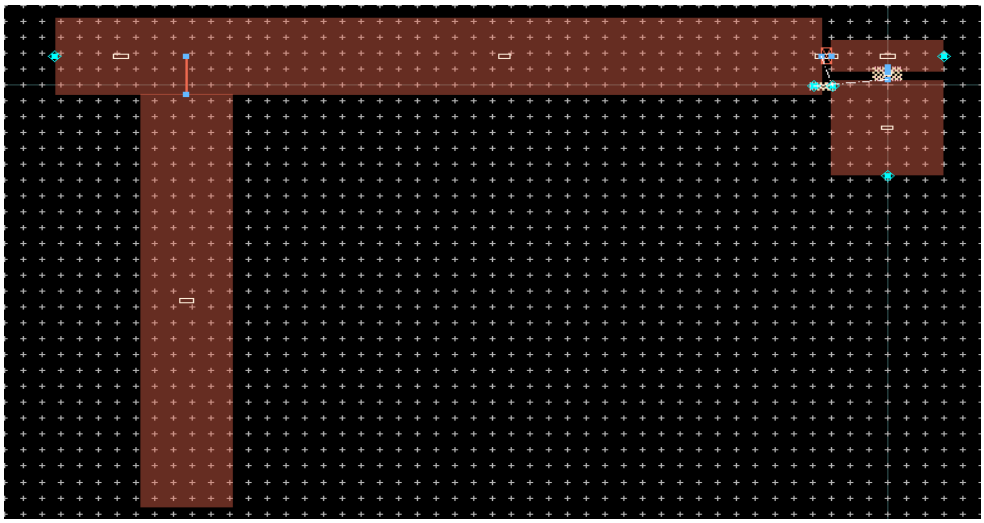

Figure 3.23: ADS layout of the rectifying circuit.

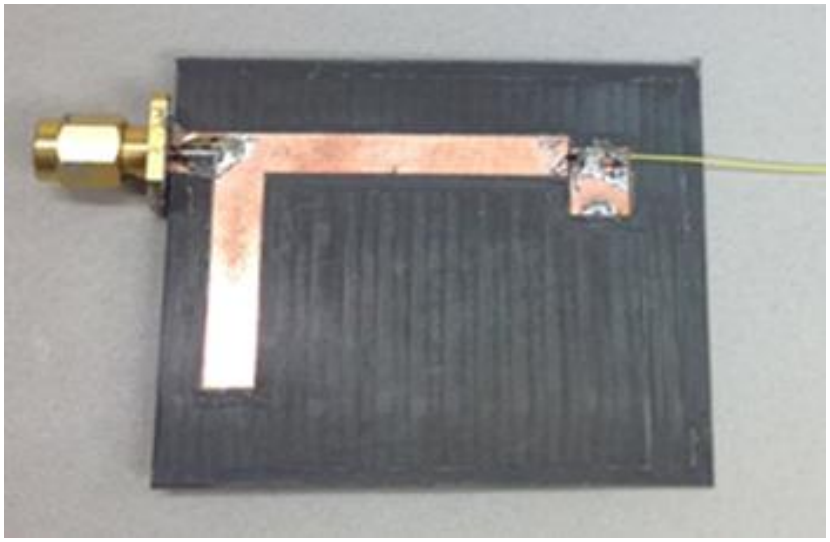

Figure 3.24: Photograph of the fabricated rectifying circuit,

After fabrication, the return loss was measured for the rectifying ciruit. In fiure 3.25, both the simulated and measured S_{11} are plotted with respect to frequency. The resonant frequency for the simulated circuit is at 2.22 GHz with -26.646 dBm power and for the measured circuit a resonant frequency of 2.24 GHz at -29.4130 dBm is observed.

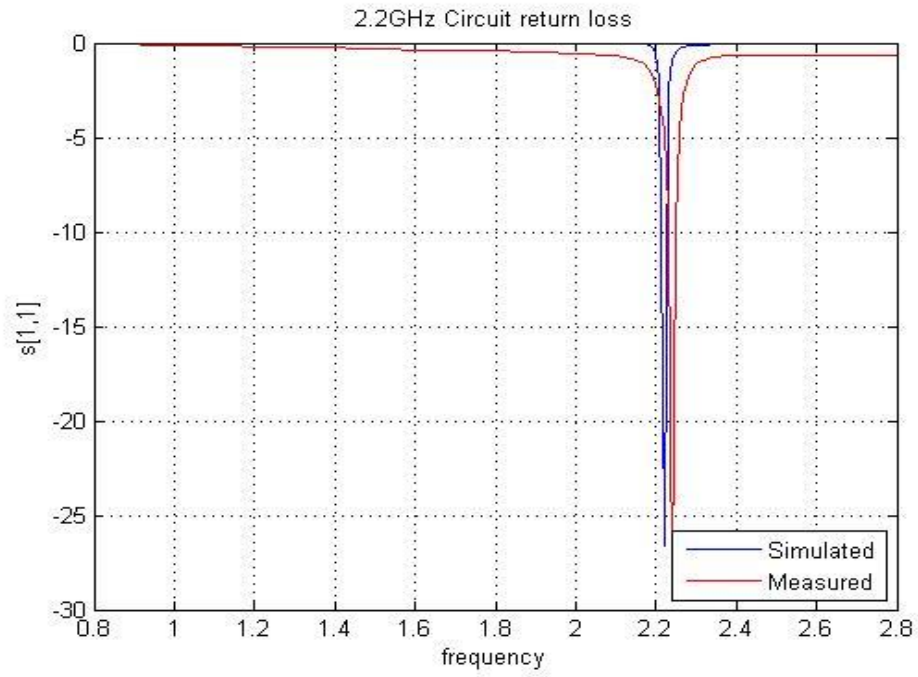

Figure 3.25: Measured S_{11} parameters versus the simulated S_{11} parameters for the rectifying circuit

To measure the DC voltage being produced by the circuit a synthesized sweeper (HP 83752b Sweeper) is attached and set to produce a 2.22 GHz frequency with the power level ranging from -10 dBm to 18 dBm. To start these measurements the losses coming from the cable that the circuit attaches too are recorded in order to ensure an accurate calculation of the conversion efficiency. The loss from the cable was measured to be about -1.5 dBm. The source power and measured power levels can be see in table 3.8.

Table 3.8: Source and measured losses from the cable connected to the HP 83752b sweeper.

Source	Measured
-10 dBm	-11.5 dBm
-5 dBm	-6.5 dBm
0 dBm	-1.5 dBm
5 dBm	3.5 dBm
10 dBm	8.5 dBm
15 dBm	13.5 dBm

With a loss of -1.5 dBm the minimum power received by the circuit is -11.5 dBm and the maximum power is 16.5 dBm. The rectifying circuit was connected to the sweeper and the DC output was measured. The results in table 3.9 show the source power, received power, resulting voltage, DC power, and conversion efficiency. The conversion efficiency was calculated by taking the ratio between the output power and input power of the circuit.

$$\eta = \frac{P_{out}}{P_{in}} \tag{31}$$

The highest voltage generated by the circuit is 1.84V and has a conversion efficiency of 75.8%.

Table 3.9: Measured DC voltage from rectifying circuit.

Source Power	Power	Voltage (V)	P_{DC}	Efficiency η
-10 dBm	-11.5 dBm	45.7 mV	2.088e-5	29.5%
-7.5 dBm	-9 dBm	58 mV	3.364e-5	26.72%
-5 dBm	-6.5 dBm	87.5 mV	7.656e-5	34.17%
-2.5 dBm	-4 dBm	130 mV	1.69e-4	42.5%
0 dBm	-1.5 dBm	187.4 mV	3.512e-4	49.6%
2.5 dBm	1 dBm	265 mV	7.0225e-4	55.7%
5 dBm	3.5 dBm	365 mV	1.3322e-3	59.5%
7.5 dBm	6 dBm	0.519 V	2.6936e-3	67.7%
10 dBm	8.5 dBm	0.706 V	4.984e-3	70.4%
12.5 dBm	11 dBm	0.955 V	9.12e-3	72.4%
15 dBm	13.5 dBm	1.287 V	0.01656	74%
16.5 dBm	15 dBm	1.544 V	0.02384	75.4%
18 dBm	16.5 dBm	1.84 V	0.033856	75.8%

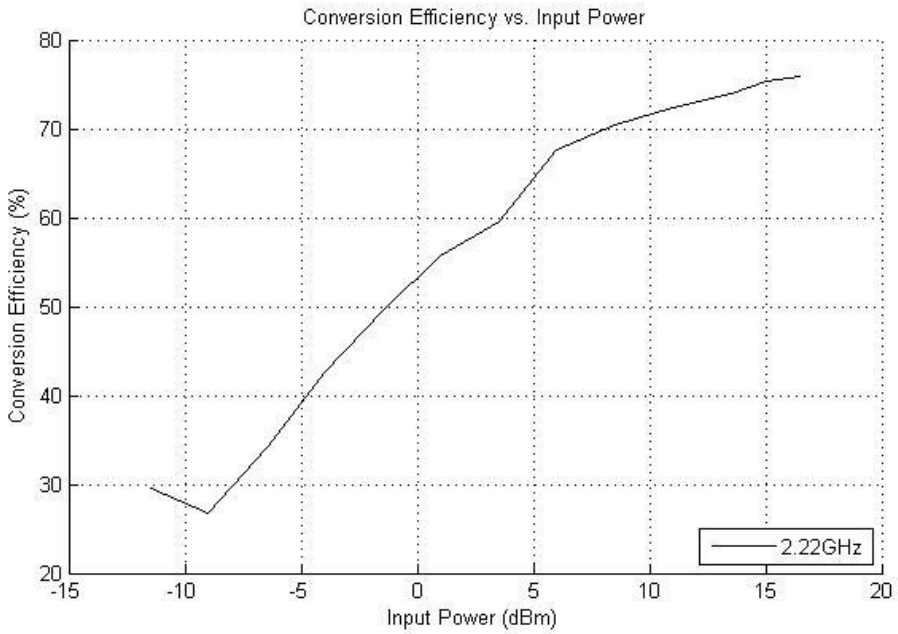

Figure 3.26: Conversion efficiency with respect to input power for the rectenna connected to the HP 83752b sweeper.

Figure 3.26 shows the efficiency of this antenna with respect to the input power levels. It is seen in this plot that the efficiency increases as the input power increases. This increase is due to the diode being able to more effectively rectify the signal when more power is available. The peak efficiency of 75.8% occures at 16.5 dBm.

The final measurements for this design were done by connecting the rectifying circuit to the patch antenna and measuring the DC output. The set up for these measurements incude the HP 83752b sweeper connected to a horn antenna that is aligned with the patch antenna. A photo of this set up is seen in figure 3.27.

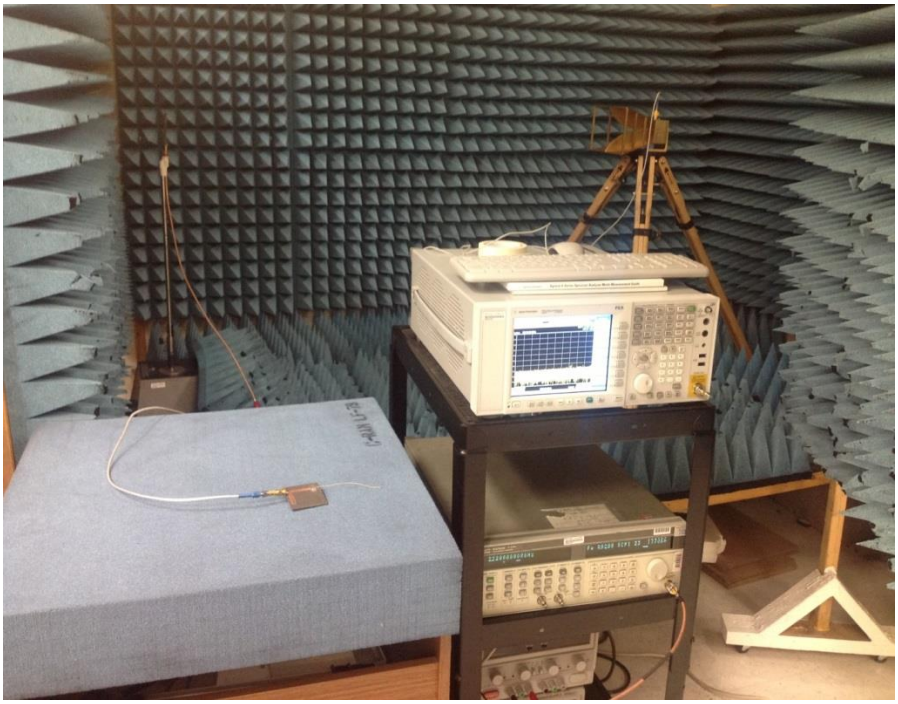

Figure 3.27: Photograph of the setup for the retenna measurments using a 2.22 GHz patch antenna.

The horn antenna is used to radiate the 2.22 GHz signal at a specified power level. As with the first set of measurements, the loss of power between the source and the circuit is measured to see how much power is actually being received by the rectifying circuit. The losses seen in this set are due to cable losses and alignment mismatch between the horn antenna and patch antenna. The source and the measured power are shown in table 3.10.

Table 3.10: Cable and alignment losses.

Source	Measured
18 dBm	-3.8 dBm
15 dBm	-6.8 dBm
10 dBm	-11 dBm
5 dBm	-16.9 dBm
0 dBm	-21 dBm
-5 dBm	-26 dBm
-10 dBm	-31 dBm

As one can see, the losses in this case are around -21 dBm which is very high. Due to the high loss value, the DC voltage is not as strong due to very low input power received by the diode. In

order to prevent this from occuring cables without a high loss value and better matching must be attained. However, even with a low input power level, a DC signal is still measured. The measured DC power from this set up is seen in table 3.11.

Table 3.11: DC voltage received by the rectenna with a 2.22 GHz radiating horn antenna.

Source Power	Received Power	Voltage	P_{DC}	Efficiency η
-10 dBm	-31 dBm	0.2 mV	4.000e-10	0.1%
-5 dBm	-26 dBm	1 mV	1.000e-8	0.4%
0 dBm	-21 dBm	3.3 mV	1.089e-7	1.4%
5 dBm	-16.9 dBm	10 mV	0.000001	5%
10 dBm	-11.9 dBm	27 mV	0.00000729	11.3%
15 dBm	-6.8 dBm	67 mV	0.00004489	21.5%
18 dBm	-3.8 dBm	107 mV	0.0001145	27.5%

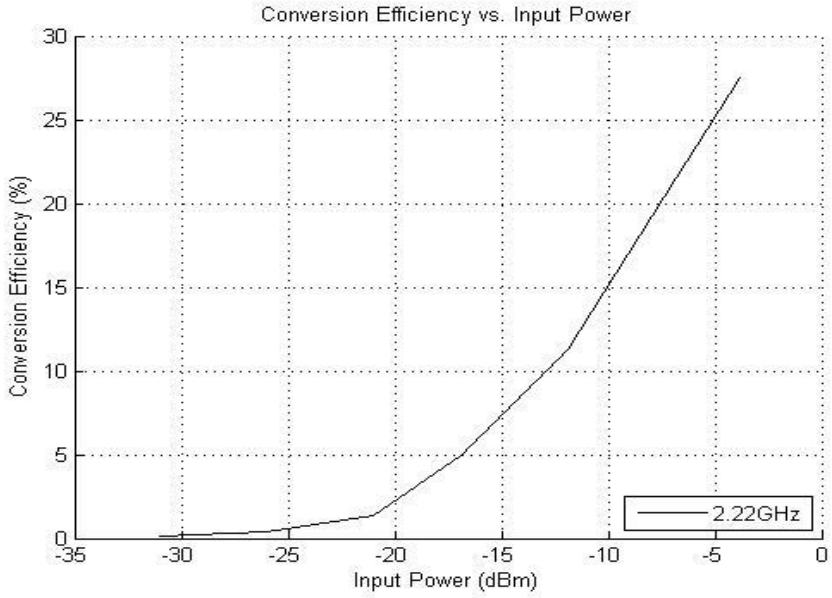

Figure 3.28: Efficiency with respect to the input power for the 2.22 GHz rectenna.

The efficiency with respect to the input power is ploted in figure 3.28. The efficiency is seen to increase with the input power and reaches a peak of 27.5% with an input power of -3.8 dBm. With these measurements it is concluded that the 2.22 GHz rectenna constructed has the capability of harvesting DC voltage even with a low input power level.

Now that a circuit that works properly to rectify the RF signal with a narrow bandwidth has been constructed, a wide bandwith rectenna can be designed. The next chapter will use what was implemented in this design to create a retenna that works for the frequencies that were found with a high power density level.

Chapter 4

Broadband Rectenna Design

In this chapter we start with a discussion of the characteristics and design of our next antenna. This second model is a more wideband antenna known as a PIFA or Planar Inverted-F Antenna. An overview of this model will be followed by the rectenna design, simulation and fabrication results.

4.1 PIFA Design

The Planar Inverted-F Antenna (PIFA) has been increasing integrated into the mobile phone world due it it's smaller size, low profile and omnidirectional pattern. This antenna design consists of a retangular planar element that is located above a ground plane, a shorting plate, and a feeding point. The inverted F of the antenna is a type of monopole where the top section has been folded down to be parallel with the ground plane. This technique is done to reduce the height of the antenna while maintaning the resonant trace length [14]. The parallel section of the antenna creates a capacitance to the input impedance, which is compensated with a short-circuit stub. For the PIFA, the ground plane plays a crucial role in the design due to the fact that that excitation of the currents in the printed planar elements causes excitation of currents in the ground plane [14]. Studies have shown that the PIFA behavior changes in relation to the ground plane size or orientation and position of the inverted F with respect to the ground plane. Ground

plane changes can affect antenna characteristics such as resonant frequency, bandwidth, gain, and radiation pattern.

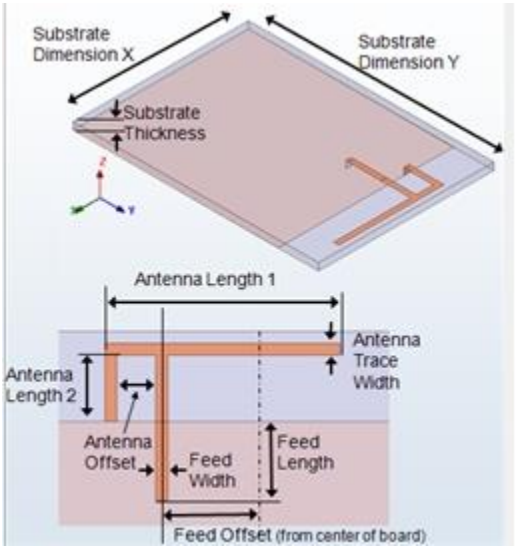

Figure 4.1: PIFA design layout.

The figure above shows the layout of the PIFA antenna. Using the lengths, L1 and L2, and width, W, the resonant frequency can be found by

$$f_r = \frac{c}{4\sqrt{\varepsilon_r}(L1 + L2 - W)} \quad [14] \tag{32}$$

The relative permitivity, ε_r, depends on the substrate used. By changing the length of the patch the resonant frequency can be shifted.

The PIFA is known to have a relatively small bandwidth, however several techniques have been introduced to increase it. Some studies have found that by adjusting the space between the feed and the short can increase the bandwidth. Also, an increased bandwidth can occur when the size of the ground plane is changed. Reducing the ground plane can effectively broaden the bandwidth of the antenna [15].

When designing the PIFA for this project, the length, L1 and L2, were 6.2 cm and 1.4 cm respectively with a width of 0.19 cm. The substrate used was Rogers 5880 which has a relative permitivity, ε_r, of 2.2 and a thickness of 1.6 mm. After the length, width, and permittivity of the antenna were found for a center frequency of 2.0 GHz, the size of the ground plane and distance between the feed and shorting plate were changed to broaden the bandwidth. The dimensions of the ground plane that provided the optimal bandwidth were 67 mm and 48 mm for the length and width respectively and the distance between the shorting plate and feed is 3.7 cm.

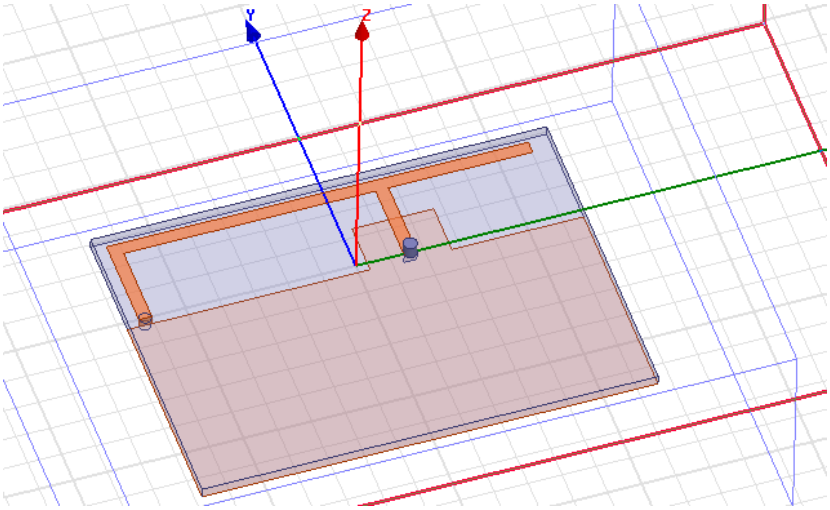

Figure 4.2: HFSS layout of the PIFA design

Figure 4.2 is the PIFA designed and simulated in HFSS. The simulation results are seen below. It is observed that the resonant frequency is approximately 2.0844 GHz and the bandwidth is from 1.87 GHz to 2.37 GHz. The gain for this antenna 3.0211 dB and has a radiation pattern seen in figure 4.3 (d) and (e) for the x- and z-axis respectively.

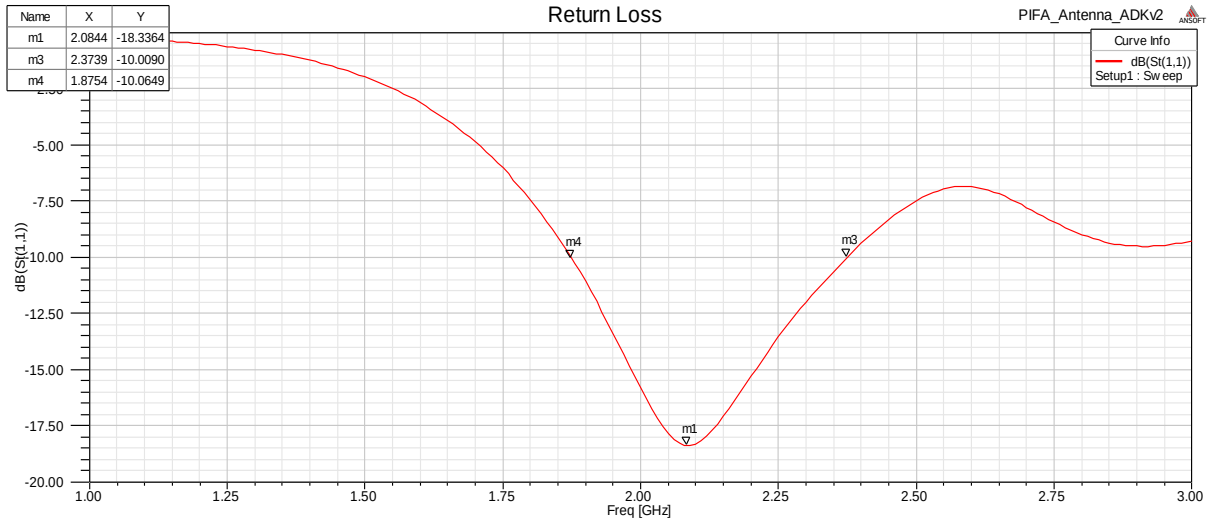
Return Loss
PIFA_Antenna_ADKv2
Name X Y
m1 2.0844 -18.3364
m3 2.3739 -10.0090
m4 1.8754 -10.0649
Curve Info
dB(St(1,1))
Setup1 : Sweep
dB(St(1,1))
Freq [GHz]
m1
m3
m4

a.

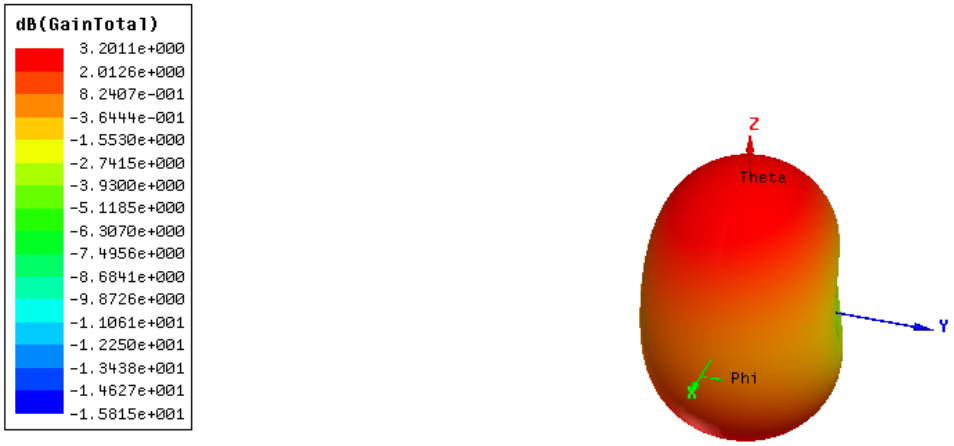
dB(GainTotal)
3.2011e+000
2.0126e+000
8.2407e-001
-3.6444e-001
-1.5530e+000
-2.7415e+000
-3.9300e+000
-5.1185e+000
-6.3070e+000
-7.4956e+000
-8.6841e+000
-9.8726e+000
-1.1061e+001
-1.2250e+001
-1.3438e+001
-1.4627e+001
-1.5815e+001
Z
Theta
Y
Phi

b.

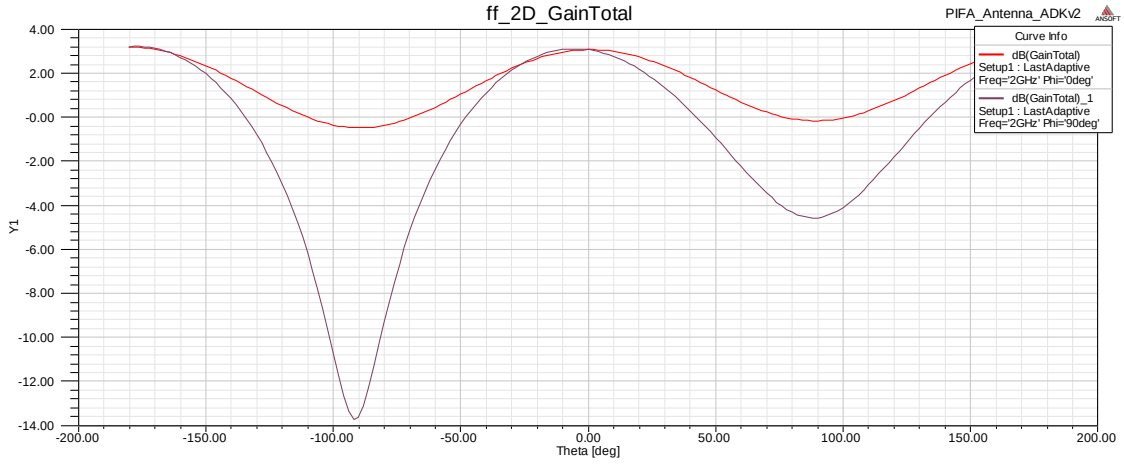
ff_2D_GainTotal
PIFA_Antenna_ADKv2
Curve Info
dB(GainTotal)
Setup1 : LastAdaptive
Freq='2GHz' Phi='0deg'
dB(GainTotal)_1
Setup1 : LastAdaptive
Freq='2GHz' Phi='90deg'
Y1
Theta [deg]

c.

d.

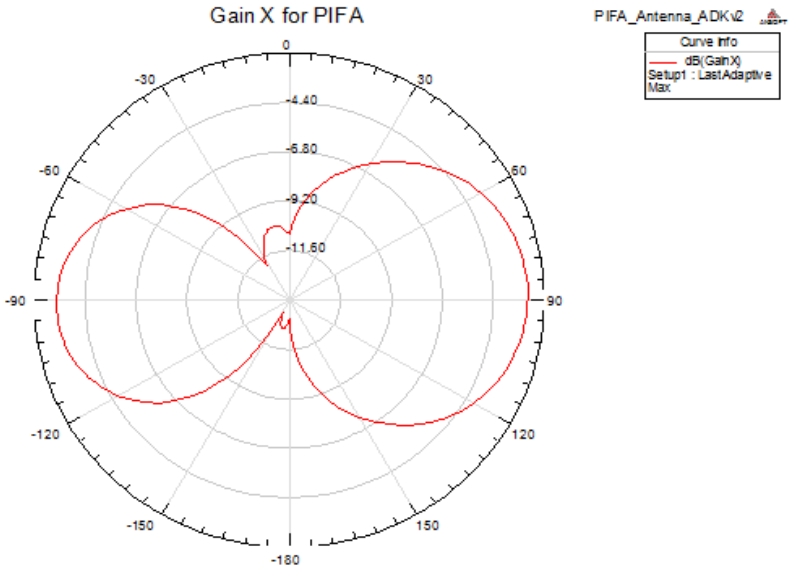

e.

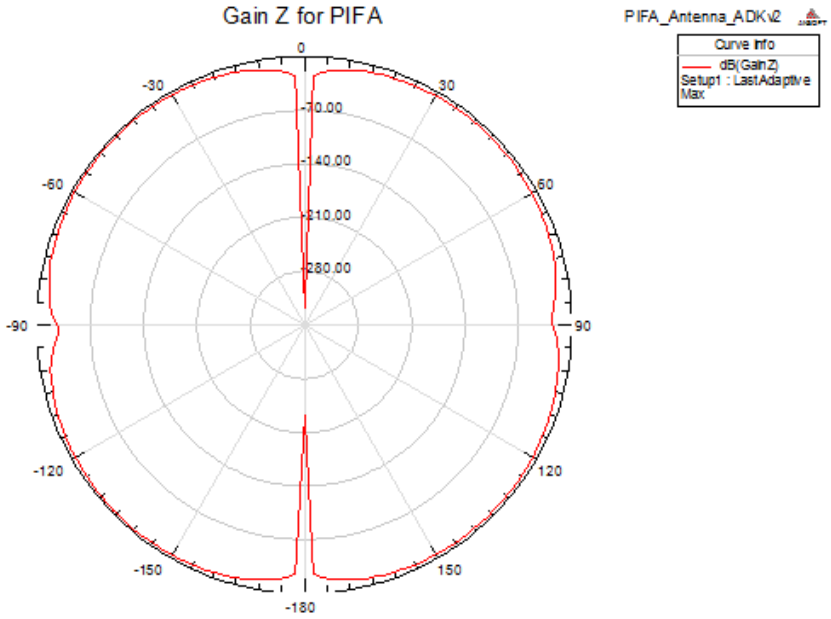

Figure 4.3: HFSS simulated results for the broadband PIFA antenna.

The PIFA design was fabricated, tested and compared with the HFSS simulation. The final fabricated model is seen in figure 4.4.

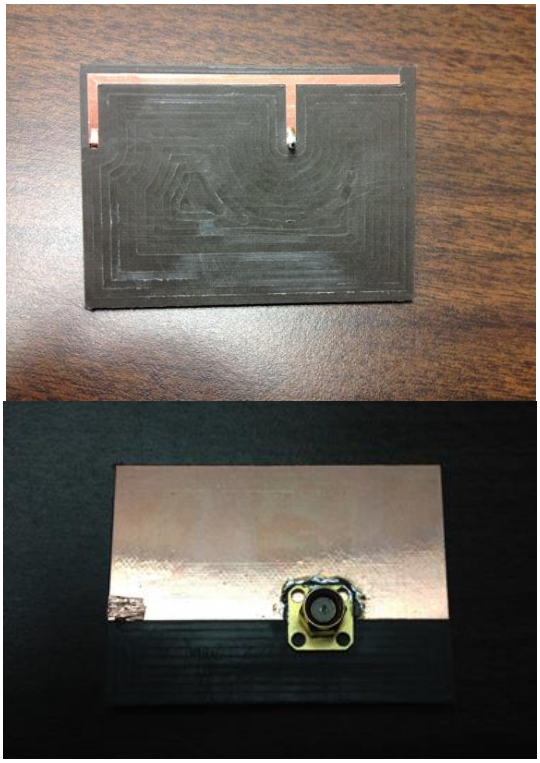

Figure 4.4: Photograph of the fabricated PIFA antenna.

The S_{11} parameters for this antenna were measured after fabrication and the results were compared with the HFSS simulation. The resonant frequency for the simulated PIFA is 2.09GHz at -18.3dBm and the measured f_r is 2.06GHz at -17dBm. Due to small differences in dimensions during fabrication, the return loss varies slightly from the simulated values. The comparison between the two is plotted in figure 4.5.

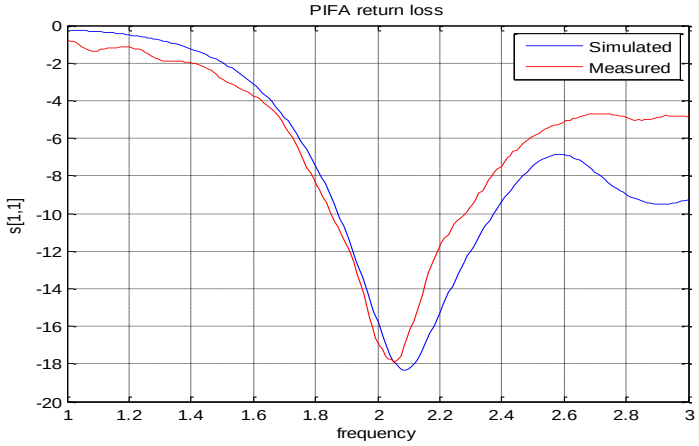

Figure 4.5: S_{11} parameters for the simulated and measured PIFA antenna

4.2 Broadband Rectifying Circuit

When is comes to designing a broadband rectenna the matching network between the output of the antenna and the input of the diode is the trickiest part. For this project the T- and pi-matching netowrks were researched and tested to maintain the broadband characteristics in our rectenna design. In this section we will discuss these matching networks and then relate them to the final broadband circuit.

4.2.1 T- and pi- matching networks

To begin this network design the quality factor, Q, must be determined. Q can be a lower value in order to increase the bandwidth of your design, or a higher value to eliminate undesired harmonics in the ouput signal. The value of Q is determined by finding the ratio between the center operating frequency (f_c) and the bandwith (BW).

$$Q = \frac{f_c}{BW} \quad [18] \tag{33}$$

Once this value is determined it can be plotted on the Smith chart to aid in the network matching. Starting at the load impedance, matching can either be accomplished using a shunt, series, shunt design (pi- matching) or a series, shunt, series design (T-matching). An example of a pi-matching network is seen if figure 4.6.

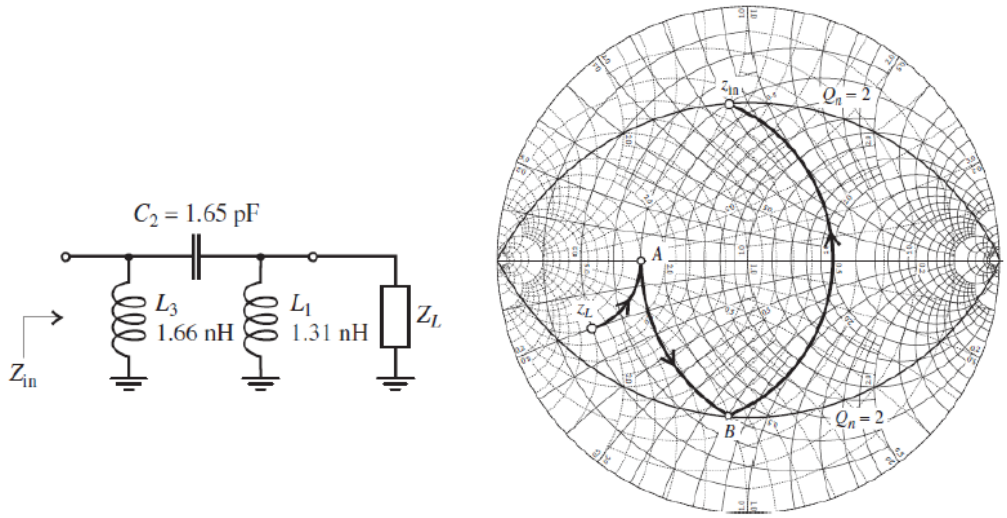

Figure 4.6: Pi-matching network example [18].

In the above figure the quality factor is equal to two. Starting at Z_L and making sure to get that Q at point B a pi- matching network is designed. The design for a T-matching network is performed the same way except the component from Z_L is in series. An example of this network is demonstrated in figure 4.7.

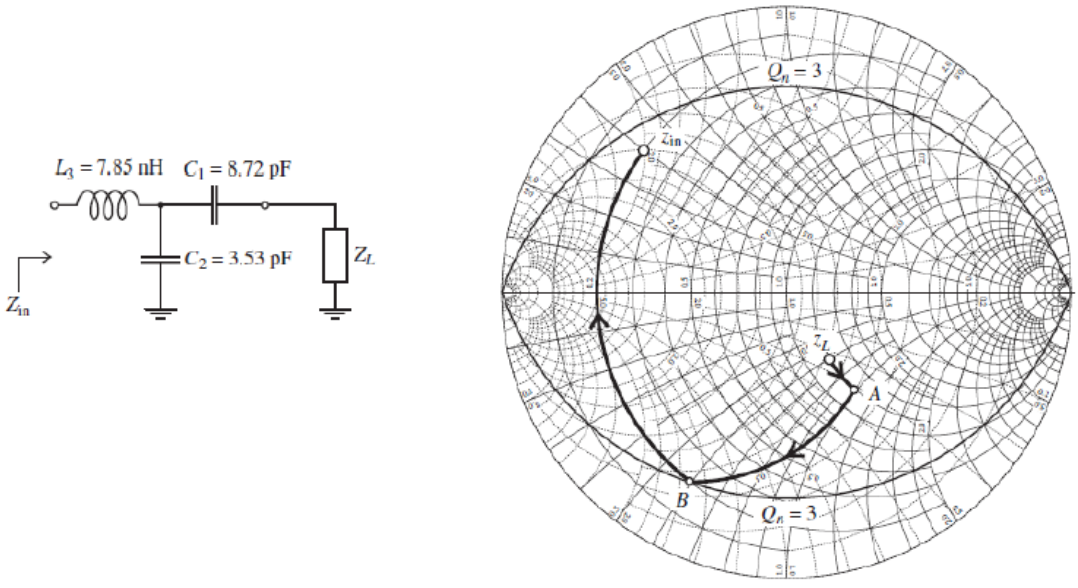

Figure 4.7: T-matching network example [18].

4.2.2 Simulated and Fabricated Broadband Rectifying Circuit

To start the broadband circuit design first one must determine the qualifying factor value, Q. As discussed earlier, in this case the ideal bandwidth is 1.5 GHz to 2.5 GHz. Therefore the f_c is equal to 2GHz with the BW equal to 1 GHz. Therefore,

$$Q = \frac{f_c}{BW} = \frac{2GHz}{1GHz} = 2 \tag{34}$$

Using ADS the impedance to the diode was found. In order to design a matching network with Q equal to 2 the load impedance and source impedance must lie inside the quality factor circle on the Smith chart. To get the load impedance inside this circle a 100 Ohm resistor was placed in front of the diode. The diode input impedance was then found to be 100.951+j54.537 Ω.

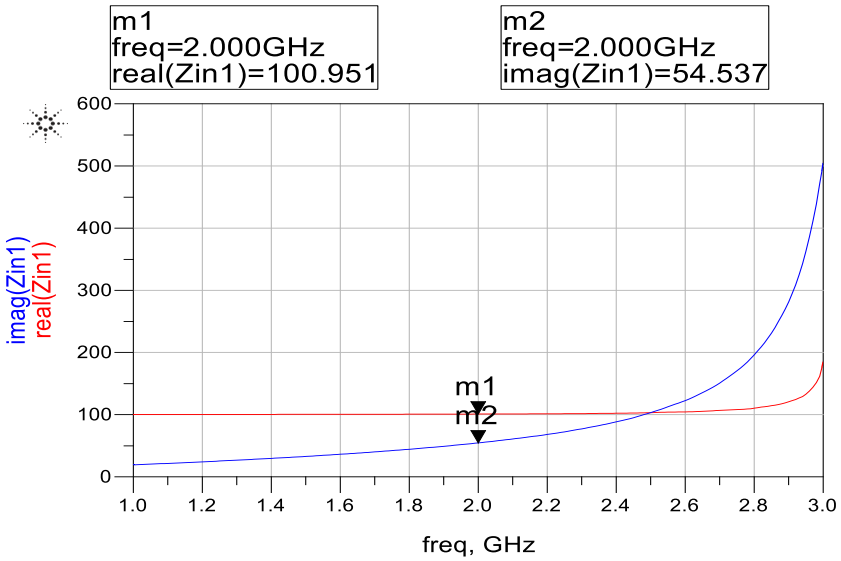

Figure 4.8: Measured input impedance to the diode at 2.0 GHz.

The impedance from the antenna is 50 Ω. Plotting the output impedance from the antenna, the input impedance to the diode and the quality factor of two on the Smith chart the matching network for this circuit was constructed (figure 4.9). The network used is a pi-matching network with two shunt capacitors and a series inductor in the middle. The value for the capacitors C1 and C2 are 1.59312 pF and 1.5913 pF, respectively and the value for the inductor is 6.05722 nH.

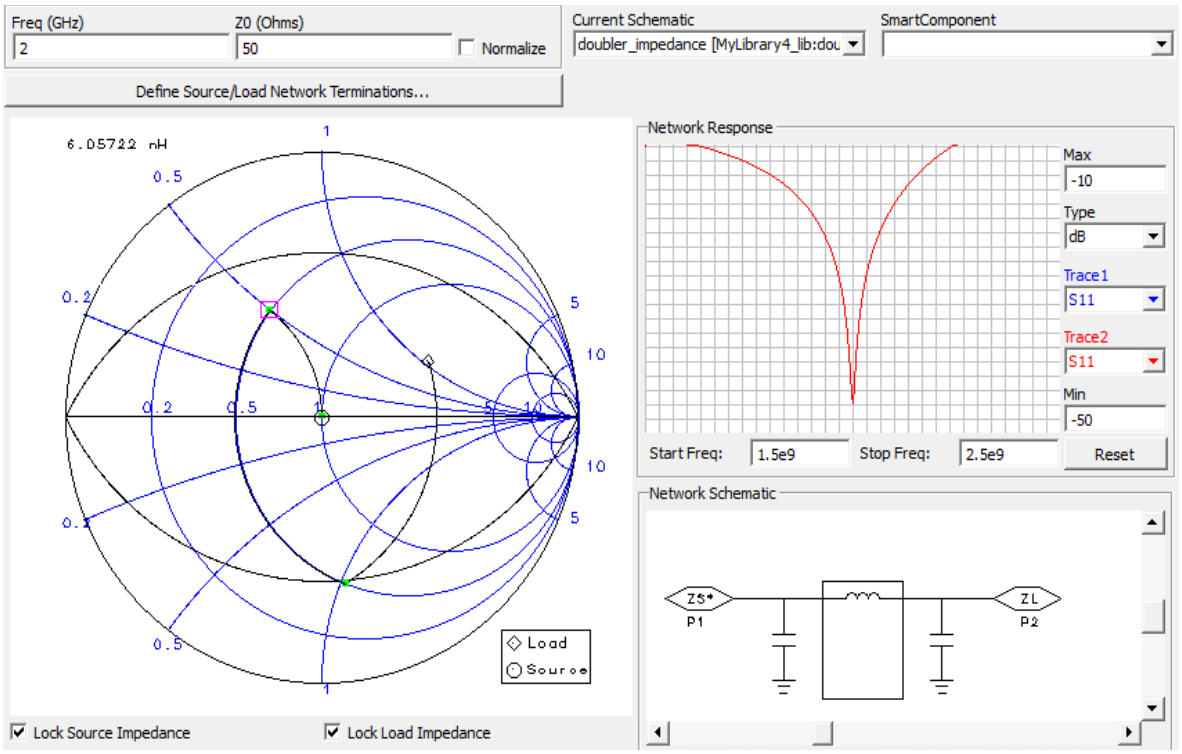

Figure 4.9: Pi-matching network for the broadband rectifying circuit.

The components for this circuit were chosen to be surface mounted devices (SMD) in order to avoid any additional resonance. The Murata library was downloaded into ADS and the SMD components that were able to provide the most accurate return loss and bandwidth were found. The first capacitor has a value of 2 pF followed by the inductor with a value of 3.9 nH and lastly a 1.6 pF capacitor. These components are connected by transmission line pads with a width of 1.722570 mm for 50 Ω impedance and the substrate used is Rogers 3206 which has a relative permittivity, ε_r, of 6.15 and a thickness of 1.27 mm. The return loss of -23.625 dBm for this circuit is shown in figure 4.10.

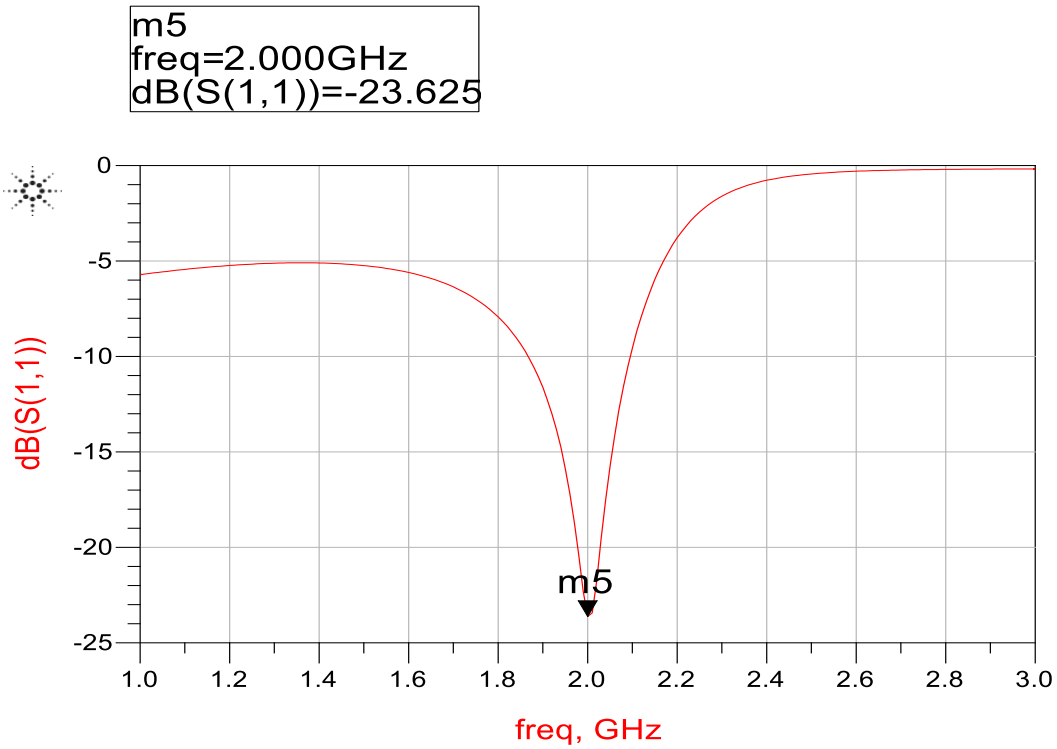

Figure 4.10: Simulated return loss for the broadband rectifying circuit.

The same set up following the diode that was used in the previous 2.22 GHz rectenna is used to rectify the signal and produce a DC voltage in this circuit. The full circuit design is illustrated in figure 4.11 and the list of all components in this circuit are in table 4.1.

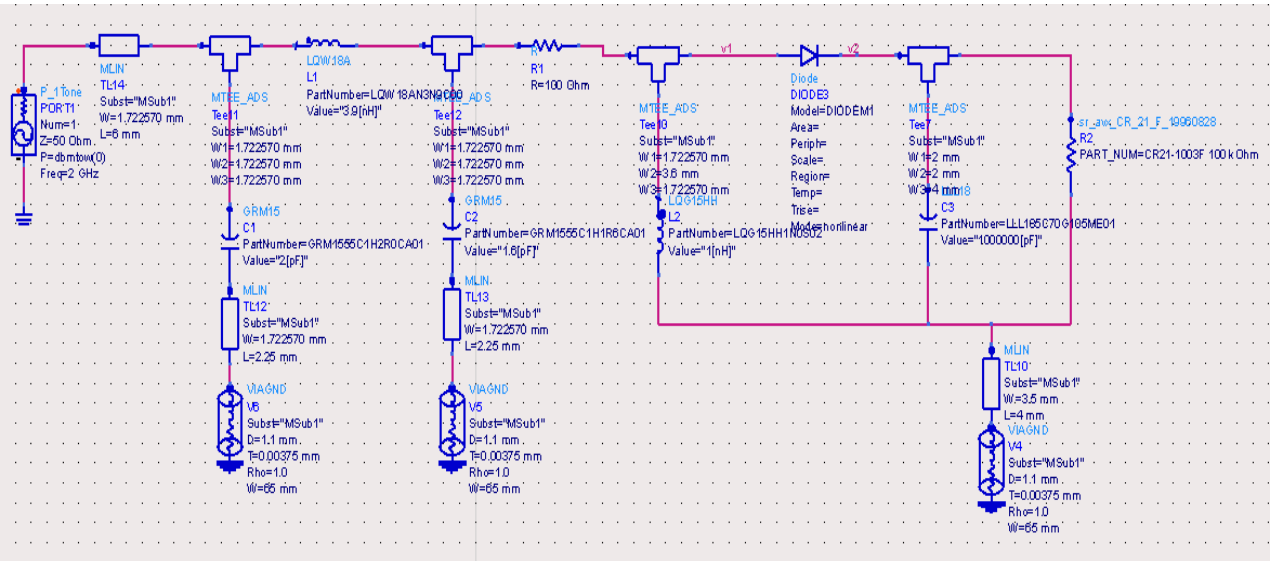

Figure 4.11: ADS layout for the braodband rectifying circuit.

Table 4.1: Component values for broadband rectifying circuit

Component	Value
C1	2pF
L1	3.9nH
C2	1.6pF
R1	100Ω
L2	1nF
C3	1µF
R2	100KΩ

As in the previous circuit, a harmonic balance simulation is perfomed to show that a DC signal is being recieved. At 0 Hz the power level is 5.697 dBm and the first harmonic at 2.0 GHz is -13.064 dBm.

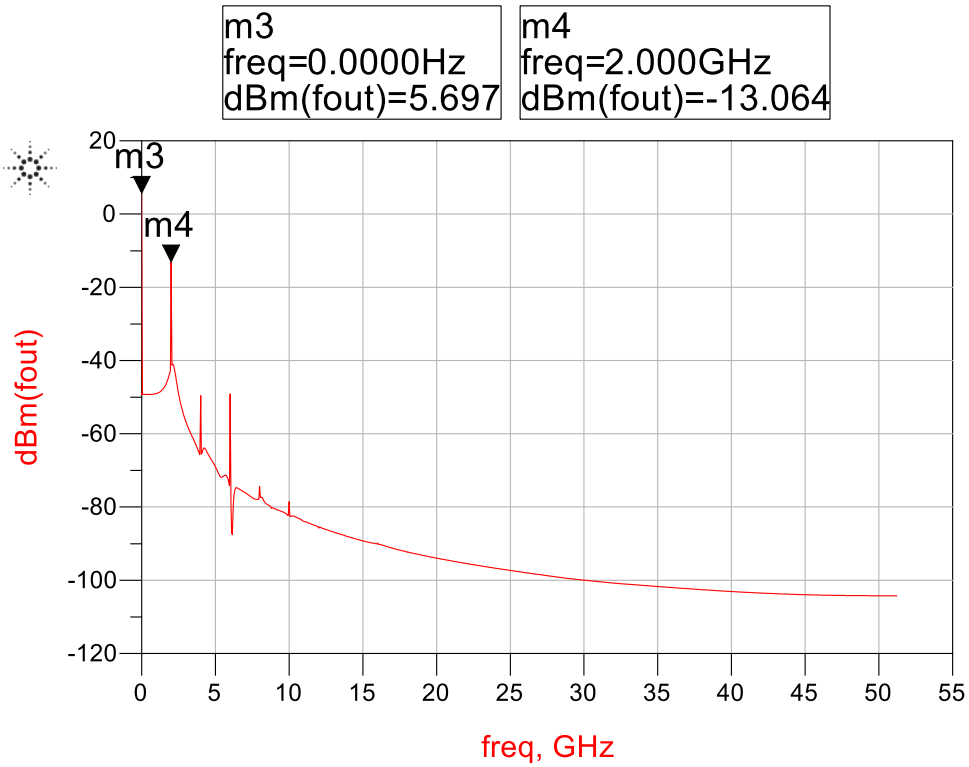

Figure 4.12: ADS harmonic balance simulation to show the DC signal.

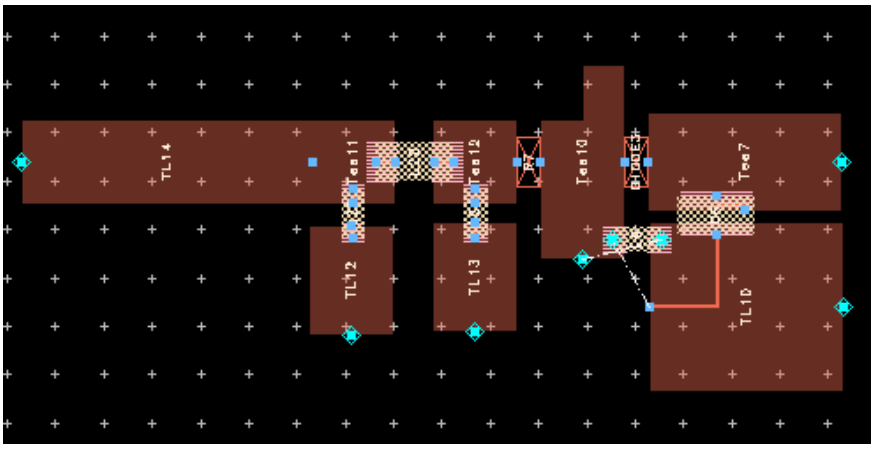

Figure 4.13: Generated schematic of the broadband rectifying circuit

Before fabriaction the schematic for the rectifying circuit is generated (figure 4.13). The final fabricated layout without the soldered components is showen in figure 4.14 and the full circuit in figure 4.15.

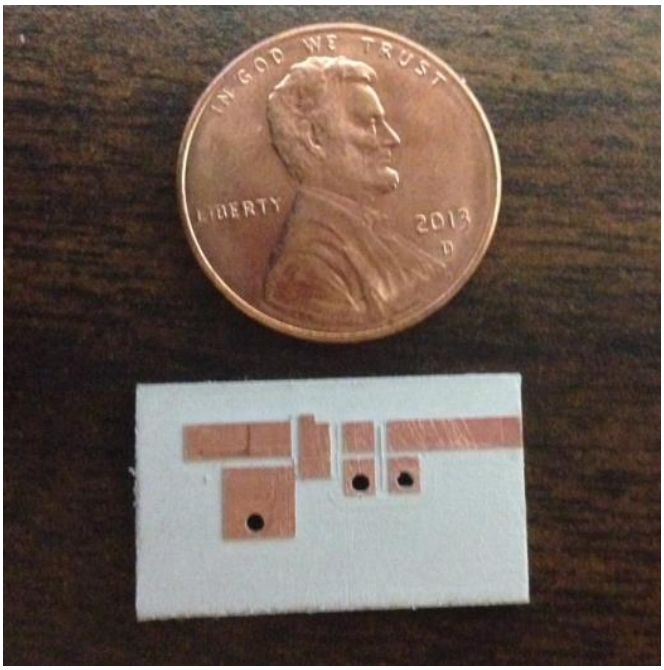

Figure 4.14: Photograph of the fabricated rectifying circuit without the soldered components.

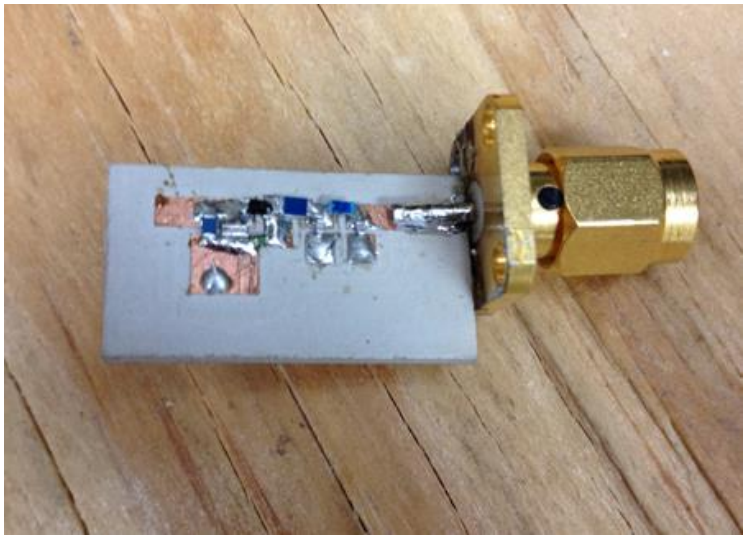

Figure 4.15: Photograph of the final fabricated rectifying circuit.

The return loss was measured and recorded for this model and are seen in figure 4.16.

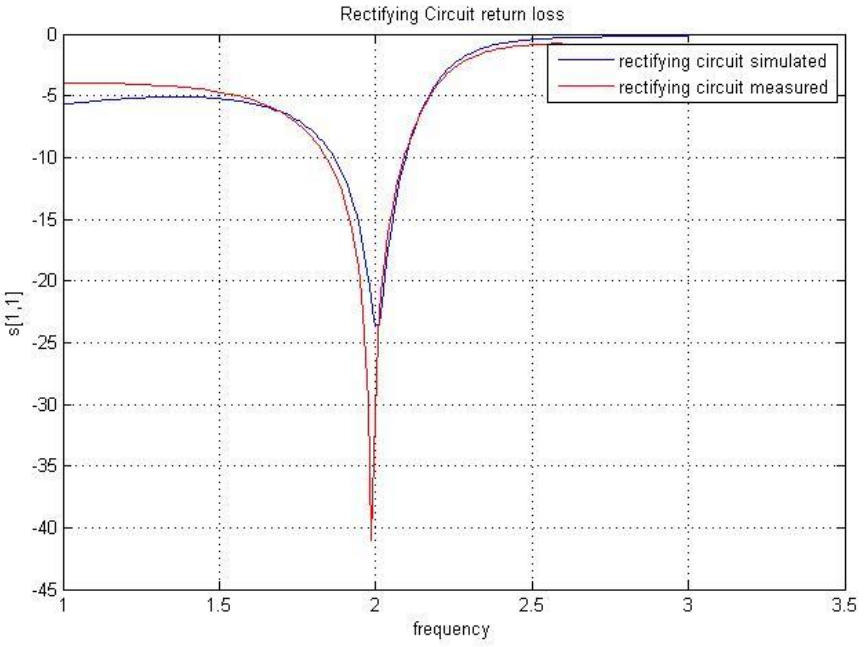

Figure 4.16: ADS simulated S_{11} versus measured S_{11} for the rectifying circuit.

In the figure above one can see that the peak of the return loss occurs at 1.99GHz and has a power level of -41 dB. Using the HP 83752b sweeper the DC power produced by our circuit was then measured. There was a DC signal being produced by the circuit from about 1.8 GHz to 2.2

GHz. The results are seen in table 4.2. The losses from the cable used to connect the circuit to the sweeper are the same as they were in the previous set of measurements, -1.5 dBm.

Table 4.2: DC voltage received from 1.8 GHz to 2.2 GHz

Source Power	Received P_{in}	Voltage	P_{DC}	Efficiency η
1.8GHz				
18 dBm	16.5dBm	494 mV	0.00244	5.5%
15 dBm	13.5dBm	333.3 mV	0.001111	5%
10 dBm	8.5dBm	169.4 mV	0.0002870	4%
5 dBm	3.5dBm	80.4 mV	0.00006464	3%
0 dBm	-1.5dBm	34.3 mV	0.00001176	1.6%
-5 dBm	-6.5dBm	12.8 mV	0.000001638	0.7%
-10 dBm	-11.5dBm	4.4 mV	1.936e-7	0.2%
1.99 GHz				
18 dBm	16.5dBm	0.685 V	0.004692	10.5%
15 dBm	13.5dBm	0.467 V	0.002181	9.7%
10 dBm	8.5dBm	241 mV	0.0005808	8.2%
5 dBm	3.5dBm	119 mV	0.0001416	6.3%
0 dBm	-1.5dBm	54 mV	0.00002916	4.1%
-5 dBm	-6.5dBm	22 mV	0.000004840	2.2%
-10 dBm	-11.5dBm	7.9 mV	6.241e-7	1%
2.0 GHz				
18 dBm	16.5dBm	0.688 V	0.004733	10.6%
15 dBm	13.5dBm	0.472 V	0.002228	10%
10 dBm	8.5dBm	241.2 mV	0.0005818	8.2%
5 dBm	3.5dBm	117.8 mV	0.0001388	6.2%
0 dBm	-1.5dBm	53.2 mV	0.00002830	4%
-5 dBm	-6.5dBm	21.3 mV	0.000004537	2%
-10 dBm	-11.5dBm	7.6 mV	5.776e-7	0.82%
2.1 GHz				
18 dBm	16.5dBm	646 mV	0.004173	9.34%
15 dBm	13.5dBm	443 mV	0.001962	8.8%
10 dBm	8.5dBm	227 mV	0.0005153	7.3%
5 dBm	3.5dBm	110.4 mV	0.0001219	5.4%
0 dBm	-1.5dBm	49.3 mV	0.00002430	3.4%
-5 dBm	-6.5dBm	19.5 mV	0.000003803	1.7%
-10 dBm	-11.5dBm	6.9 mV	4.761e-7	0.67%
2.2 GHz				
18 dBm	16.5dBm	491 mV	0.002411	5.4%
15 dBm	13.5dBm	328.7 mV	0.001080	4.8%
10 dBm	8.5dBm	164.8 mV	0.0002716	3.8%
5 dBm	3.5dBm	77.3 mV	0.00005975	2.7%
0 dBm	-1.5dBm	33 mV	0.00001089	1.5%

-5 dBm	-6.5dBm	12.4 mV	0.000001538	0.7%
-10 dBm	-11.5dBm	4.2 mV	1.764e-7	0.3%

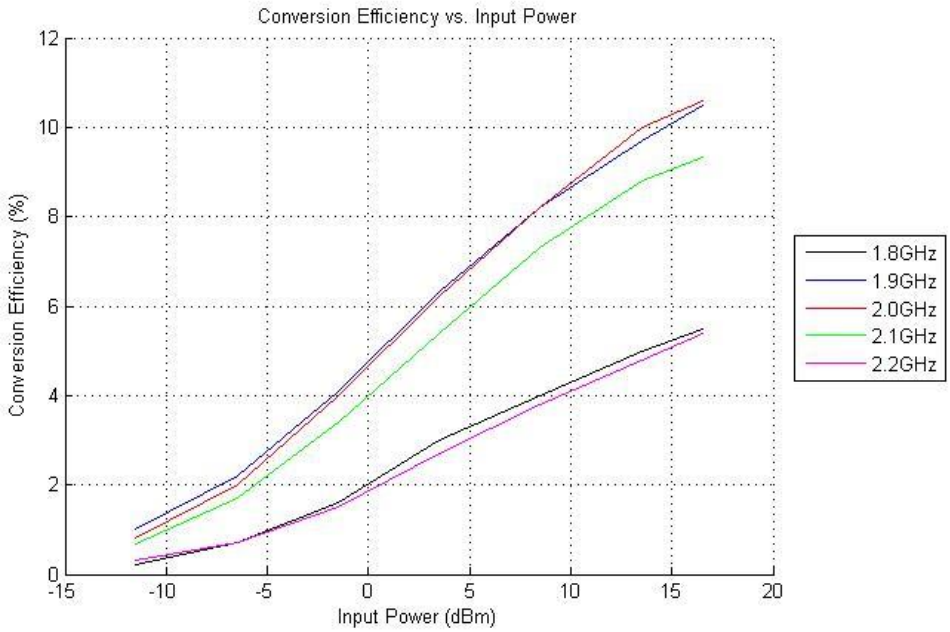

Figure 4.17: Efficiency with respect to input power for frequecies ranging from 1.8 GHz to 2.2 GHz.

The highest RF to DC converstion efficiency occurred at 2.0GHz with a power level of 16.5 dBm, as seen in figure 4.17. The results found in this study show that the circuit design was not converting the AC to DC power efficiently. Although some power was received, the maximum conversion efficiency was only 10.6% as compared to 79% in the narrowband rectenna study.

After further review, a voltage doubler rectenna was designed in order to increase the DC output. The layout of this circuit is discussed in chapter one and can be seen in figure 4.18.

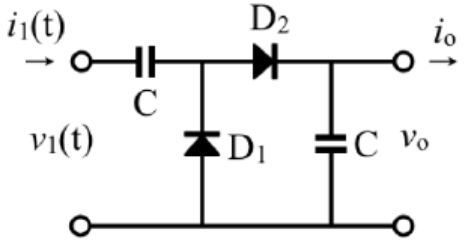

Figure 4.18: Voltage doubler rectifying circuit layout [4].

In this circuit the output of the two diodes are added in series which results in, ideally, double the DC voltage. This circuit layout will also increase the value of the voltage sensitivity for the network and improve the conversion efficiency. The diode used for this design was HSMS-286C by Agilent Technologies. This diode was chosen because there are two diodes connected in a series-parallel manner in one component [19]. The diode also has a low impedance to aide in impedance matching between the antenna and the diode and high detection sensitivity, up to 35mV/μW at 2.45GHz. The layout of this diode is seen in figure 4.19.

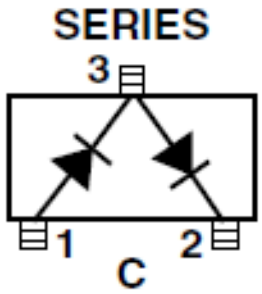

Figure 4.19: Layout of Agilents HSMS-286C diode [20].

When finding the quality factor, Q, a bandwidth of 1.3 GHz and a center frequency of 2.0 GHz is used. The equation to find Q is

$$Q = \frac{f_c}{BW} = \frac{2GHz}{1.3GHz} \simeq 1.5 \tag{35}$$

The value Q is plotted on the smith cart to aide in matching between impedances. As in the previous design, a resistor was added in front of the capacitor and diode in order to place the load impedance inside Q.

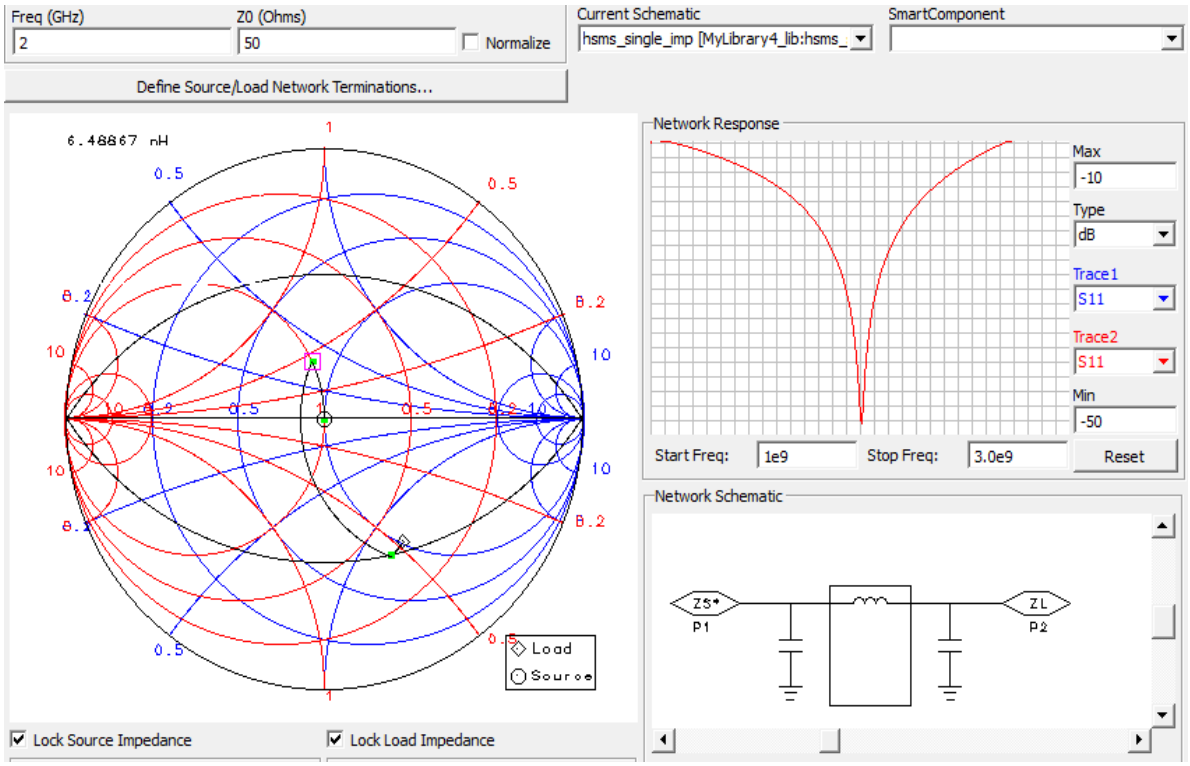

Figure 4.20: Matching for the voltage doubler rectifying circuit.

The matching done for the voltage double circuit is seen in figure 4.20. This network consists of a shunt capacitor with a value of 705.50309 fF, a series inductor with a value of 6.48867 nH, and a shunt capacitor with a value of 115.02263 fF. These components were then found as SMD components which altered their values slightly. The SMD values of all the components used in this circuit are presented in table 4.3.

Table 4.3: Component list and corresponding values for voltage doubler

Component	Value
C1	0.7pF
L1	5.6nH
C2	0.1pF
R1	50Ω
C3	12pF
C4	5pF
R2	1MΩ

These components are connected by transmission line pads with a width of 1.722570 mm for 50 Ω impedance. The substrate used for this design was Rogers 3206 which has a relative permittivity, ε_r, of 6.15 and a thickness of 1.27 mm.

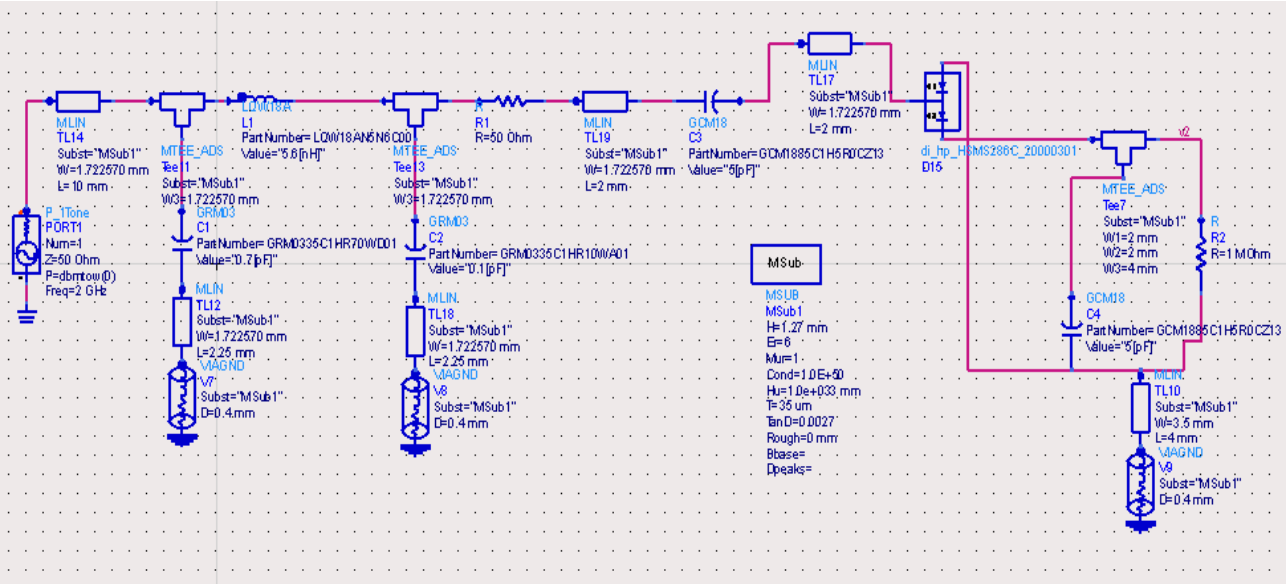

Figure 4.21: ADS voltage doubler layout.

Figure 4.21 shows the ADS schematic for the voltage doubler layout. This layout was then used to simulate the S_{11} parameters and harmonic balance for this cirucit. The return loss peaks with a value of -35.577 dB at 1.98 GHz and the bandwidth ranges from 1.65 GHz to 2.33 GHz.

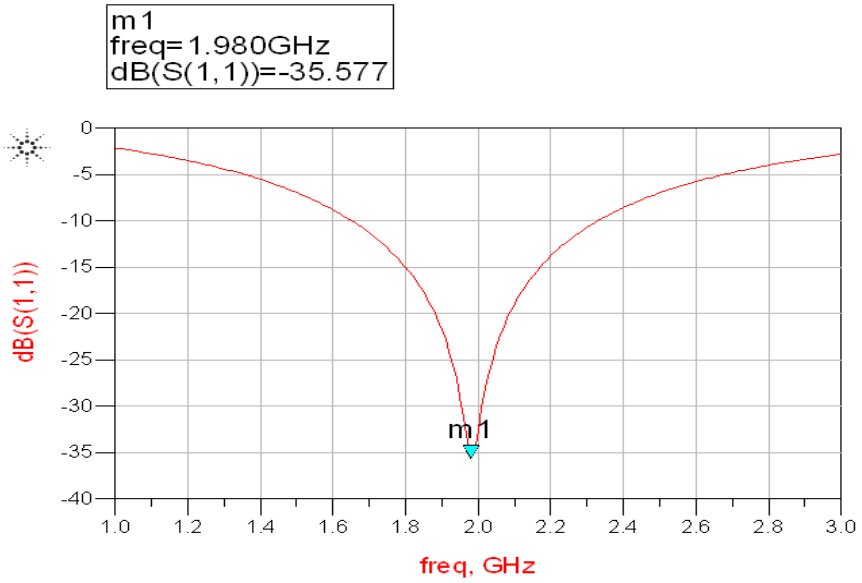

Figure 4.22: Simulated return loss for voltage doubler circuit.

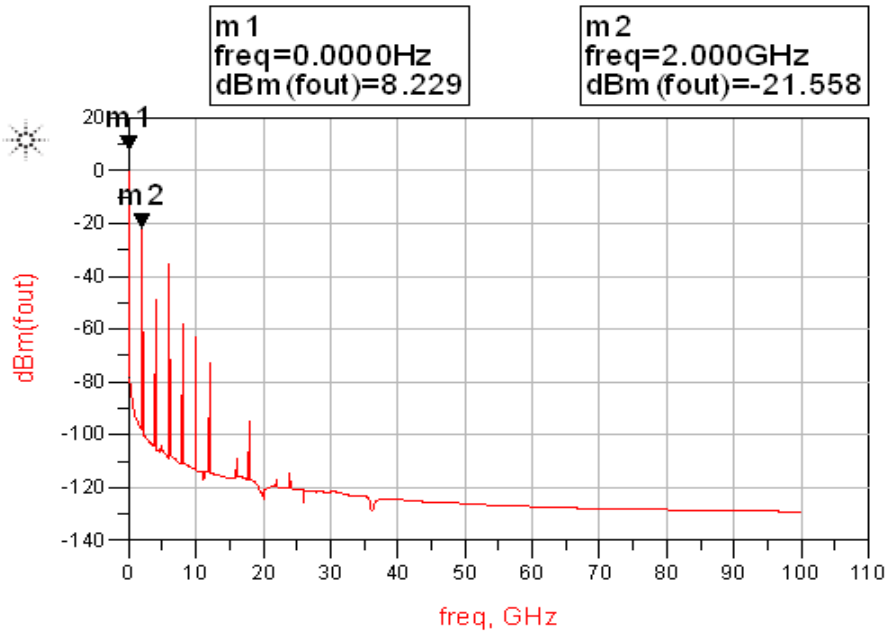

Figure 4.23: ADS harmonic balance simulation for voltage doubler circuit.

The harmonic balance simulation was performed at 2.0 GHz with an input power of 0 dBm. In the previous circuit design the power level at 0 GHz in the harmonic balance simulation was 5.697dBm which is 2.532 dBm less than the power received by this voltage doubler circuit. This circuit design was fabricated and measured. The fabricated design is seen in figure 4.24.

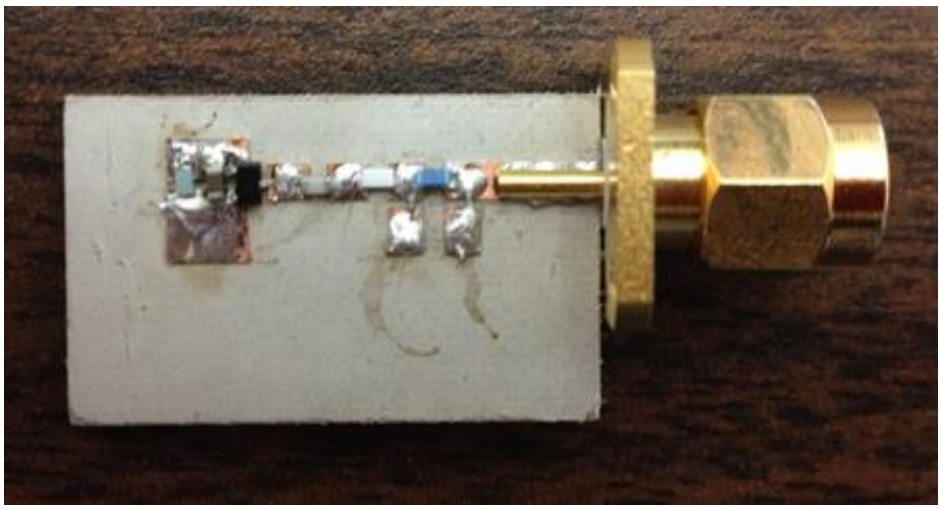

Figure 4.24: Photograph of the fabricated voltage doubler circuit.

After fabrication the circuit's return loss was measured and compared with the ADS simulation. In the ADS simulation the resonant frequency is 1.97 GHz with a power level of -36.4 dBm and for the fabricated circuit the observed resonant frequency occurs at 1.9 GHz with a power level of -23.64 dBm. The comparison of the simulated and measured S_{11} values are seen in figure 4.25. The difference in the simulated and measured frequecies is a result of dimension mismatch during fabrication and ADS diode model inconsistencies.

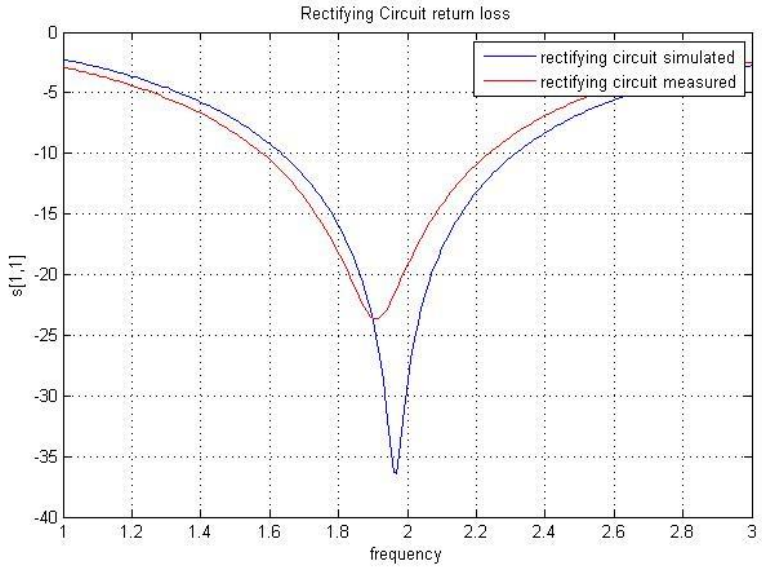

Figure 4.25: ADS simulation return loss versus fabricated circuit return loss.

Using the HP 83752b synthesized sweeper the voltage doubler was tested for frequencies from 1.3 GHz to 2.4 GHz with input power from -10 dBm to 18 dBm. The results are recorded in table 4.4.

Table 4.4: Results from voltage doubler for frequencies 1.3GHz to 2.4GHz. Table displays the input power (dBm), ouput voltage, output power (dBm), and conversion efficiency respectively.

Voltage Doubler Measurements								
1.3GHz					**1.4GHz**			
18dBm	7.39V	0.05461	86.55%		18dBm	7.45V	0.05550	87.96%
15 dBm	5.26V	0.02767	87.50%		15 dBm	5.25V	0.02756	87.15%
10 dBm	2.80V	0.007840	78.40%		10 dBm	2.77V	0.007673	76.73%
5 dBm	1.43V	0.002045	64.67%		5 dBm	1.41V	0.001988	62.87%

0 dBm	.687V	0.0004720	47.20%		0 dBm	.676V	0.0004570	45.70%
-5 dBm	.301V	0.00009060	28.65%		-5 dBm	.297V	0.00008821	27.89%
-10 dBm	.118V	0.00001392	13.92%		-10 dBm	.116V	0.00001346	13.46%
1.5GHz					**1.6GHz**			
18dBm	7.36V	0.05417	85.85%		18dBm	7.2V	0.05184	82.16%
15 dBm	5.18V	0.02683	84.84%		15 dBm	5.0V	0.02500	79.06%
10 dBm	2.74V	0.007508	75.08%		10 dBm	2.68V	0.007182	71.82%
5 dBm	1.39V	0.001932	61.10%		5 dBm	1.36V	0.001850	58.50%
0 dBm	.668V	0.0004462	44.62%		0 dBm	.655V	0.0004290	42.90%
-5 dBm	.292V	0.00008526	26.96%		-5 dBm	.288V	0.00008294	26.23%
-10 dBm	.113V	0.00001277	12.77%		-10 dBm	.114V	0.00001300	13.00%
1.7GHz					**1.8GHz**			
18dBm	7.0V	0.04900	77.66%		18dBm	6.9V	0.04761	75.46%
15 dBm	4.93V	0.02430	76.84%		15 dBm	4.79V	0.02294	72.54%
10 dBm	2.60V	0.006760	67.60%		10 dBm	2.52V	0.006350	63.50%
5 dBm	1.32V	0.001742	55.09%		5 dBm	1.27V	0.001613	51.01%
0 dBm	.631V	0.0003982	39.82%		0 dBm	.602V	0.0003624	36.24%
-5 dBm	.275V	0.00007563	23.92%		-5 dBm	.2595V	0.00006734	21.29%
-10 dBm	.107V	0.00001145	11.45%		-10 dBm	.100V	0.00001000	10.00%
1.9GHz					**2.0GHz**			
18dBm	6.67V	0.04449	70.51%		18dBm	6.30V	0.03969	62.90%
15 dBm	4.62V	0.02134	67.48%		15 dBm	4.36V	0.01901	60.11%
10 dBm	2.42V	0.005856	58.56%		10 dBm	2.27V	0.005153	51.53%
5 dBm	1.24V	0.001538	48.64%		5 dBm	1.135V	0.001288	40.73%
0 dBm	.578V	0.0003341	33.41%		0 dBm	.526V	0.0002767	27.67%
-5 dBm	.244V	0.00005954	18.83%		-5 dBm	.220V	0.00004840	15.31%
-10 dBm	.094V	0.000008836	8.84%		-10 dBm	.083V	0.000006889	6.89%
2.1GHz					**2.2GHz**			
18dBm	5.95V	0.03540	56.11%		18dBm	5.69V	0.03238	51.32%
15 dBm	4.12V	0.01697	53.66%		15 dBm	3.92V	0.01537	48.60%
10 dBm	2.15V	0.004622	46.22%		10 dBm	2.029V	0.004117	41.17%
5 dBm	1.069V	0.001143	36.14%		5 dBm	.998V	0.0009960	31.50%
0 dBm	0.491V	0.0002411	24.11%		0 dBm	.453V	0.0002052	20.52%
-5 dBm	.203V	0.00004121	13.03%		-5 dBm	.1857V	0.00003448	10.90%
-10 dBm	.076V	0.000005776	5.78%		-10 dBm	.0691V	0.000004775	4.78%
2.3GHz					**2.4GHz**			
18dBm	5.21V	0.02714	43.01%		18dBm	4.92V	0.02421	38.37%
15 dBm	3.576V	0.01279	40.45%		15 dBm	3.35V	0.01122	35.48%
10 dBm	1.837V	0.003375	33.75%		10 dBm	1.71V	0.002924	29.24%
5 dBm	.899V	0.0008082	25.56%		5 dBm	.832V	0.0006922	21.89%
0 dBm	.403V	0.0001624	16.24%		0 dBm	.372V	0.0001384	13.84%
-5 dBm	.163V	0.00002657	8.40%		-5 dBm	.148V	0.00002190	6.93%
-10 dBm	.060V	0.000003600	3.60%		-10 dBm	.054V	0.000002916	2.92%

The greatest efficiency recorded of 87.96% occurs at 1.4 GHz with an input power of 18 dBm. These conversion efficiencies are plotted with respect to input power in figure 4.26.

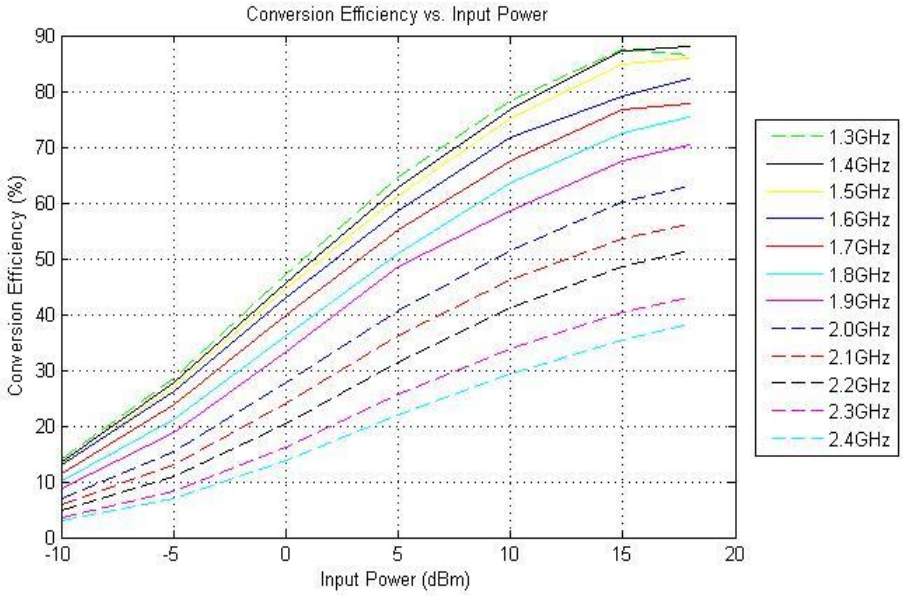

Figure 4.26: Conversion efficiency plotted with respect to input power for frequencies ranging from 1.3 GHz to 2.4 GHz

It is clear that the voltage received from this broadband circuit is significantly greater then that of the single diode circuit. The difference between the voltages of the two circuits is seen in table 4.5.

Table 4.5: Difference between the DC output voltage of the single diode circuit and the voltage doubler circuit

Singe Diode and Voltage Doubler Output Differences						
1.8GHz				**2.0GHz**		
Single diode	Double Voltage	Difference		Single diode	Double Voltage	Difference
494 mV	6.9V	6.406V		0.688 V	6.30V	5.612V
333.3 mV	4.79V	4.4567V		0.472 V	4.36V	3.888V
169.4 mV	2.52V	2.3506V		241.2 mV	2.27V	2.0288V
80.4 mV	1.27V	1.1896V		117.8 mV	1.135V	1.0172V
34.3 mV	.602V	0.5677V		53.2 mV	.526V	0.4728V
12.8 mV	.2595V	0.2467V		21.3 mV	.220V	0.1987V
4.4 mV	.100V	0.0956V		7.6 mV	.083V	0.0754V

2.1GHz				2.2GHz		
Single diode	Double Voltage	Difference		Single diode	Double Voltage	Difference
646 mV	5.95V	5.304V		491 mV	5.69V	5.199V
443 mV	4.12V	3.677V		328.7 mV	3.92V	3.5913V
227 mV	2.15V	1.923V		164.8 mV	2.029V	1.8642V
110.4 mV	1.069V	0.9586V		77.3 mV	.998V	0.9207V
49.3 mV	0.491V	0.4417V		33 mV	.453V	0.42V
19.5 mV	.203V	0.1835V		12.4 mV	.1857V	0.1733V
6.9 mV	.076V	0.0691V		4.2 mV	.0691V	0.0649V

Next, it is important to measure the efficiency of the rectifyig circuit when connected to a PIFA design. In order to measure the DC power received a linearly polarized horn antenna was used to radiate at different frequencies from 1.5 GHz to 2.2 GHz with the input power varying from -10 dBm to 18 dBm. The power being received from the antenna was measured first in order to accurately determine how much power is going into the rectifying circuit. In table 4.6 the source and received power is recorded to show how much of a loss is generated. These losses are due to cable losses and alignment mismatch.

Table 4.6: Recorded losses due to cable losses and alignement mismatch

Source Power	Received Power
18 dBm	1.5dBm
15 dBm	-1.5dBm
10 dBm	-7dBm
5 dBm	-11.5dBm
0 dBm	-16.5dBm
-5 dBm	-21.5dBm
-10 dBm	-26.5dBm

The circuit is then connected to the PIFA antenna and the output DC power is measured. A photograph of the setup for these measurements is shown in figure 4.27.

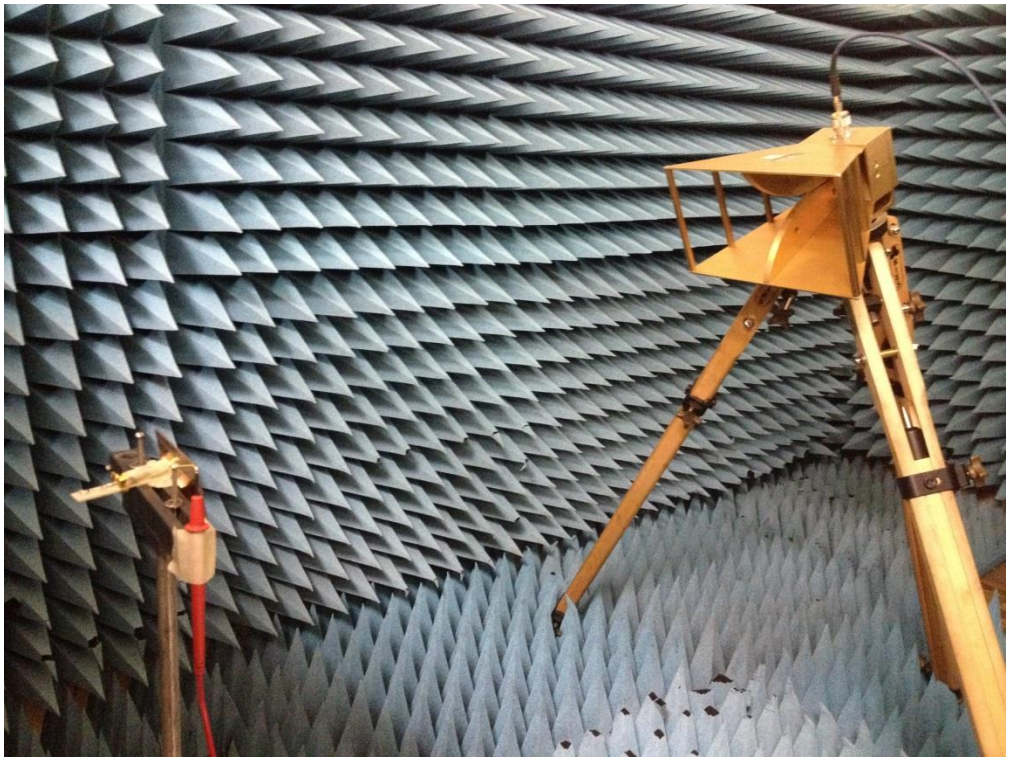

Figure 4.27: A photograph of the setup used to test the broadband rectenna design.

Due to the low power levels, the efficiency is not as high as in the previous set of measurements however, it is important to note that the signal is still being rectified and delivered to the load despite the low power level. The source power, received power, voltage, DC output and conversion efficiency are recorded in table 4.7.

Table 4.7: Results measured from broadband PIFA rectenna design with a radiating horn antenna

Source Power	Received P_{in}	Voltage	P_{DC}	Efficiency η
1.5 GHz				
18 dBm	1.5dBm	385 mV	0.0001482	10.49%
15 dBm	-1.5dBm	224 mV	0.00005018	7.09%
10 dBm	-7dBm	81 mV	0.000006561	3.29%
5 dBm	-11.5dBm	26 mV	6.760e-7	0.95%
0 dBm	-16.5dBm	8.7 mV	7.569e-8	0.34%
-5 dBm	-21.5dBm	3.3 mV	1.089e-8	0.15%
-10 dBm	-26.5dBm	1.5 mV	2.250e-9	0.10%
1.6 GHz				
18 dBm	1.5dBm	470mV	0.0002209	15.64%
15 dBm	-1.5dBm	283mV	0.00008009	11.31%

10 dBm	-7dBm	107mV	0.00001145	5.74%
5 dBm	-11.5dBm	35.6mV	0.000001267	1.79%
0 dBm	-16.5dBm	11.6mV	1.346e-7	0.60%
-5 dBm	-21.5dBm	4.0mV	1.600e-8	0.23%
-10 dBm	-26.5dBm	1.8mV	3.240e-9	0.14%
1.7 GHz				
18 dBm	1.5dBm	410mV	0.0001681	11.90%
15 dBm	-1.5dBm	246mV	0.00006052	8.55%
10 dBm	-7dBm	90mV	0.000008100	4.06%
5 dBm	-11.5dBm	30.8mV	9.486e-7	1.34%
0 dBm	-16.5dBm	9.4mV	8.836e-8	0.39%
-5 dBm	-21.5dBm	3.5mV	1.225e-8	0.17%
-10 dBm	-26.5dBm	1.6mV	2.560e-9	0.11%
1.8 GHz				
18 dBm	1.5dBm	290 mV	0.00008410	5.95%
15 dBm	-1.5dBm	168 mV	0.00002822	3.99%
10 dBm	-7dBm	50 mV	0.000002500	1.25%
5 dBm	-11.5dBm	17.6 mV	3.098e-7	0.44%
0 dBm	-16.5dBm	6.1 mV	3.721e-8	0.17%
-5 dBm	-21.5dBm	2.3 mV	5.290e-9	0.07%
-10 dBm	-26.5dBm	1.3 mV	1.690e-9	0.08%
1.9 GHz				
18 dBm	1.5dBm	520mV	0.0002704	19.14%
15 dBm	-1.5dBm	289mV	0.00008352	11.80%
10 dBm	-7dBm	110mV	0.00001210	6.06%
5 dBm	-11.5dBm	38mV	0.000001444	2.04%
0 dBm	-16.5dBm	11.5mV	1.322e-7	0.59%
-5 dBm	-21.5dBm	4.1mV	1.681e-8	0.24%
-10 dBm	-26.5dBm	1.9mV	3.610e-9	0.16%
2.0 GHz				
18 dBm	1.5dBm	1.0V	0.001000	70.79%
15 dBm	-1.5dBm	640mV	0.0004096	57.86%
10 dBm	-7dBm	272mV	0.00007398	37.08%
5 dBm	-11.5dBm	100mV	0.00001000	14.13%
0 dBm	-16.5dBm	32mV	0.000001024	4.57%
-5 dBm	-21.5dBm	10.4mV	1.082e-7	1.53%
-10 dBm	-26.5dBm	3.8mV	1.444e-8	0.65%
2.1 GHz				
18 dBm	1.5dBm	918mV	0.0008427	59.66%
15 dBm	-1.5dBm	574mV	0.0003295	46.54%
10 dBm	-7dBm	243mV	0.00005905	29.60%
5 dBm	-11.5dBm	88.9mV	0.000007903	11.16%
0 dBm	-16.5dBm	28.2mV	7.952e-7	3.55%
-5 dBm	-21.5dBm	9.1mV	8.281e-8	1.17%
-10 dBm	-26.5dBm	3.4mV	1.156e-8	0.52%

2.2 GHz				
18 dBm	1.5dBm	615mV	0.0003782	26.77%
15 dBm	-1.5dBm	371mV	0.0001376	19.44%
10 dBm	-7dBm	143mV	0.00002045	10.25%
5 dBm	-11.5dBm	48mV	0.000002304	3.25%
0 dBm	-16.5dBm	15.0mV	2.250e-7	1.01%
-5 dBm	-21.5dBm	5.3mV	2.809e-8	0.40%
-10 dBm	-26.5dBm	2.1mV	4.410e-9	0.20%

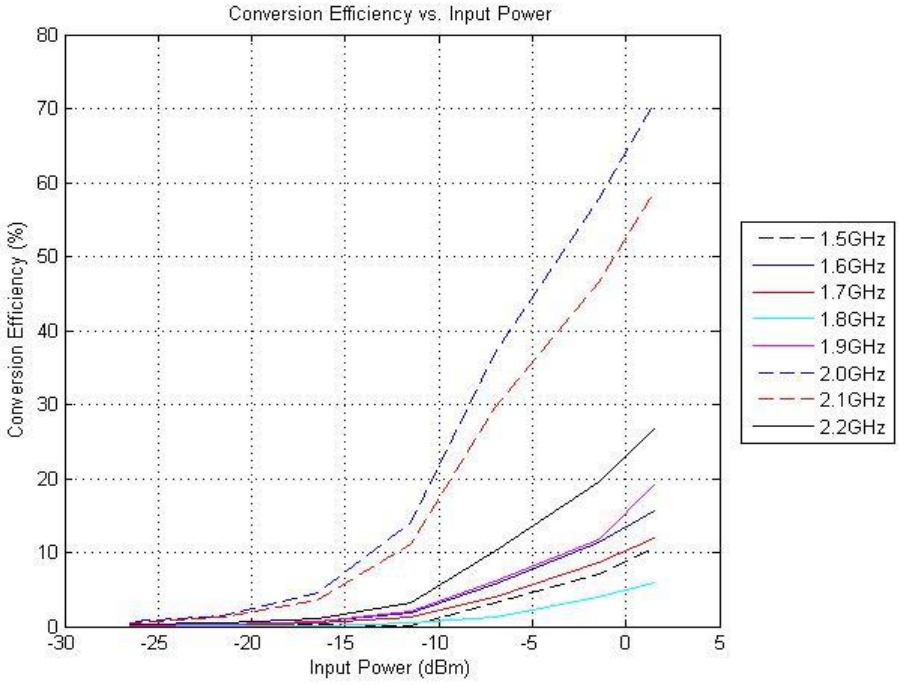

Figure 4.28: Conversion efficiency plotted with respect to input power for frequencies ranging from 1.5 GHz to 2.2 GHz

The highest converstion efficiency of 70.79% is observed at 2.0 GHz with an input power of 1.5 dBm. The PIFA rectenna is now operable from approximately 1.5 GHz to 2.4 GHz.

Chapter 5

PIFA and Solar Cell Integration

The main goal of this project is to create a multi-source energy harvesting device; therefore, it is important to discuss the designed PIFA antenna is affected when integrated with a solar cell. Also, it is important to measure how the power harvested from the solar cell will change. This chapter begins with a breif discussion of solar energy harvesting followed by the experiments done to test how the integration will affect both devices and their results.

5.1 Solar Energy Harvesting

Solar energy harvesting is a process that uses photovoltaic solar panels that convert solar radiation to DC power. This type of energy harvesting is the most efficient conversion technique used today. Table 5.1 shows solar power density compared to other harvesting techniques.

Table 5.1: Harvesting technology and corresponding power density [16]

Harvesting technology	Power density
Solar cells (outdoors at noon)	$15mW/cm^2$
Piezoelectric (shoe inserts)	$330\mu W/cm^3$
Vibration (small microwave oven)	$116\mu W/cm^3$
Thermoelectric (10^oC gradient)	$40\mu W/cm^3$
Acoustic noise (100dB)	$960nW/cm^3$

Solar panels are characterized by two parameters which are the open circuit voltage (V_{oc}) and short circuit current (I_{sc}). Both of these parameters form the x- and y- intercepts of the V-I curve [16]. Once the solar power is received from the panels, the power is sent to the core of the

module which is the harvesting circuit. This circuit takes power from the solar panels, manages the energy storage and routes the power to the battery that is to be charged. It is imporant in this circuit to maximize efficiency to receive the optimal amount of power.

Solar energy is the most widely used means of harvesting energy today because of it's harvesting efficiency and available input solar power. For this reason, a solar cell was chosen to interate with our rectifying antenna. To test the effect of the antenna on the solar cell and visa verca several test were perfomed and recorded.

5.2 PIFA Effect on a Solar Cell

Since the solar cell is so efficient in ambient energy harvesting, it is important to take precaution when integrating a rectifying antenna. If a rectenna design has a large area then some of the solar energy will not be harvested. For this reason the PIFA design was chosen for this thesis. As stated earlier, the PIFA has a very small aperture size and low profile which will be necessary when placing it on a solar cell. The first few measurements were taken with the fabricated PIFA, a solar cell, and a radiating horn antenna. The setup for these measurements is shown in figure 5.1.

Figure 5.1: Photograph of the setup for the measurements recorded on the effects of a rectenna on a solar cell

First it was important to measure the solar cell with the radiating horn antenna on and off to make sure there were not any changes in the received solar power. The results are shown in table 5.2 and show no drastic changes in received solar power.

Table 5.2: Solar cell measurements take with and without the horn antenna radiating at the specified freuqency and power level

	Voltage, V	Current (I), A
No Antenna No horn	0.524V	1.95A
No Antenna Horn ON: 2.24GHz, P_{in}=18dBm	0.516V	1.95A

The antenna was then slid behind the solar cell with the ground facing up (figure 5.2) to see if any changes occurred in received voltage or current.

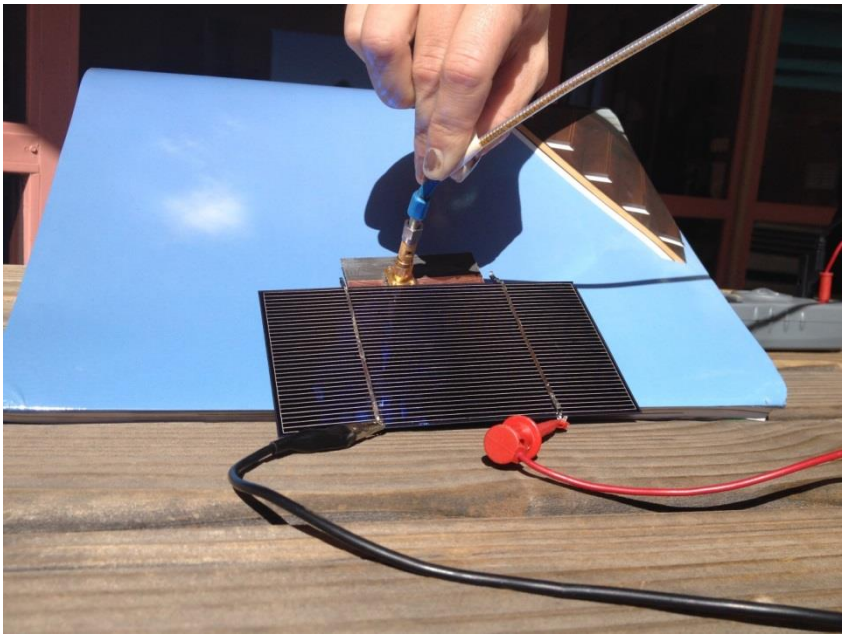

Figure 5.2: PIFA antenna with the solar cell with the ground of the antenna facing upwards.

When the antenna is placed behind the solar cell with the ground up, as seen in the photo above, at one point the current was increasing to 2.4 A. This occurred for the first couple tests but was not consistent. The inconsistency in this test could be due to cloud coverage. The antennas received power was also measured when the antenna was slid behind the solar cell. The antenna was receiving -16 dBm power when in this position without the solar cell and -23-24 dBm power with the solar cell. Therefore, the solar cell was causing a 7-8 dBm power loss for the antenna. It is important to note that the antenna was not aligned with the horn antenna for these measurements.

The next set of measurements were taken with the PIFA antenna behind the solar cell to see if there is any effect on harvested energy. The set up for this measurement is see below.

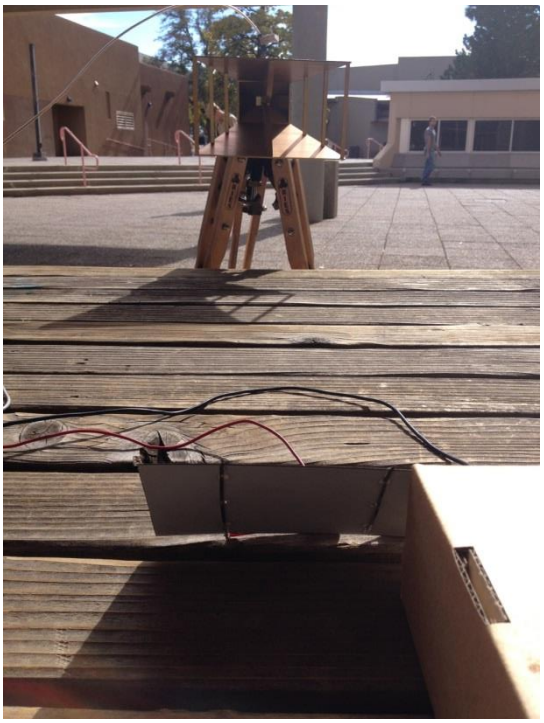

Figure 5.3: Photograph showing the area where antenna was positioned facing upward

In the figure above, the antenna was placed, face up, behind the solar cell. When the antenna was positioned this way behind the solar cell with the antenna up there was no noticeable change in the solar cell output. However, the antenna received power dropped from -11 dBm without the solar cell to around -20 – -23 dBm with the solar cell in place. Therefore, the solar cell was causing a 9-12 dB power loss for the antenna.

From the previous measurements, it was concluded that a more accurate representation of the PIFA and solar cell integration would be to design a replica of the PIFA shape to attach to the front of the cell. The PIFA design was cut from copper tape (figure 5.4) in order to be an accurate representation of the antenna that is to be integrated.

Figure 5.4: PIFA design cut from copper tape for solar cell integration.

Two solar cells were used for these measurements. One solar cell had the PIFA antenna design attached to it and the other was a reference panel to compare the change in power received. The set up for these measurements is displayed in figure 5.5.

Figure 5.5: Photograph of the setup to test the effects of a PIFA antenna design on a solar cell.

The results showed that there was very little loss between the two solar cells. The difference in the received voltage and current was approximately 0.01V and 0.24A respectively. It is also important to take into consideration any mismatch in dimension between the two cells or angle differences.

Table 5.3: Differences between voltage and current for a solar cell with and without an integrated PIFA on the front panel

	Voltage	**Current**
Without PIFA	.574V	3.3A
With PIFA	.564V	3.06A

The placement of the PIFA on the back of the solar cell was also tested to see if there was any variation in output power. The follow figure shows the placement on the back of the solar cell.

Figure 5.6: Photograph of the PIFA placement on the back of a solar cell.

These measurements showed little to no change in the output power of the solar cell. Again, the solar cell dimensions and angle can also cause slight changes in output power.

Table 5.4: Differences between voltage and current for a solar cell with and without an integrated PIFA on the back of the panel

	Voltage	**Current**
Without PIFA	.570V	3.03A
With PIFA	.550V	2.95A

With these various tests it is seen that, if integrated correctly, this antenna design has very little effect on the received output DC power from the solar cell.

5.3 Solar Cells Effect on a PIFA

It is also important to measure what kind of effects the solar cell will have on the antennas efficiency. Some differences in the power received by the antenna are recorded in the previous section, however, in this section the main focus will be on the antennas changes prior to integration. The first set of measurements were perfomred by placing the solar cell on various areas of the antenna and using a radiating horn antenna to measure the power received by the PIFA. The amount of power received by the PIFA sans the solar cells was measured first to provide as a reference.

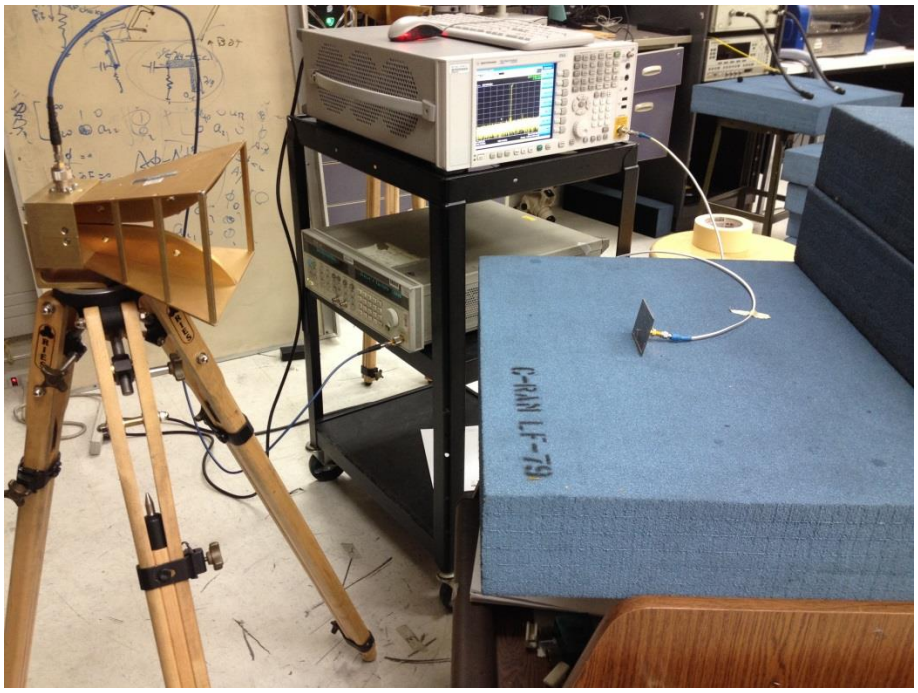

Figure 5.7: Photograph of the setup to measure power received from the PIFA antenna by the radiating horn antenna.

The horn antenna was set to radiate at 2.06 GHz with an input power of 18 dBm and the power received from the PIFA antenna was then read on the spectrum analyzer. Without the precense of

a solar cell the PIFA antenna was receiving a power of -7.68 dBm. This power level will become a reference for the remainder of the measurements.

The next test was performed by placing the solar cell covering the ground of the antenna. In this set up the antenna is pointed towards the horn and the solar cell is facing away. An image of layout is shown in figure 5.8.

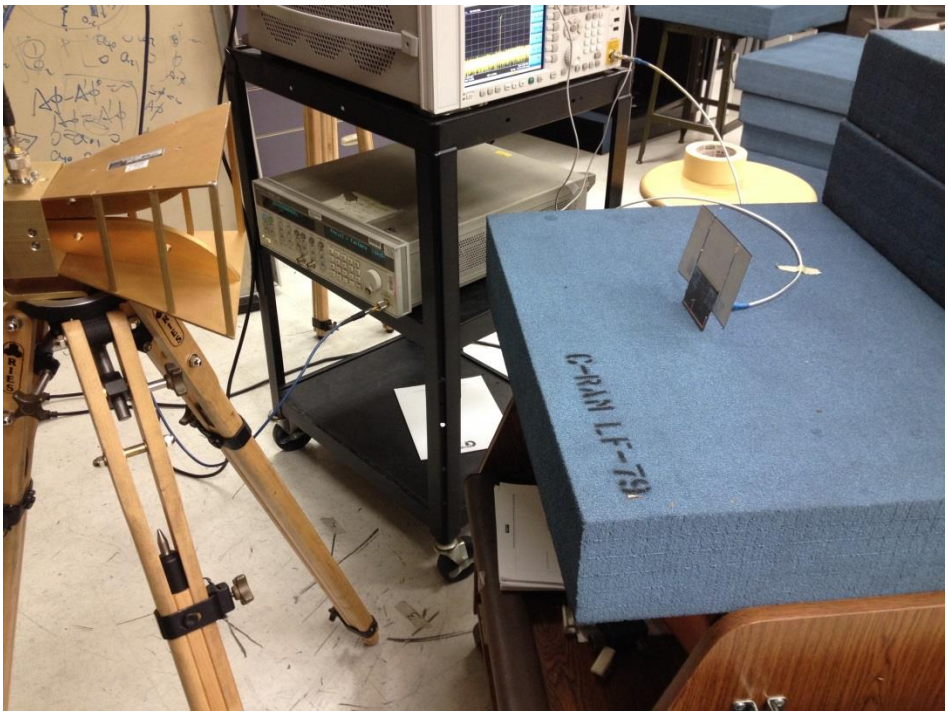

Figure 5.8: Photograph of the est performed with solar cell covering the ground plane of the antenna

The power received from the PIFA antenna with the solar cell in this position was -18.09 dBm. This is a drop of 10.49 dBm in received power from the antenna. The possible reason for this change in received power is that the solar cell connected to the ground in such a way could have shifted the resonant frequency.

The next solar cell placement was on the front of the antenna below the PIFA design. Here both the solar cell and the antenna are facing the radiating horn, as seen in figure 5.9.

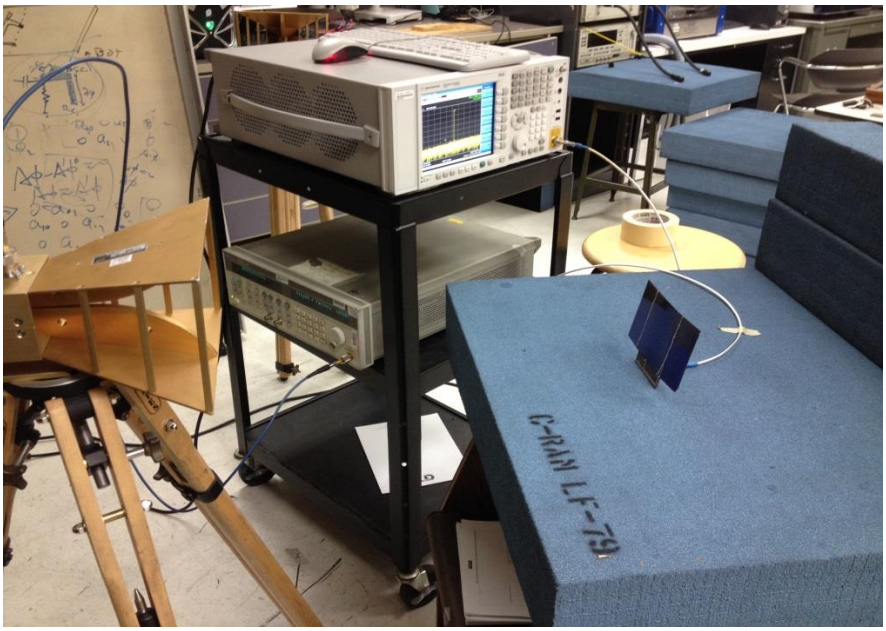

Figure 5.9: Photograph of the test performed with solar cell covering the front of the antenna underneath the PIFA design.

This placement did not see as much of a loss in antenna power as in the previous test. The measured power received by the PIFA was -13.99 dBm which is a loss of approximately 6.3 dBm. As in the previous test, this loss could be due to the effect the solar cell has on the ground plane which could result in a shit in resonant frequency.

To see what kind of effects the solar panel has on the resonant frequency, the return loss was measured with the integrated solar panel. The S_{11} parameters were measured for both the placement of the solar cell covering the ground and on the antenna side over the ground.

a.  b. 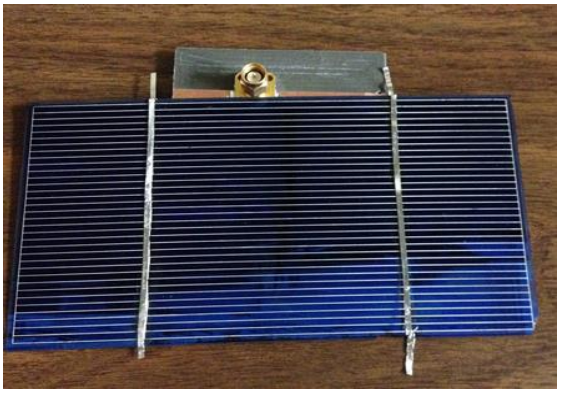

Figure 5.10: Photograph of the (a) placement of solar cell on the front side of the antenna (b) placement of the solar cell covering the ground.

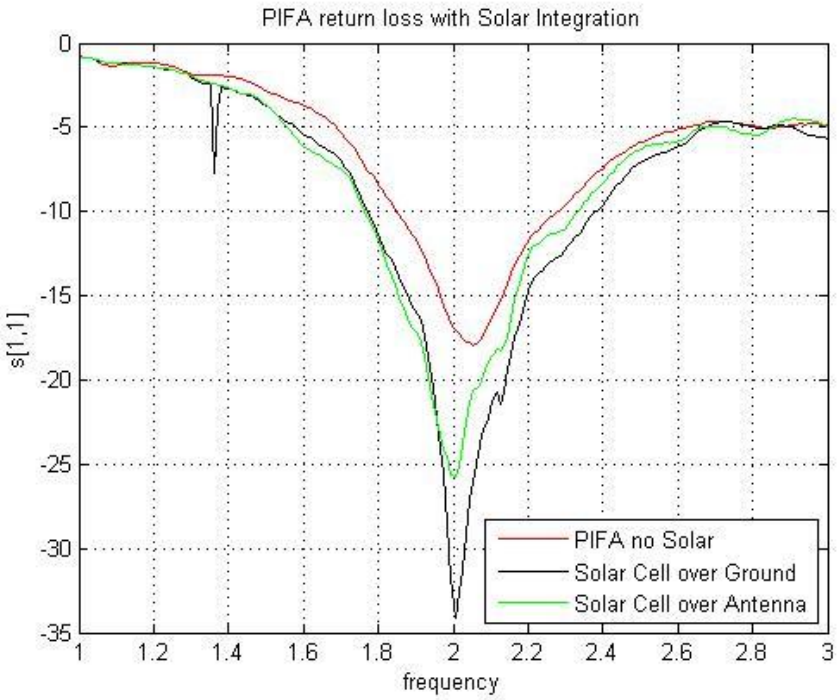

Figure 5.11: Measured return loss for the PIFA with and without the integration of a solar cell.

The results of the return loss measurements are diplayed in a graph in figure 5.11. It is seen in this plot that, the resonant frequency for the antenna with the solar cell, does shift slightly to the left to about 2.0 GHz. This shift could slightly affect the received power from the antenna, however the bandwidth of the PIFA with the solar panel still remains broad and encompasses the initial bandwidth of the antenna without the solar panels. While these results are useful to determine how an existing solar panel can shift the frequency of the antenna, the PIFA design of the antenna is not covered and, therefore, if we can integrate the PIFA on the same plane as the solar panel, the solar will not distort the performance of the antenna in terms of S_{11} parameters.

The final return loss test conducted was to see how the antenna would react if the solar cell was surrounding the antenna. To do this, several solar panels were placed around the antenna and the return loss was measured. Figure 5.12 shows the antenna and solar cell placement.

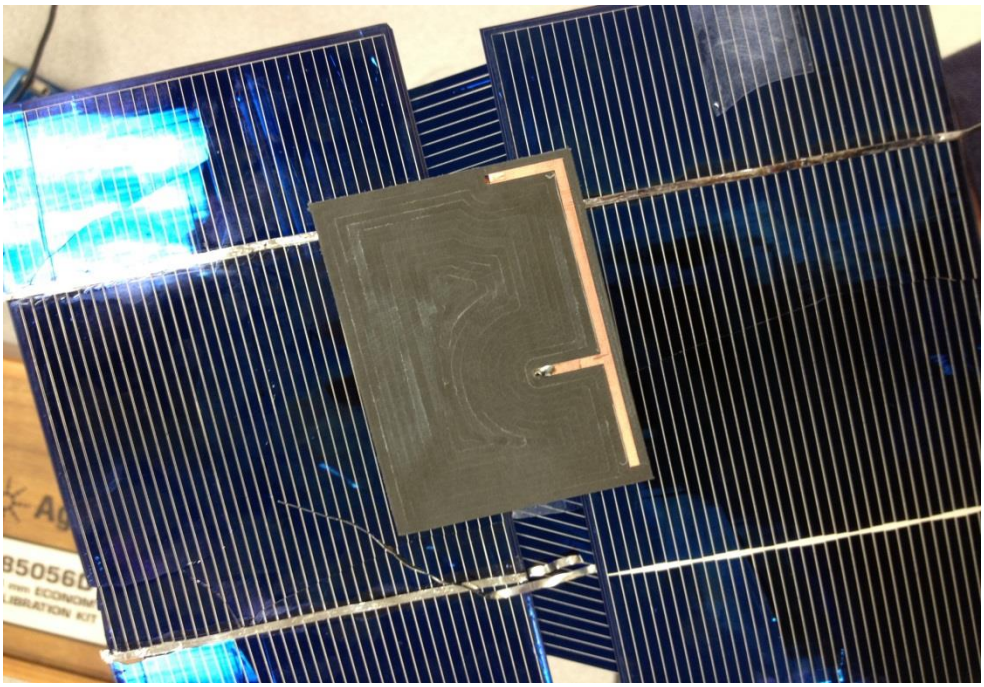

Figure 5.12: Photograph of the PIFA antenna surrounded by solar cells.

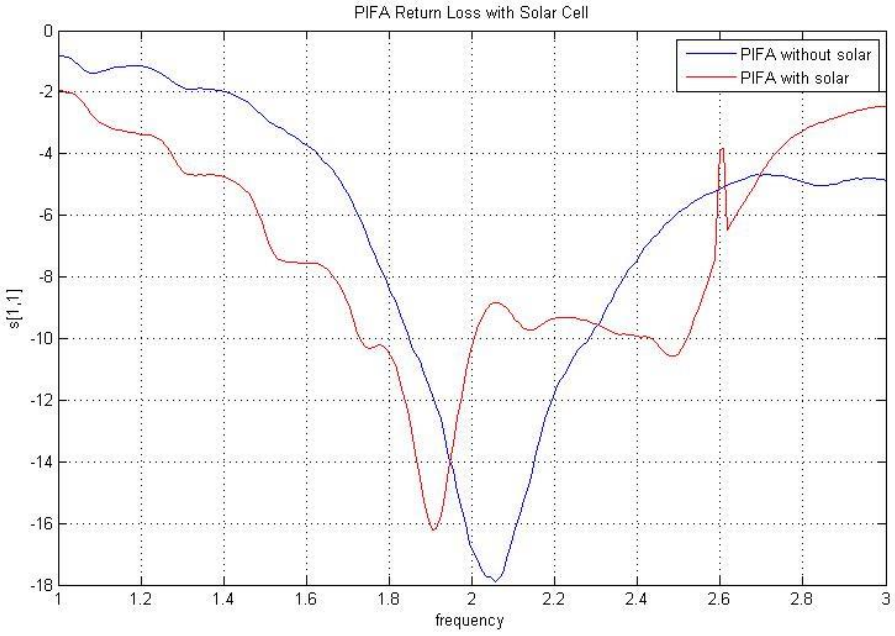

Figure 5.13: Return loss for the PIFA with surrounding solar cells.

It is seen if figure 5.13 that surrounding the PIFA with solar panes does shift the resonant frequency approximately 200 MHz. The original PIFA f_r is 2.06 GHz and the f_r with the solar panels is recorded at 1.9 GHz.

To complete this study of the integration of a broadband PIFA antenna with a solar cell, a model of PIFA was constructed in HFSS with the Si material of the solar cell used for the substrate. Table 5.5 shows the characteristics for Si that are needed to incorporate this material as the antennas substrate.

Table 5.5: Si conditions needed create the substrate for the PIFA antenna

Si Conditions	
ε_r	11.7
tanδ	0.004
thickness	5.9055 mil

The PIFA design was simulated on this substrate for a resonant freuency of ~2.1 GHz. The dimensions for this antenna design are listed in table 5.6.

Table 5.6: PIFA design dimensions with solar panel substrate

PIFA Design Dimensions	
Length – L1	4.1cm
Length – L2	0.9cm
Width - W	0.16cm
Ground Plane Length	14cm
Ground Plane Width	8cm
Length between short and feed	1.6cm

The PIFA model is seen in figure 5.14 and the simulation reults are in figure 5.15 a-c.

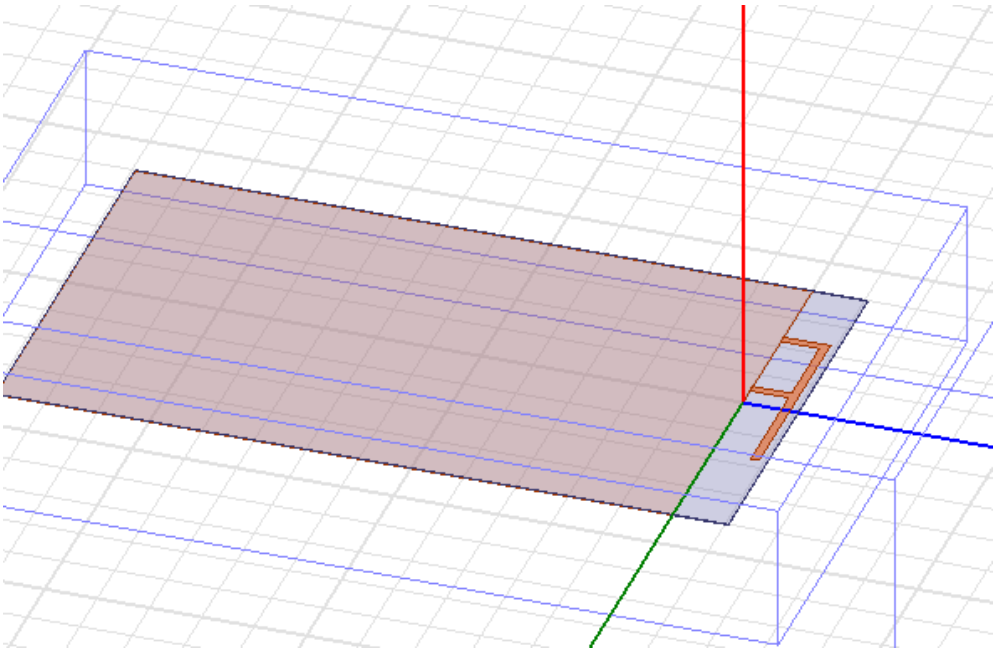

Figure 5.14: HFSS model of PIFA design with Si substrate.

a.

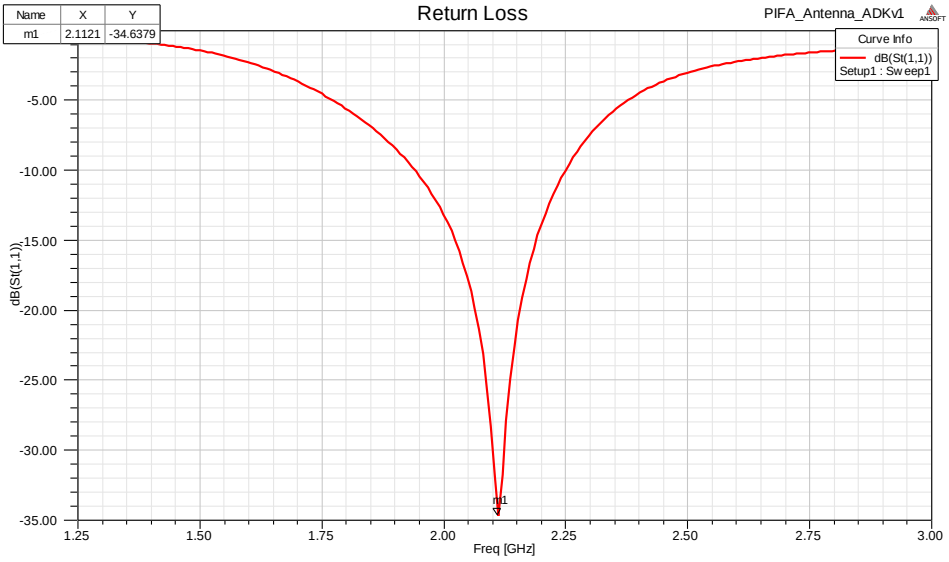

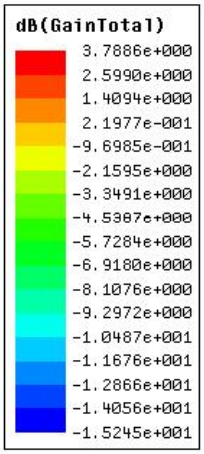
dB(GainTotal)
3.7886e+000
2.5990e+000
1.4094e+000
2.1977e-001
-9.6985e-001
-2.1595e+000
-3.3491e+000
-4.5387e+000
-5.7284e+000
-6.9180e+000
-8.1076e+000
-9.2972e+000
-1.0487e+001
-1.1676e+001
-1.2866e+001
-1.4056e+001
-1.5245e+001

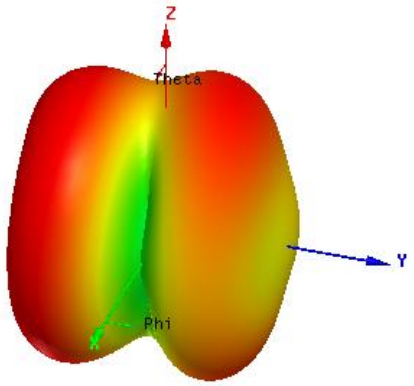
Z
Theta
Y
Phi

b.

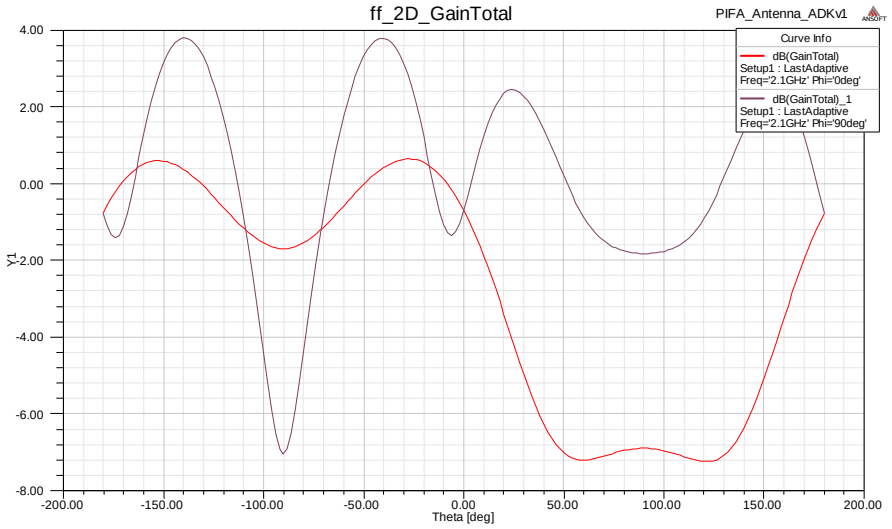
ff_2D_GainTotal
PIFA_Antenna_ADKv1
Curve Info
dB(GainTotal)
Setup1 : LastAdaptive
Freq='2.1GHz' Phi='0deg'
dB(GainTotal)_1
Setup1 : LastAdaptive
Freq='2.1GHz' Phi='90deg'
4.00
2.00
0.00
-2.00
-4.00
-6.00
-8.00
Y1
-200.00
-150.00
-100.00
-50.00
0.00
50.00
100.00
150.00
200.00
Theta [deg]

c.

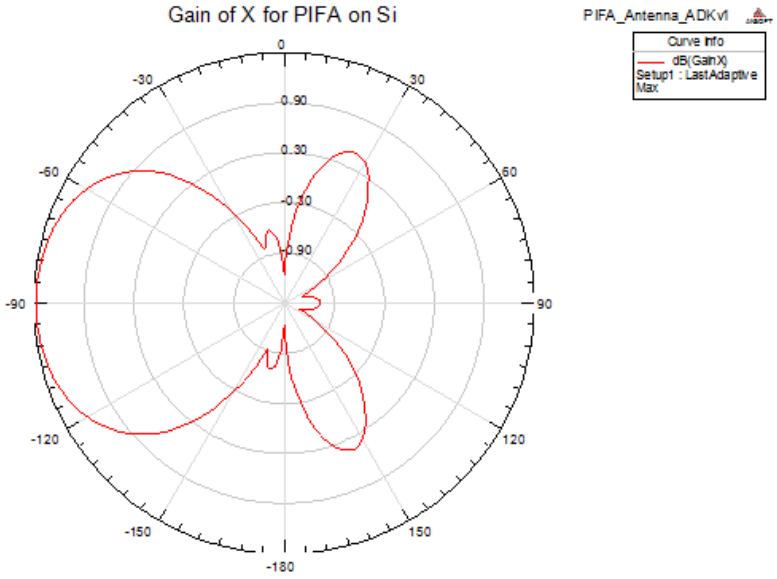
Gain of X for PIFA on Si
PIFA_Antenna_ADKv1
Curve Info
dB(GainX)
Setup1 : LastAdaptive
Max
0
30
60
90
120
150
-180
-150
-120
-90
-60
-30
0.90
0.30
-0.30
-0.90

d.

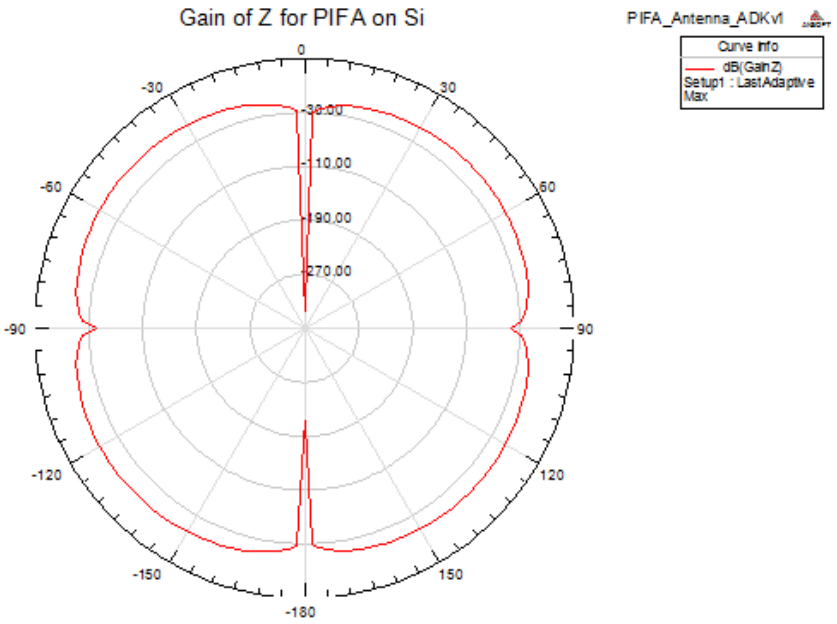

e.

Figure 5.15: HFSS simulation resutls (a) return loss (b) 3D gain plot (c) 2D gain total (d-e) radiation pattern for x- and z- axis.

The resonant frequency is recorded at 2.11 GHz of -35 dBm, the bandwidth ranges from around 1.9 GHz to 2.3 GHz and the gain reaches to 3.7 dBm. In conclusion, this PIFA design can be integrated on top of a solar panel with an Si base to produce similar results however, due to the fragile state of the substrate, a laser may need to be used in order to create the holes in the panel for the feed and short.

Chapter 6

Conclusions and Furture Work

Throughout the course of this thesis the ambient energy from RF has been measured and recorded to determine the optimal frequency and bandwidth of operation for the rectifying antenna. The design and fabrication of narrowband and broadband antennas were discussed, the design and fabrication of a narrowband, broadband and broadband voltage doubler rectifyig circuit are also presented and discussed. Furthermore, the integration of the rectenna with a solar panel is presented. The broadband PIFA rectenna functions with approximately 88% efficiency at high input power and 13.9% efficiency at low input power. The highest voltage harvested with this design is 7.45 V at 1.4 GHz with an input power of 18 dBm. This design integrated with a solar panel shows it does not cause a significant solar power loss and although there is a slight shift in resonant frequency, the bandwidth is not greatly effected.

Future work for this project would include the construction of a PIFA array integrated with a photovoltaic array to receive the optimal amount of harvestable energy. A PIFA array can be used to provide different radiation patterns to receive signals in different directions. An example layout of such array can be seen in figure 6.1.

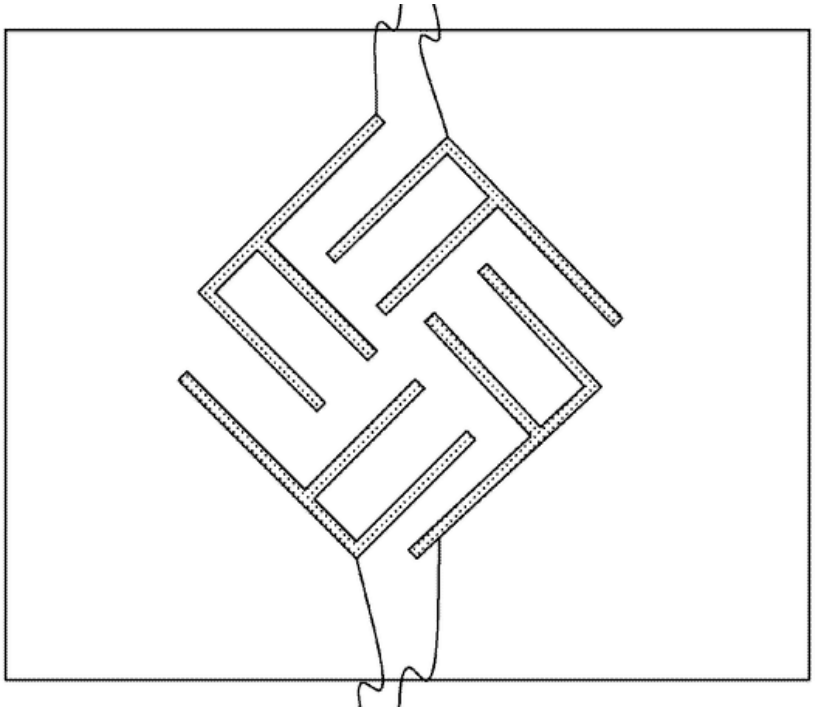

Figure 6.1: Layout of a PIFA array [17].

The separation between the antenna elements in an array is the most crucial part of the design. Spacing in an array can affect mutual coupling which can affect both the elements radiation pattern and the input impedance. Studies have shown that for little to no coupling, the distance between the antenna elements need to be at least a half wavelength ($\lambda/2$) apart. The design and fabrication of a PIFA array and its integration with a solar cell could greatly increase the amount of harvested RF energy.

Resources

[1] “SEPTET: Sustainable Energy Pathways Through Education and Technology” University of New Mexico, Albuquerque, New Mexico

[2] Zhang, Jingwei and Huang, Yi. “Rectennas for Wireless Energy Harvesting” Department of Electrical Engineering and Electronics, University of Liverpool, Liverpool UK

[3] Brown, William C. "The History of the Development of the Rectenna." *Microwave Power Transmission and Reception*. Vol. 1. 1980.

[4] Ohira, Takashi. "Power efficiency and optimum load formulas on RF rectifiers featuring flow-angle equations." *IEICE Electronics Express* 10.11 (2013): 20130230-20130230.

[5] Gao, Yan-Yan, et al. "A circularly polarized rectenna with low profile for wireless power transmission." *Progress In Electromagnetics Research Letters* 13 (2010): 41-49.

[6] Hagerty, Joseph A., et al. "Recycling ambient microwave energy with broad-band rectenna arrays." *Microwave Theory and Techniques, IEEE Transactions on* 52.3 (2004): 1014-1024.

[7] Marian, Vlad, et al. "Strategy for microwave energy harvesting from ambient field or a feeding source." *Power Electronics, IEEE Transactions on* 27.11 (2012): 4481-4491.

[8] Heikkinen, Jouko, and Markku Kivikoski. "A novel dual-frequency circularly polarized rectenna." *Antennas and Wireless Propagation Letters, IEEE* 2.1 (2003): 330-333.

[9] Baroudi, Uthman, Samir Mekid, and Abdelhafid Bouhraoua. "Radio Frequency Energy Harvesting Characterization: An Experimental Study." *Trust, Security and Privacy in Computing and Communications (TrustCom), 2012 IEEE 11th International Conference on*. IEEE, 2012.

[10] Turpin, Timothy W., and Reyhan Baktur. "Meshed patch antennas integrated on solar cells." *Antennas and Wireless Propagation Letters, IEEE* 8 (2009): 693-696.

[11] Roo-Ons, M. J., et al. "Transparent patch antenna on a-Si thin-film glass solar module." *Electronics letters* 47.2 (2011): 85-86.

[12] "Microstrip (Patch) Antennas." *Microstrip Antennas: The Patch Antenna*. N.p., n.d. Web. 08 Nov. 2013. <http://www.antenna-theory.com/antennas/patches/antenna.php>.

[13] Balanis, Constantine A. *Antenna theory: analysis and design*. John Wiley & Sons, 2012.

[14] Rosu, Iulian. “PIFA – Planar Inverted F Antenna” YO3DAC/VA3IUL – RF Technical Articles. 2008

[15] Firoozy, Nariman, and Mahmoud Shirazi. "Planar Inverted-F Antenna (PIFA) Design Dissection for Cellular Communication Application." *Journal of Electromagnetic Analysis and Applications* 3.10 (2011).

[16] Raghunathan, Vijay, et al. "Design considerations for solar energy harvesting wireless embedded systems." *Proceedings of the 4th international symposium on Information processing in sensor networks*. IEEE Press, 2005.

[17] "PIFA ARRAY - Diagram, Schematic, and Image." *PIFA ARRAY - Diagram, Schematic, and Image*. N.p., n.d. Web. 08 Nov. 2013. <http://www.faqs.org/patents/imgfull/20120319919_11>.

[18] Tawk, Youssef. "Chapter 8: Matching Networks" Spring 2013. University of New Mexico.

[19] Sun, Jwo-Shiun, et al. "Wireless Power Transmission with Circularly Polarized Rectenna." *Microwave Journal. ii* (2011).

[20] Avago technologies,"HSMS 286X series, surface mount microwave Schottky detector diode" Data sheet, May 2009.

[21] Huynh, M-C., and Warren Stutzman. "Ground plane effects on planar inverted-F antenna (PIFA) performance." *Microwaves, Antennas and Propagation, IEE Proceedings*. Vol. 150. No. 4. IET, 2003.